# Aalborg University

# Modeling and Control of an Autonomous Racing Car



Electronics and IT:
Master Thesis

Group:
19gr1038

6. September 2019

**Theme:**

Complex Systems

**Project:**

Master Thesis

**Project period:**

February 2019 - September 2019

**Project group:**

19gr1038

**Participants:**

Jonatan Fuglsang Jensen

**Supervisors:**

Jesper A. Larsen

Copies: 1
Pages: 54
Appendix: 11
Completed: 06-09-2019

**Abstract:**

This thesis describes the design and analysis of an nonlinear model and a control strategy for Aalborg University Race team's G8 race car and has been motivated by the need for an Autonomous Racing Car (ARC) to compete in the Formula Student event in 2021. The performance of the designed model is evaluated in a simulation environment, implemented in Matlab Simulink. Effort has been put in to keep it reusable for extensions in future work. The equations of motion have been formulated, including tire dynamic together with aerodynamic disturbance and take into account longitudinal and lateral slip. A linearization of the nonlinear model has be performed to allow an implementation of a linear quadratic controller (LQR) design, to regulate the speed. The model shows good performance in regions above 36 kilometer per hour, but region below suffer from a simplified engine model.

# Preface

This thesis has been written by group 19gr1038, to document the work at Aalborg University. The documentation includes the modeling, design and development of a control strategy for an Autonomous Racing Car. It is written as part of a Master program in the Department of Electronic Systems, started on February 1, with a submission deadline on September 6.

The report is written in cooperation with the supervisor:

- Jesper A. Larsen, Associate Professor at Aalborg University.

The figures in the report have been produced by the group unless a source is specified. Sources are indicated by [Number] or [Number, p. Page-number] and can be found in the bibliography. Appendixes are indicated by A.number. The paper is structured in chapters, sections and subsections. Every figure, table, equation and code is numbered according to the section they belong. Figures can be diagrams, flowcharts and graphs. The following is uploaded on the Database:

- Matlab files
- Simulink files
- SolidWorks files

The author would like to thank students of Aalborg University Race team who have been involved in this project, providing data and consultation regarding the race car.

Jonatan Fuglsang Jensen

# Contents

# Introduction 1

This thesis describes the modeling, design and development of a control strategy for an Autonomous Racing Car (ARC). The car is designed by a team of students from Aalborg University (AAU) to compete in the Formula Student, which is a worldwide engineering competition. Changes to the rules has motivated the need for an autonomous system to be implemented on the car.

A description of the competition, events and possible subsystems are first introduced, followed by an outline of the thesis at the end of this chapter.

## 1.1 Formula Student Competition

Formula Student (FS) is an educational engineering competition that aims to encourage people to take up a career in engineering. The competition combines practical engineering with other skills such as business planning and project management and have teams from around the globe. Students are required to build a single seat formula race car for the competition, but a team is also scored in terms of construction, performance and financial. This can be compared to developing and manufacturing a prototype car, that is evaluated for production [7].

The competition is divided into three classes, which are Internal Combustion Engine Vehicle (CV), Electric Vehicle (EV) and Driverless Vehicle (DV), where DV class can be either CV or EV. The university can register one team per class, but by 2021 all vehicles are supposed to have a driverless mode as DV merge with CV and EV [4]. All classes must meet a set of requirements, but there are also specific requirements depending on the class. These are specified in the FS rule book. An inspection is performed to ensure the vehicle is in compliance with the rules [5].

The competition is split into static and dynamic events. The static events consider the ability to develop a business model, understand manufacturing and costs and evaluate the engineering process associated with construction of the prototype race car [5].

The dynamic events focus on the performance of the car. For all events the track is marked with cones that have specific characteristics. Entry/exit lanes are marked with small orange cones while large orange cones is placed before and after the start/finish lines. Borders to the left of the track are marked with small blue cones, while borders to the right are marked with small yellow cones, with a distance of max 5 $[m]$ between two cones in driving direction [6].

Both static and dynamic events has a maximum amount of points that can be awarded as seen in Tab. 1.1. The team with most points wins the competition [5].

| Static Events: | CV & EV | DV |
|---|---|---|
| Business Plan Presentation | 75 points | 75 points |
| Cost and Manufacturing | 100 points | 100 points |
| Engineering Design | 150 points | 300 points |
| **Dynamic Events:** | | |
| Skid Pad | 75 points | 75 points |
| Acceleration | 75 points | 75 points |
| Autocross | 100 points | 100 points |
| Endurance | 325 points | - |
| Efficiency | 100 points | 75 points |
| Trackdrive | - | 300 points |
| Overall | 1000 points | 1000 points |

Table 1.1: Table of maximum amount of points that can be awarded in static and dynamic events [7].

### 1.1.1   Dynamic Events

A description of each dynamic events can be found in FS rule book, defining the objective, layout and placement of cones on the track. Since driverless mode will be a requirement in 2021 only DV is considered.
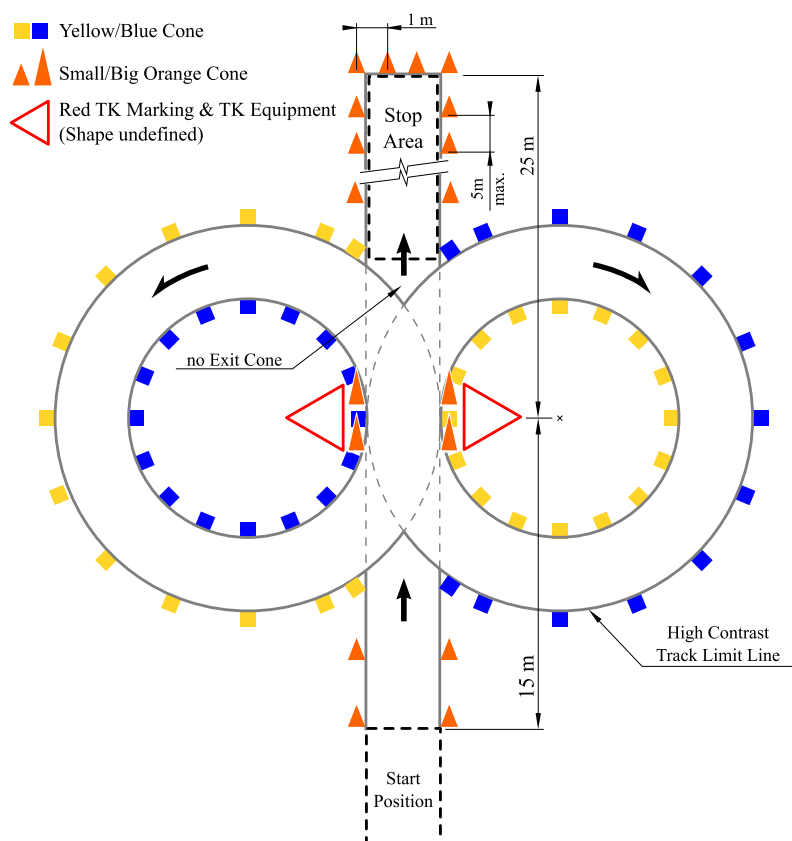


Figure 1.1: Figure of the dynamic event skid pad [6].

In the skid pad event, see in Fig. 1.1, the vehicle enters a eight figure track and take one

full lap on the right circle. The second lap is timed, still on the right circle. Following the second lap, the vehicle enter the left circle for a full lap. The fourth lap is timed on the left circle. After finishing the fourth lap, the vehicle exits the track [5].
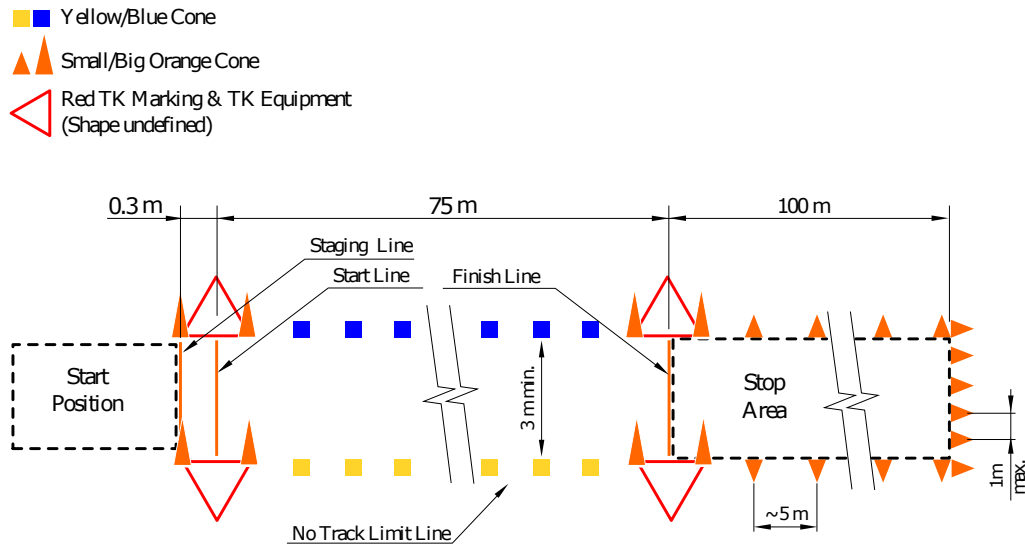
Figure 1.2: Sketch of the dynamic event acceleration [6].

In the acceleration event, see in Fig. 1.2, the track is a straight line having a length of 75 [m] from start to finish. The timing starts after the vehicle crosses the start line and stops after it crosses the finish line. The vehicle is required be fully stop within 100 [m] [5].
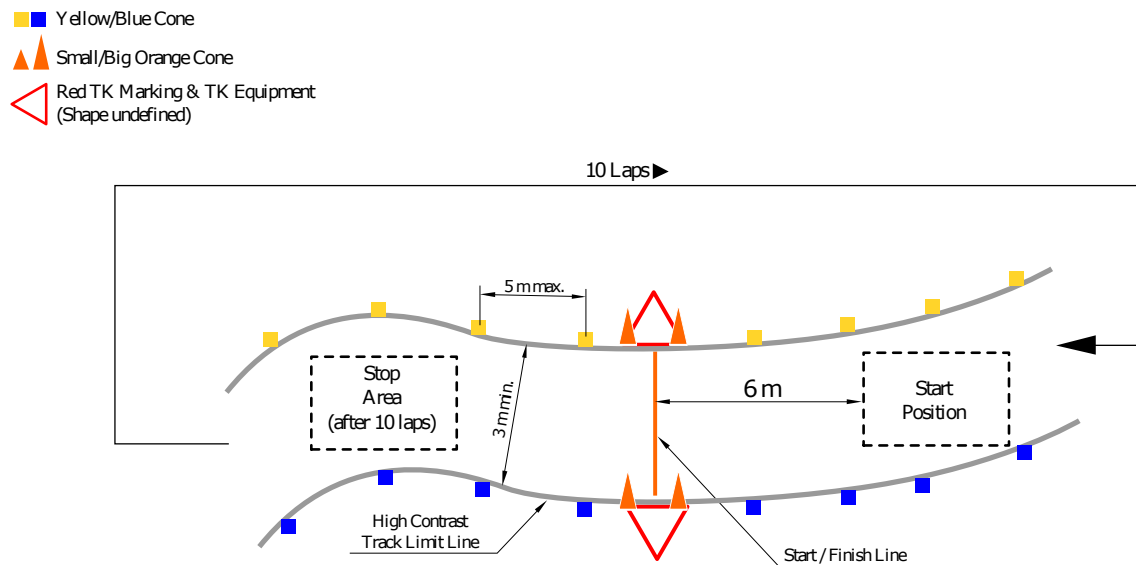
Figure 1.3: Figure of the dynamic event autocross/trackdrive [6].

The autocross event, see in Fig. 1.3, is a handling track that follows a set of guidelines, such as no straights segments longer than 80 [m], constant turns up to 50 [m] in diameter and can include hairpin turns, slaloms and chicanes. The length of the track is less than 1500 [m]. The timing starts after the vehicle crosses the start line and stops after it crosses the finish line, having completed a specified number of laps. The vehicle is required be fully stopped within 30 [m] [5].

The efficiency event is connected to the trackdrive event for DV. It uses the same track as the autocross event and follows a similar procedure, but includes points for energy efficiency. It should be noted that no data of the track layout may be obtained prior the event and can't be stored for a second run. The vehicle is also required to count the lap by itself [5].

## 1.2   ARC Subsystem

Currently there are no implementation on the AAU G8 racing car that would enable it to function autonomously. Therefore it is necessary to incorporate actuation, sensing and processing to the platform. However the car must still be able to be driven by a human operator and any addition must be implemented such that the safety of the operator remain intact. Given the confined space of the racing car it may also be difficult to ensure optimal placement for the actuators and sensor and probably requires modification to the body frame.

The AAU racing team are considering to change the current combustion vehicle to an electrical, which complicates upgrading the car ever further. Therefore should the subsystem and their placement discussed in this section not be considered a finalized version for the ARC.

One of the primary task the ARC has to be able to perform, is tracking the position and following a path. As mentioned in the previous section, the track is marked with cones, which could be detected using a Light Detection and Ranging (LIDAR) sensor. It is also possible to use a camera to determine the color of the cones, which particular could be helpful in the skid pad event to ensure correct left or right hold. Furthermore could a Global Positioning System (GPS) and a inertial measurement unit (IMU) be added and by combining all four, using sensor fusion. Together with a Kalman filter, a relative high position accuracy for the ARC should be ensured. This is important since no data of the track layout is known prior.

The placement of the LIDAR in the ARC could be in the front section as seen in Fig. 1.4 and thereby be able to detect the cones. Depending of the Field Of View (FOV) and maximum range of the LIDAR, a reference path can be determined ahead of the vehicle and stored using a processing system. Assuming the size of the processing system is relative small and sufficient space beneath the driver seat, the processing system and IMU could be placed there. The GPS receiver and camera could be placed in front of the dashboard, giving the camera an overview of the track ahead of the ARC.

The reasoning for placing the LIDAR in the front section closer to the surface is to avoid possible ground cluttering, making the cones relative easy to distinguish from the surface. The camera on the other hand might benefit from the contrast between the cones and the typically dark tarmac and is place higher above the surface. There is an argument to place the LIDAR and camera on the roll bar seen in Fig. 1.5, giving a 360 degree view around the vehicle. But it is specified in the rules that placement can not be outside the roll bar and the inside area is where the drivers head would be. Note that the driver would not be present in the vehicle during a run, however as stated before the ARC must be able to be driven by a person. Furthermore the vehicle is not designed or allowed to drive in reverse.
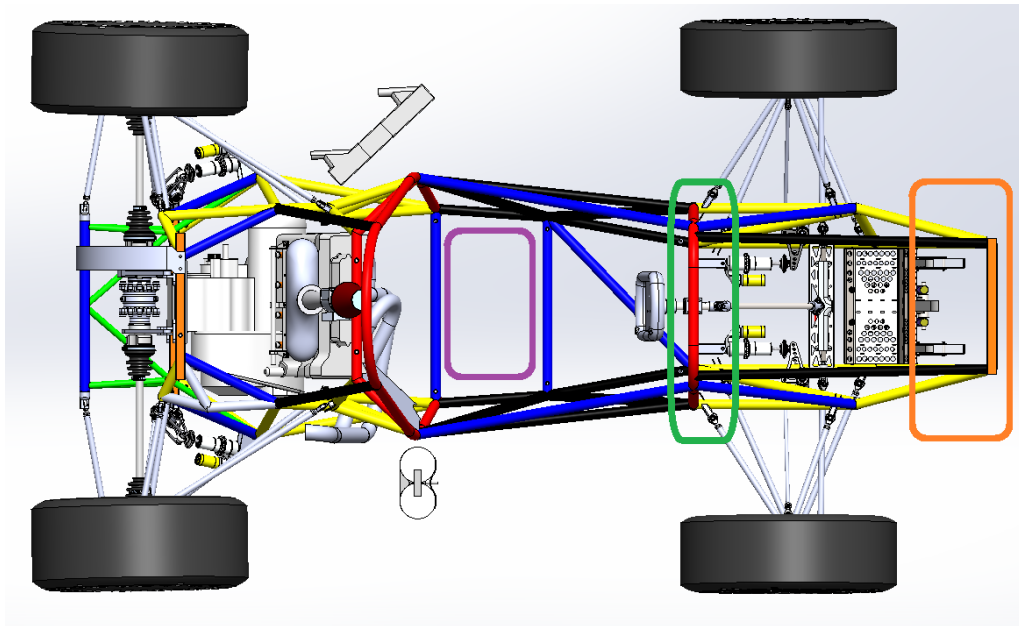
Figure 1.4: Sketch of sensor placement for LIDAR (orange), camera and GPS (green) and processing system and IMU (magenta).
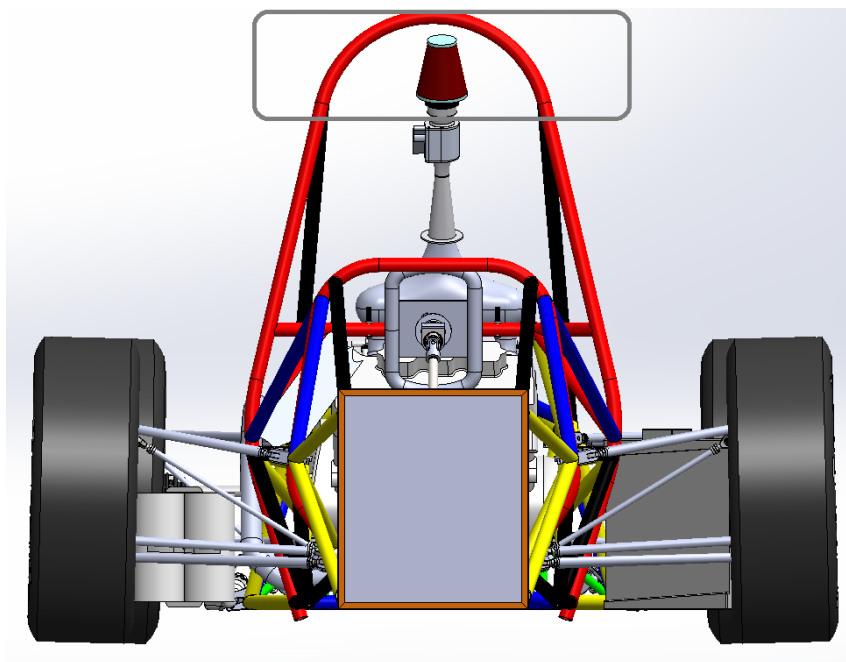


Figure 1.5: Sketch of sensor placement on the roll bar for LIDAR and camera (gray).

## 1.3   Thesis Outline

The focus of this project is to develop a nonlinear model for simulation of the ARC in MatLab Simulink, design a speed controller to verify its functionality. Furthermore is relevant disturbances investigated and include in the model. Going forward, this thesis is organized as follows:

**Chapter 2** introduces the nonlinear model required to obtain a description of the vehicle behavior including disturbances model, engine model, drivetrain model and tire model. The reference frames and equation of motion are defined leading to verification of the model using parameters from the G8 race car.

**Chapter 3** gives an introduction to a possible track design, covering multiple aspect of a driving environment for the ARC, were requirements for a possible control scenario are described. It furthermore includes a short evaluation of possible control strategies leading to a linearization of the nonlinear model for use in a Linear Quadratic Regulator design.

**Chapter 4** discusses the implemented model and control and summarizes the thesis, leading to recommendations for future work.

# Vehicle Modelling 2

In this Chapter, a physically description of the behavior for the vehicles when driving is studied using a simplified model. Only a nonlinear model is considered as a description for the drivetrain and the vehicle behavior at larger steering angles and higher lateral accelerations above 0.4 $[m/s^2]$ is needed (vehicle speed above 5 m/s). For convenience purposes the notation and illustration throughout this chapter often refers to [2], which is the source of the model.

## 2.1 Nonlinear Single Track Model

A nonlinear model is required to obtain a description for vehicle behavior at larger steering angles and higher lateral accelerations. However a single track model still only cover planar translation and yaw and not dynamics, such as roll and pitch. including more dynamics would require a two track model, which increase the complexity significantly as the number of Degrees of freedom (DOF) increases. Particular the wheel suspension is important for accurate wheel movements, vibration behavior of vehicles and driving dynamics. If these dynamics could be considered relative small, given optimal condition, the single track model may still be viable for control purpose. The single track model is also often referred to as the bicycle model where the two front wheels are represented by one single wheel and similarly the rear wheels are represented by one rear wheel, both place centrally to the vehicle wheelbase [2].

The model consist of a chassis, considered a rigid body, with two translational degrees of freedom and the rotation about the vertical axis. An imaginary front and rear wheel, that are characterized by speed and tire forces and includes steering at the front wheel. The driving torques of the wheel is approximated from the engine torque, the chosen gear ratio, the final drive ratio and can be distributed onto the front and rear wheel. Brake torques on the wheels is determined from the brake pedal position and can also be distributed. The engine torque is fund from the Revolutions Per Minute (RPM) of the engine and the acceleration pedal position. Finally the model includes the air resistance as a disturbance [2].

The model do not account for all lifting, rolling and pitching motions, aligning torque and assumes that the mass is concentrated at the center of gravity. Also the load between front and rear axle is assumed to be constant [2].

## 2.2 Aerodynamic Disturbances

Aerodynamic forces has significant influence on the vehicle performance and dynamic behavior at higher velocities. The air resistance can be associate with three physical

effects, the air stream turbulence (form resistance), the flow onto the chassis (friction resistance) which depend on the surface area and the air stream flows through the chassis (inner resistance) which cool the motor, each accounts for approximately 85 percent, 10 percent and 5 percent of the complete air resistance respectively [2].

Based on this, wind forces is generally caused by the turbulent streams and according to [2], are proportional to the ram pressure $p_L$, which is a pressure exerted on a body moving through a fluid medium causing drag:

$$p_L = \frac{1}{2}\rho_L v_L^2 \tag{2.1}$$

Where $\rho_L$ is the air density and $v_L$ is the flow velocity. The air density at sea level is 1.2 $[kg/m^3]$ [11].

By considering an effective cross-sectional area $A$ of the vehicle, with a dimensionless air resistance coefficient $c_W$, which for a typical vehicle is between 0.2 and 0.4. The force due to wind resistance $F_W$ is given as [2]:

$$F_W = c_W A \rho_L \tag{2.2}$$

If the environmental wind $v_W$ is consider with the flow velocity, the relative velocity $v_R$ is needed as illustrate in Fig. 2.1. Note that the air resistance coefficient mentioned above is based on the vehicle seen in the figure. The ARC is not necessarily aerodynamic efficient and might require a higher coefficient value.
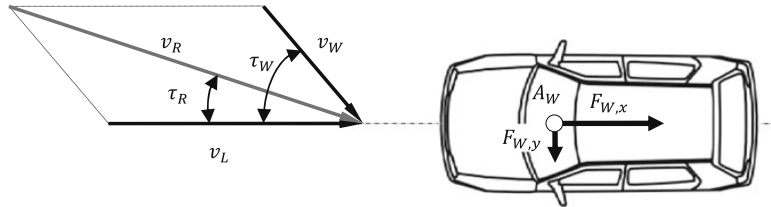


Figure 2.1: Illustration of the relative velocity [2].

The direction of the environmental velocity is given with the angle $\tau_W$. By applying the cosine law, the relative velocity is obtained [2]:

$$v_R = \sqrt{v_L^2 + v_W^2 + 2v_L + v_W cos(\tau_W)} \tag{2.3}$$

The air flow angle $\tau_R$ can then be obtained as [2]:

$$\tau_R = arcsin\left(\frac{v_W}{v_R}sin(\tau_W)\right) \tag{2.4}$$

The slanted inflow cause changes in the direction of the longitudinal, lateral and aerodynamic lift forces giving the following force components for the air resistance [2]:

$$F_{W,x} = c_x A_W \frac{\rho_L}{2} v_R^2 \tag{2.5a}$$

$$F_{W,y} = c_y A_W \frac{\rho_L}{2} v_R^2 \tag{2.5b}$$

$$F_{W,z} = c_z A_W \frac{\rho_L}{2} v_R^2 \tag{2.5c}$$

Note that the cross-sectional area $A_W$ is assumed to be the same. Furthermore will coefficients $c_x, c_y$ and $c_z$ depend on the angle of inflow. For simplicity is $F_{W,z}$ neglected and $\tau_R$ is considered to be zero and therefore is $c_x, c_y$, become $c_W$.

## 2.3 Engine Model

The engine that is currently used for the ARC is from a Honda CBR600-RR motorcycle. A simple model of the engine, is to consider it as a black box. illustrated in Fig. 2.2, where an input is applied and a output is measured. Here, the angular velocity (converted to RPM) of the wheels is the input, giving a torque output.
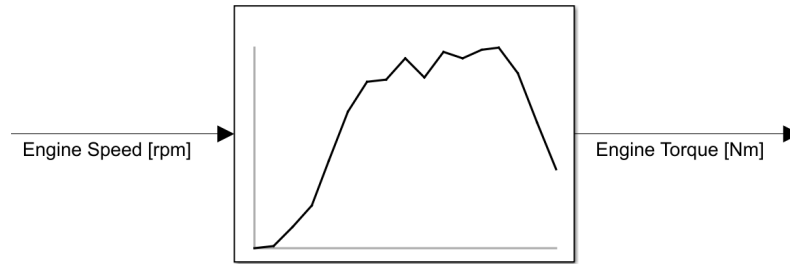


Figure 2.2: Black Box of the engine where the input is angular velocity of the wheel and the output is torque.

The AAU Racing Team have provided data from the engine as seen in Fig. 2.3. The torque can then be interpolated from the one dimensional characteristic curve. However data is from 4000 to approximately 12000 RPM, it is therefore not clear if the engine have a minimum velocity of 4000 RPM.

As the torque is approximated form the angular velocity of the wheels, data from 0 to 4000 RPM have to be added. According to [2] this could be assumed to be linear. Considering a low velocity for the wheels, this should lead to relative low torque output from the engine.

It should be mentioned that the characteristic of the torque curve is assumed to be the same regardless of the accelerator pedal position, which is not necessarily correct. Furthermore consideration such as fuel efficiency, optimal torque output and gear changes will not be taken into account in this thesis.
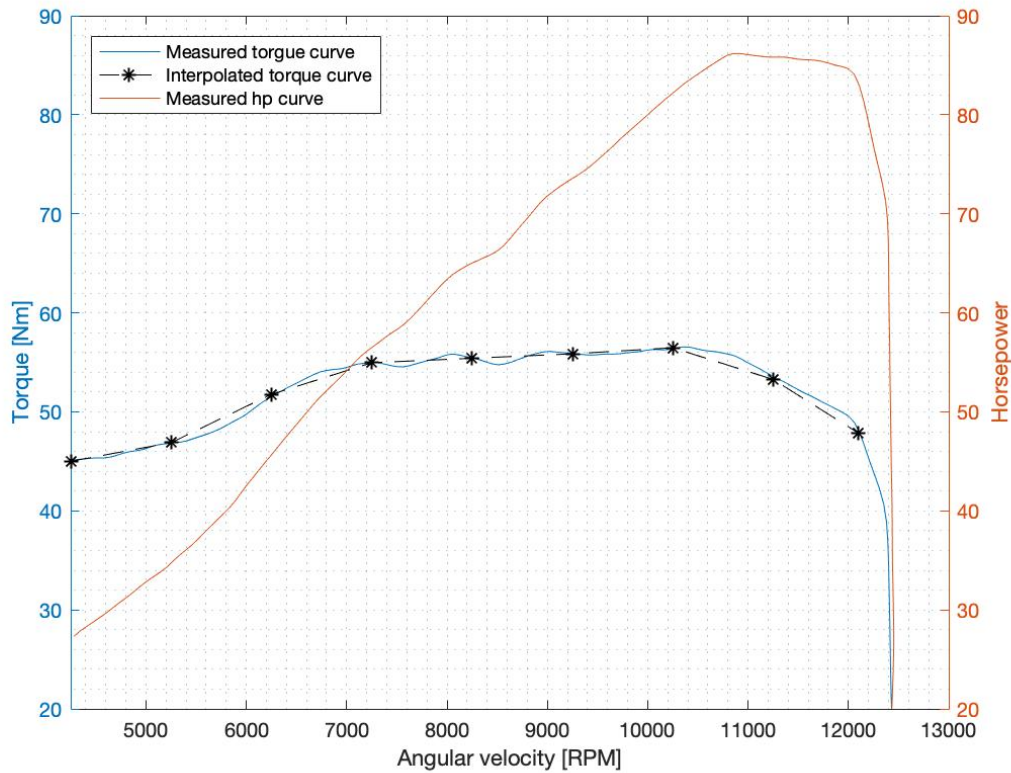
Figure 2.3: Plot of torque and horsepower given the angular velocity of the engine.

## 2.4   Drivetrain Model

A simple model of the drivetrain can be considered, where the torque from the engine goes to the gearbox, the final drive and then to the wheels. For simplicity, it is assumed there is no loss of torque in the drivetrain. Given the engine is placed above the rear shaft with no connection to the front wheels, this is considered reasonable.

The AAU Racing Team informed there is no clutch on the ARC and the gear shift are sequential. As the model does not account for a clutch and optimal gear change is not considered, no further investigation will be done to this part. However the different gear ratio and the Final Drive Ratio (FDR) is needed. In Table 2.1 are the provided gear ratio from AAU Racing Team.

| Gear: | Gear ratio [-] |
|:-----:|:--------------:|
| 1 | 2.67 |
| 2 | 1.94 |
| 3 | 1.61 |
| 4 | 1.41 |
| 5 | 1.26 |
| FDR | 6.99 |

Table 2.1: Table of gear and gear ratio.

## 2.5   Tire Model

Knowledge of the interaction between the tires and the road surface is importance to describe the dynamics of vehicles. If one do not consider the aerodynamic influence, only the contact between road and tire, have influence on the motion of the vehicle. All the forces is transmitted over a relative small sized patch known as the tire contact patch. The wheel is spinning about the axis, of the vehicle undercarriage and is fitted to the suspension. In general the wheels have three important properties, the absorption and the protection of vehicle components including the driver from impact loads, the transmission of acceleration and braking forces and the lateral forces during cornering [2].

Transmission of forces between tire and road surface is through the tire contact patch, which is formed due to the tire load in the contact area. The forces can be described through a single contact point as a function of position and velocity variables, relative to a wheel fixed coordinate system, where the velocity of the wheel center $v$ is comprised of a longitudinal component and a lateral component as seen in Fig. 2.4 [2].
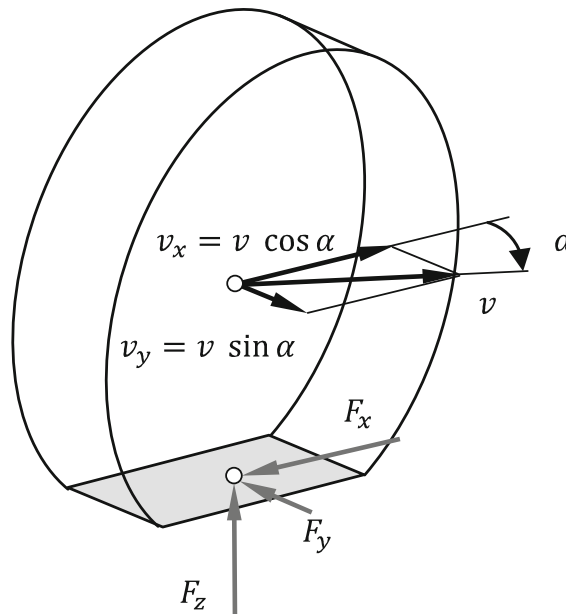


Figure 2.4: Contact forces of a tire [2].

Now considering longitudinal slip, which describes the state of motion of a driven, braked or rolling wheel. Assuming the wheel is a rigid body, the planar motion of the wheel can be described with the wheel radius $r$, the velocity of the wheel center $v$, the velocity of the wheel contact point $v_P$ and the angular velocity of the wheel $\omega$. Assuming an ideal rolling wheel, the velocity of the contact patch will vanish, which is not the case in reality, hence there will be always be a small slip. The deviation, relative to the wheel speed is known as the slip. In Fig. 2.5 the acceleration slip $s_A$ and the brake slip $s_B$ are illustrated. Here the value of the relative velocity of the tire contact point $P$ is given relative to the larger of the two values $v$ and $v_P$ [2].
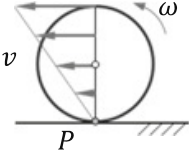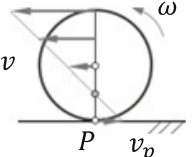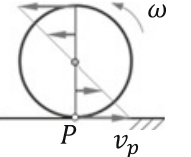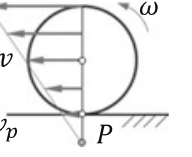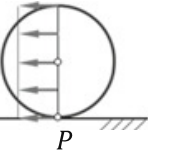
| $v = \omega r$ | $v < \omega r$ | | $v > \omega r$ | |
|---|---|---|---|---|
| Rolling wheel | Driven wheel | Spinning wheel | Braked wheel | Blocked wheel |
|  |  |  |  |  |
| No slip | Drive slip | | Brake slip | |
| $s_A = 0$ $\quad$ $s_B = 0$ | $s_A = \dfrac{v_P}{\omega r} = \dfrac{\omega r - v}{\omega r}$ | $s_A = 1$ | $s_B = \dfrac{v_P}{v} = \dfrac{v - \omega r}{v}$ | $s_B = 1$ |

Figure 2.5: Illustration of the acceleration slip $s_A$ and the brake slip $s_B$ of a tire, under different driving situation [2].

The slip is typically given in percentage, this guarantees that the value of the slip in the extreme conditions (spinning or blocked) is one. Note that motion at low velocities such as at startup can introduce fluctuation between acceleration slip and the brake slip [2].

Now considering a free rolling wheel with no longitudinal force but acted upon by a lateral force $F_y$ and therefore a velocity component, lateral to the rolling direction. The angle between the direction of motion of the tire center point and a vector, in the cross-sectional area of the wheel and parallel to the road, is known as the slip angle $\alpha$ and according to Fig. 2.4:

$$tan(\alpha) = \frac{v_y}{v_x} \tag{2.6a}$$

$$sin(\alpha) = \frac{v_y}{v} \tag{2.6b}$$

The variable $tan(\alpha)$ is known as the lateral slip and the angle $\alpha$ as the slip angle. For normal driving conditions $|\alpha| < 12 \ [deg]$, the lateral slip and the slip angle can be approximated to be the same [2].

Pure longitudinal or lateral forces can only be considered during straight line driving or cornering with a constant velocity. For general driving situations the longitudinal and the lateral slip occur simultaneously. However the resulting force must be less or equal to the maximum adhesion forces (the transition point between adhesion and sliding) according to the Coulomb's friction law. To consider the effects of both longitudinal and lateral slip during driving situations, one can define an absolute slip $s_a$ variable from the longitudinal $s$ and lateral $\alpha$ slip. [2]:

$$s_a = \sqrt{s^2 + \tan^2(\alpha)} \tag{2.7}$$

with the effect direction $\psi_a$ given by [2]:

$$\psi_a = arctan\left(\frac{\tan(\alpha)}{s}\right) \tag{2.8}$$

The (absolute) tire forces $F_{\psi_a}(s_a)$ in the direction of the given angle $\psi_a$ [2]:

$$F_{\psi_a}(s_a) = \sqrt{\frac{s^2 F_x^2(s_a) + \tan^2(\alpha) F_y^2(s_a)}{s_a^2}} \tag{2.9}$$

The resulting horizontal components of the tire force are then applied in the coordinate directions of the wheel carrier [2]:

$$\begin{bmatrix} F_{a,x} \\ F_{a,y} \end{bmatrix} = F_{\psi_a}(s_a) \begin{bmatrix} \cos(\psi_a) \\ \sin(\psi_a) \end{bmatrix} \tag{2.10}$$

Note that both acceleration slip brake slip must be evaluated for the front and rear wheel for (2.7) through (2.10), but only acceleration slip is shown.

AAU racing team have obtained tire data from The Formula SAE Tire Test Consortium (FSAE TTC) that has been measured at Calspan's Tire Research Facility. Plots of the longitudinal and lateral forces given the slip angle and slip ratio can be found in Appendix A.3.

Till now the assumption was that the tire were stationary or at least quasi stationary. Meaning the introduced parameters, such as the slip, slip angle and tire forces remain constant over time or small fluctuation. These conditions are typically not met for maneuvers, such as high steer angle jump, ABS-braking and ESP-intervention. Here the longitudinal slip and the slip angle change very fast with time. In these cases the tire forces build up with a time delay. The simplest case is a first order system. This way the longitudinal and lateral force can be approximated as [2]:

$$F_{x,stat} = T_x \frac{dF_x}{dt} + dF_x \tag{2.11}$$

$$F_{y,stat} = T_y \frac{dF_y}{dt} + dF_y \tag{2.12}$$

Where the time constants are:

$$T_x = \frac{c_{s,stat}}{c_{x,stat} v_x}, \quad T_{v,y} = \frac{c_{\alpha,stat}}{c_{y,stat} v_x} \tag{2.13}$$

Requiring the parameters, the longitudinal stiffness $c_{s,stat}$ and the cornering stiffness $c_{\alpha,stat}$ as well as the (static) tire longitudinal stiffness $c_{x,stat}$ and the (static) lateral stiffness $c_{y,stat}$:

$$c_{s,stat} = \left[ \frac{dF_x}{ds} \right]_{s=0}, \quad c_{\alpha,stat} = \left[ \frac{dF_x}{ds} \right]_{\alpha=0} \tag{2.14}$$

The inlet length $\sigma_s$ is the distance dependence of the tire forces. The inlet angle $\sigma_\alpha$ is the length the tires have to travel, to generate two thirds of the dynamic tire forces:

$$\sigma_s = \frac{c_{s,stat}}{c_{x,stat}}, \quad \sigma_\alpha = \frac{c_{\alpha,stat}}{c_{y,stat}} \tag{2.15}$$

According to [1], Typical run-in lengths for a passenger car are between 0.2 and 0.7 $[m]$, however the parameters $c_{x,stat}$ and $c_{y,stat}$ can be approximated for a chosen slip, given the function for the slopes of (2.14) are fund. Note that multiple inlet may be necessary to cover a larger region of the slip.

## 2.6   Reference frames

For this model the chassis is considered a rigid body, with two translational degrees of freedom $x_V$, $y_V$ and the rotation about the vertical axis $\psi_V$. The four wheel will be considered as one imaginary front and rear wheel (single track) with the indices $v$ and $h$ respectively and with contact points V and H, that are characterized by the wheel velocity and the tire forces for a given steering angle $\delta$ at the front axle.

An inertial reference frame $\boldsymbol{K}_E : \{\mathcal{O}_E; x_E, y_E, z_E\}$ is fixed to the ground. To describe the chassis's position and orientation, a vehicle-fixed reference frame $\boldsymbol{K}_V : \{\mathcal{O}_V; x_V, y_V, z_V\}$ placed in the center of mass $S$ of the vehicle, with the x-axis in the driving direction (see Fig. 2.6 and Fig. 2.7).
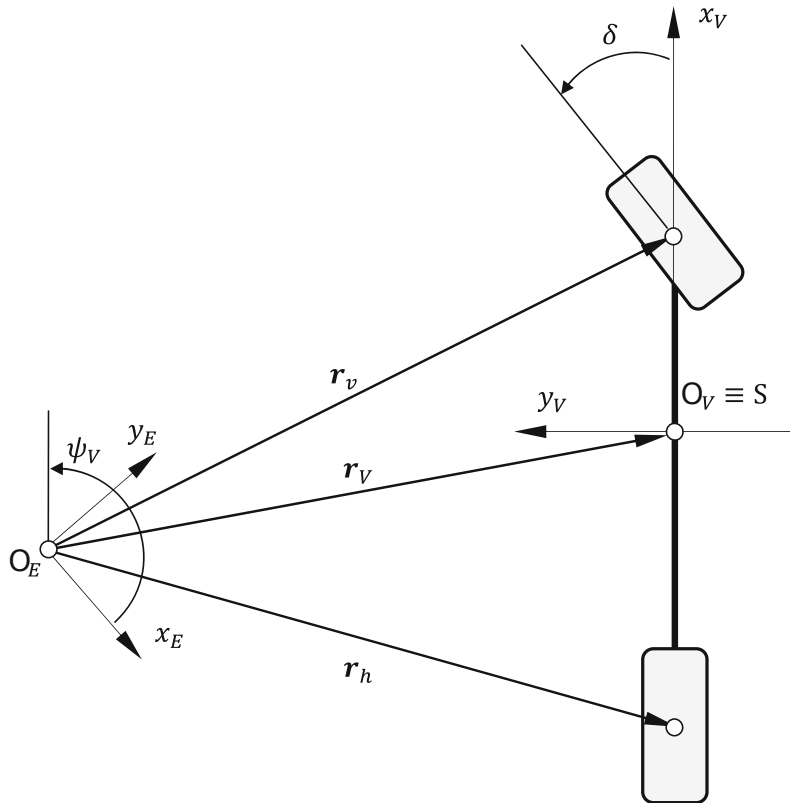


Figure 2.6: Top view of the nonlinear single track model, showing the reference frames [2].
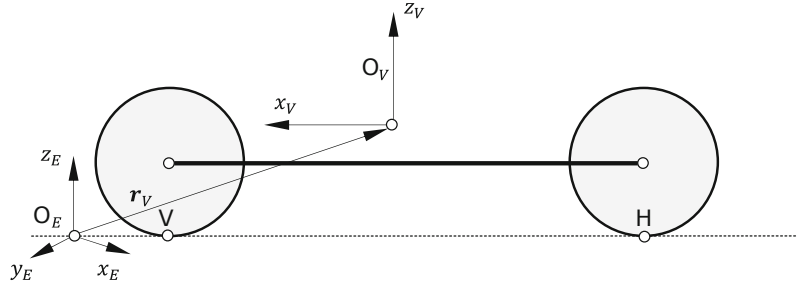
Figure 2.7: Side view of the nonlinear single track model, showing the reference frames [2].

## 2.7   Equations of motion

In this section, the equations of motion for the ARC will be described, with later sections adding different parts, leading to the final equations of motion. Based on Newton's laws of motion, the principle of linear momentum on the chassis can be considered [2]:

$$m\ddot{\boldsymbol{r}}_V = \boldsymbol{F}_v + \boldsymbol{F}_h + \boldsymbol{F}_W + \boldsymbol{F}_G \tag{2.16}$$

Where $m$ is the mass of the vehicle. $\ddot{\boldsymbol{r}}_V$ is acceleration of the vehicle, obtained from the position vector $\boldsymbol{r}_V$ to the center of gravity $S$ of the vehicle in the inertial frame $\boldsymbol{K}_E$, by differentiation with respect to time:

$$\boldsymbol{r}_V = \begin{bmatrix} x_V \\ y_V \\ h_S \end{bmatrix}, \dot{\boldsymbol{r}}_V = \begin{bmatrix} \dot{x}_V \\ \dot{y}_V \\ 0 \end{bmatrix}, \ddot{\boldsymbol{r}}_V = \begin{bmatrix} \ddot{x}_V \\ \ddot{y}_V \\ 0 \end{bmatrix} \tag{2.17}$$

Were $h_S$ is the distance from the ground to the center of mass. $\boldsymbol{F}_v$ and $\boldsymbol{F}_h$ are the forces on the front and rear wheel and $\boldsymbol{F}_G$ is the gravitational force, in the inertial frame $\boldsymbol{K}_E$:

$$\boldsymbol{F}_v = \begin{bmatrix} F_{v,x} \\ F_{v,y} \\ F_{v,z} \end{bmatrix}, \boldsymbol{F}_h = \begin{bmatrix} F_{h,x} \\ F_{h,y} \\ F_{h,z} \end{bmatrix}, \boldsymbol{F}_G = \begin{bmatrix} 0 \\ 0 \\ -mg \end{bmatrix}, \tag{2.18}$$

$\boldsymbol{F}_W$ is the air resistance, interaction on the vehicle as an external force, where the air flow is opposite to the trajectory of the vehicle that is given as [2]:

$$\boldsymbol{F}_W = \frac{1}{2} c_w \rho_L A \dot{\boldsymbol{r}}_V |\dot{\boldsymbol{r}}_V| \tag{2.19a}$$

$$\boldsymbol{F}_W = \begin{bmatrix} F_{W,x} \\ F_{W,y} \\ 0 \end{bmatrix} \tag{2.19b}$$

$$\boldsymbol{F}_W = \begin{bmatrix} \frac{1}{2} c_w \rho_L A \dot{x}_V \sqrt{\dot{x}_V^2 + \dot{y}_V^2} \\ \frac{1}{2} c_w \rho_L A \dot{y}_V \sqrt{\dot{x}_V^2 + \dot{y}_V^2} \\ 0 \end{bmatrix} \tag{2.19c}$$

Where $c_w$ is the air resistance coefficient, $\rho_L$ is the air density and $A$ is the front surface of the vehicle. The complete principle of linear momentum in the inertial frame $\boldsymbol{K}_E$ using equation (2.16) to (2.19) is then:

$$
\begin{bmatrix} m\ddot{x}_V \\ m\ddot{y}_V \\ 0 \end{bmatrix} = \begin{bmatrix} F_{v,x} + F_{h,x} - F_{W,x} \\ F_{v,y} + F_{h,y} - F_{W,y} \\ F_{v,z} + F_{h,z} - mg \end{bmatrix}
\tag{2.20}
$$

Adding the forces described above to the reference frames figures, gives Fig. 2.8 and Fig. 2.9. It should be note the figures also include additional vectors and parameters that will be induced later. Note that $\beta$ is the slip angle at center mass.
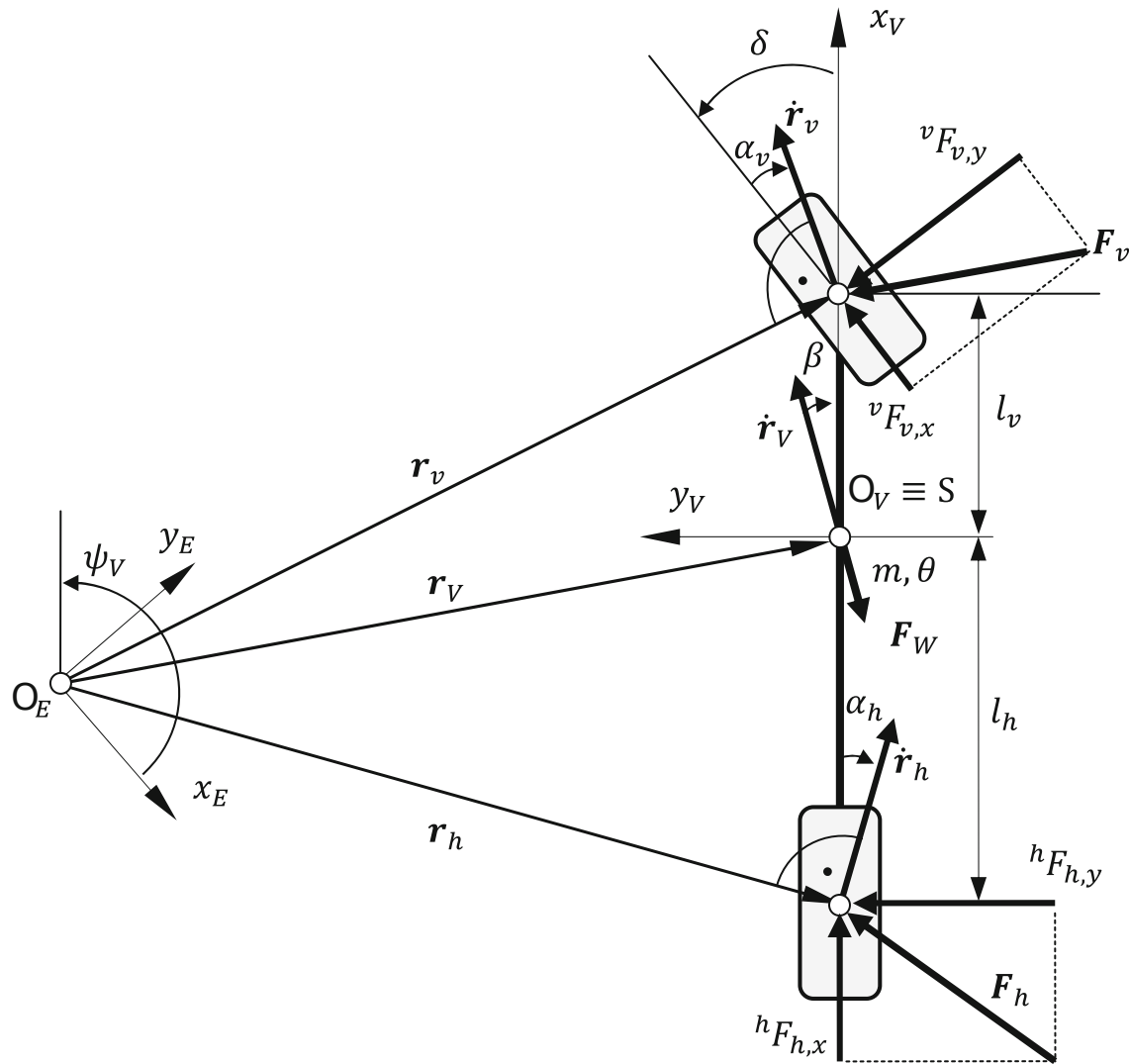


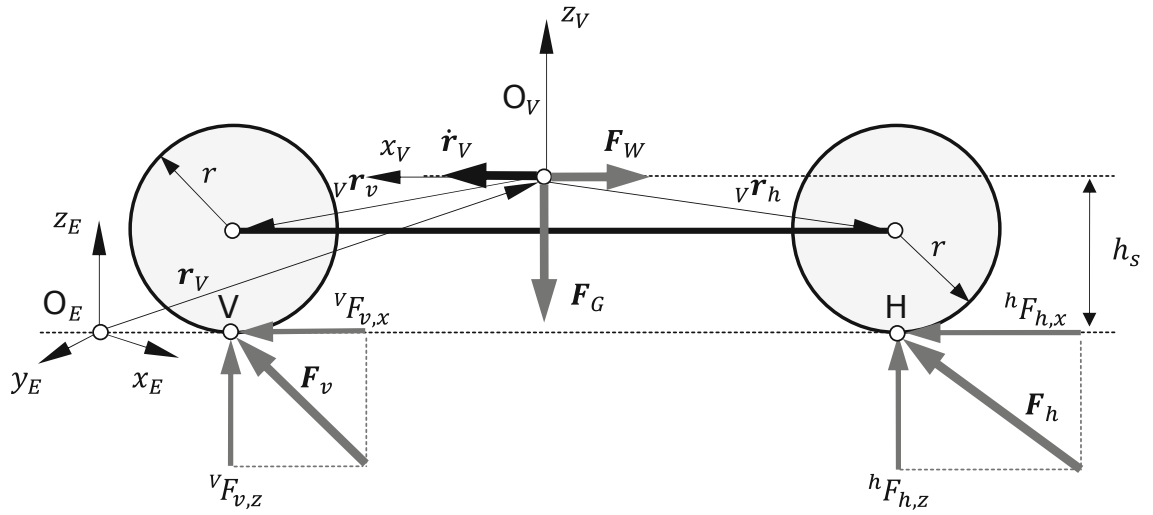Figure 2.8: Top view of the nonlinear single track model [2].

Figure 2.9: Side view of the nonlinear single track model [2].

Similarly to linear momentum the principle of angular momentum of the vehicle with respect to its center of gravity can be found in the general form as [2]:

$$\mathbf{\Theta}_V \dot{\boldsymbol{\omega}}_V + \boldsymbol{\omega}_V \times (\mathbf{\Theta}_V \cdot \boldsymbol{\omega}_V) = {}_V\boldsymbol{r}_v \times \boldsymbol{F}_v + {}_V\boldsymbol{r}_h \times \boldsymbol{F}_h \tag{2.21}$$

Were $\mathbf{\Theta}_V$ is the moment of inertia in the vehicle frame $\boldsymbol{K}_V$:

$$\mathbf{\Theta}_V = \begin{bmatrix} 0 & 0 & 0 \\ 0 & 0 & 0 \\ 0 & 0 & \theta_{zz} \end{bmatrix} \tag{2.22}$$

With ${}^V\boldsymbol{\omega}_v$ and ${}^V\dot{\boldsymbol{\omega}}_v$, as the angular velocity and acceleration:

$$ {}^V\boldsymbol{\omega}_V = \begin{bmatrix} 0 \\ 0 \\ \dot{\psi}_V \end{bmatrix} , {}^V\dot{\boldsymbol{\omega}}_V = \begin{bmatrix} 0 \\ 0 \\ \ddot{\psi}_V \end{bmatrix} \tag{2.23}$$

${}^V_V\boldsymbol{r}_v$ and ${}^V_V\boldsymbol{r}_h$ is the points of application of the tire forces on the surface:

$$ {}^V_V\boldsymbol{r}_v = \begin{bmatrix} l_v \\ 0 \\ -h_s \end{bmatrix} , {}^V_V\boldsymbol{r}_h = \begin{bmatrix} -l_h \\ 0 \\ -h_s \end{bmatrix} \tag{2.24}$$

Bye simplifying (2.21) one can obtain [2]:

$$\theta_{zz}\ddot{\psi}_V = l_v {}^VF_{v,y} - l_h {}^VF_{h,y} \tag{2.25}$$

Note that a lower left index denotes the reference body or the reference coordinate system while the coordinate system is indicated by a left upper index.

### 2.7.1  Tire Forces

For evaluation of (2.20) and (2.25), it is necessary to find the tire forces in the wheel fixed coordinate system. The tire is initially stationary and linear with respect to cornering stiffness and slip variables $c_{s,v/h}$, $c_{\alpha,v/h}$ and $s_{v/h}$, $\alpha_{v/h}$ respectively [2]:

$$
\begin{bmatrix} {}^v F_{v,x,stat} \\ {}^v F_{v,y,stat} \end{bmatrix} = \begin{bmatrix} c_{s,v} s_v \\ c_{\alpha,v} \alpha_v \end{bmatrix}, \begin{bmatrix} {}^h F_{h,x,stat} \\ {}^h F_{h,y,stat} \end{bmatrix} = \begin{bmatrix} c_{s,h} s_h \\ c_{\alpha,h} \alpha_h \end{bmatrix}
\tag{2.26}
$$

An alternative to (2.26) that is more detailed when considering higher lateral accelerations, is based on a simplified version of the Magic Formula mentioned in Appendix A.3, that includes friction coefficient, tire parameters and variable tire loads. Since data for the tires is available through AAU Racing Team it is convenient to apply it instead in the model.

For calculation of the slip variables, the velocity of the wheel center point is needed. This is represented in the inertial frame $\boldsymbol{K}_E$ for the front and rear tire respectively as [2]:

$$
\dot{\boldsymbol{r}}_v = \dot{\boldsymbol{r}}_V + \boldsymbol{\omega}_V \times \boldsymbol{T}_V(\psi_V) {}^V_V \boldsymbol{r}_v
\tag{2.27a}
$$

$$
\dot{\boldsymbol{r}}_v = \begin{bmatrix} \dot{x}_V \\ \dot{y}_V \\ 0 \end{bmatrix} + \begin{bmatrix} 0 \\ 0 \\ \dot{\psi}_V \end{bmatrix} \times \begin{bmatrix} \cos(\psi_V) & -\sin(\psi_V) & 0 \\ \sin(\psi_V) & \cos(\psi_V) & 0 \\ 0 & 0 & 1 \end{bmatrix} \begin{bmatrix} l_v \\ 0 \\ -(h_s - r) \end{bmatrix}
\tag{2.27b}
$$

$$
\dot{\boldsymbol{r}}_v = \begin{bmatrix} \dot{x}_v \\ \dot{y}_v \\ \dot{z}_v \end{bmatrix} = \begin{bmatrix} \dot{x}_v - l_v \dot{\psi}_V \sin(\psi_V) \\ \dot{y}_v + l_v \dot{\psi}_V \cos(\psi_V) \\ 0 \end{bmatrix}
\tag{2.27c}
$$

$$
\dot{\boldsymbol{r}}_h = \dot{\boldsymbol{r}}_V + \boldsymbol{\omega}_V \times \boldsymbol{T}_V(\psi_V) {}^V_V \boldsymbol{r}_h
\tag{2.28a}
$$

$$
\dot{\boldsymbol{r}}_h = \begin{bmatrix} \dot{x}_V \\ \dot{y}_V \\ 0 \end{bmatrix} + \begin{bmatrix} 0 \\ 0 \\ \dot{\psi}_V \end{bmatrix} \times \begin{bmatrix} \cos(\psi_V) & -\sin(\psi_V) & 0 \\ \sin(\psi_V) & \cos(\psi_V) & 0 \\ 0 & 0 & 1 \end{bmatrix} \begin{bmatrix} -l_h \\ 0 \\ -(h_s - r) \end{bmatrix}
\tag{2.28b}
$$

$$
\dot{\boldsymbol{r}}_h = \begin{bmatrix} \dot{x}_h \\ \dot{y}_h \\ \dot{z}_h \end{bmatrix} = \begin{bmatrix} \dot{x}_v + l_v \dot{\psi}_V \sin(\psi_V) \\ \dot{y}_v - l_v \dot{\psi}_V \cos(\psi_V) \\ 0 \end{bmatrix}
\tag{2.28c}
$$

Where $\boldsymbol{T}_V(\psi_V)$ is a transformation matrix around $\psi_V$. To calculate the slip values, the velocities are however required in the wheel fixed coordinate system $\boldsymbol{K}_W$. By consider the rotation of the wheels with respect to the vehicle frame $\boldsymbol{K}_V$ [2]:

$$
{}^v \dot{\boldsymbol{r}}_v = \begin{bmatrix} {}^v \dot{x}_v \\ {}^v \dot{y}_v \\ {}^v \dot{z}_v \end{bmatrix} = {}^v \boldsymbol{T}_E \dot{\boldsymbol{r}}_v
\tag{2.29a}
$$

$$
{}^v \dot{\boldsymbol{r}}_v = \begin{bmatrix} \cos(\psi_V + \delta) & \sin(\psi_V + \delta) & 0 \\ -\sin(\psi_V + \delta) & \cos(\psi_V + \delta) & 0 \\ 0 & 0 & 1 \end{bmatrix} \begin{bmatrix} \dot{x}_v \\ \dot{y}_v \\ \dot{z}_v \end{bmatrix}
\tag{2.29b}
$$

$$^h\dot{\boldsymbol{r}}_h = \begin{bmatrix} ^h\dot{x}_h \\ ^h\dot{y}_h \\ ^h\dot{z}_h \end{bmatrix} = {}^h\boldsymbol{T}_E\dot{r}_h \tag{2.30a}$$

$$^h\dot{\boldsymbol{r}}_h = \begin{bmatrix} \cos(\psi_V) & \sin(\psi_V) & 0 \\ -\sin(\psi_V) & \cos(\psi_V) & 0 \\ 0 & 0 & 1 \end{bmatrix} \begin{bmatrix} \dot{x}_h \\ \dot{y}_h \\ \dot{z}_h \end{bmatrix} \tag{2.30b}$$

With the components of the velocity vector from above, subtracting the rolling velocity $r\dot{\rho}_v$ and normalizing, the longitudinal and lateral slips at the front axle, the following can be obtained [2]:

$$s_v = \frac{r\dot{\rho}_v - {}^v\dot{x}_v}{max\left(|r\dot{\rho}_v|, |{}^v\dot{x}_v|\right)} \tag{2.31}$$

$$\alpha_v = -\frac{{}^v\dot{y}_v}{|r\dot{\rho}_v|} \tag{2.32}$$

where the index $v$ is front axle, $r$ is the wheel radius, $\dot{\rho}_v$ is the angular velocity of the wheel and ${}^v\dot{x}_v$ and ${}^v\dot{y}_v$ is the velocity of the wheel center point. As described in Sec. 2.5, the normalized total slip, the direction of action of the slip and the resulting tire forces are:

$$s_{v,a} = \sqrt{s_v^2 + \tan^2(\alpha_v)} \tag{2.33}$$

$$\psi_v = atan\left(\frac{\alpha_v}{s_v}\right) \tag{2.34}$$

$$F_{\psi_v}(s_{v,a}) = \sqrt{\frac{s_v^2 F_{v,x,stat}^2 + \alpha_v^2 F_{v,y,stat}^2}{s_{v,a}^2}} \tag{2.35}$$

Then, the tire forces in the wheel fixed coordinate system are [2]:

$$\begin{bmatrix} ^vF_{v,x,stat} \\ ^vF_{v,y,stat} \end{bmatrix} = F_{\psi_v}(s_{v,a}) \begin{bmatrix} \cos(\psi_V) \\ \sin(\psi_V) \end{bmatrix} \tag{2.36a}$$

$$\begin{bmatrix} ^vF_{v,x,stat} \\ ^vF_{v,y,stat} \end{bmatrix} = \frac{1}{s_{v,a}} F_{\psi_v}(s_{v,a}) \begin{bmatrix} s_v \\ \alpha_v \end{bmatrix} \tag{2.36b}$$

For the rear axle, the index $v$ is replaced with $h$. When considering changes for course or velocity, a suitable time delay constant $T_{v,x}$ and $T_{v,y}$ can be chosen to represent the first order response of the system [2]:

$$\begin{bmatrix} {}^v\dot{F}_{v,x} \\ {}^v\dot{F}_{v,y} \end{bmatrix} = \begin{bmatrix} \frac{1}{T_{v,x}} & 0 \\ 0 & \frac{1}{T_{v,y}} \end{bmatrix} \left( \begin{bmatrix} {}^vF_{v,x,stat} \\ {}^vF_{v,y,stat} \end{bmatrix} - \begin{bmatrix} {}^vF_{v,x} \\ {}^vF_{v,y} \end{bmatrix} \right) \tag{2.37a}$$

$$\begin{bmatrix} {}^v\dot{F}_{v,x} \\ {}^v\dot{F}_{v,y} \end{bmatrix} = \begin{bmatrix} \frac{c_{v,x,stat}|r\dot{\rho}_v|}{c_{v,s,stat}} & 0 \\ 0 & \frac{c_{v,y,stat}|r\dot{\rho}_v|}{c_{v,\alpha,stat}} \end{bmatrix} \left( \begin{bmatrix} {}^vF_{v,x,stat} \\ {}^vF_{v,y,stat} \end{bmatrix} - \begin{bmatrix} {}^vF_{v,x} \\ {}^vF_{v,y} \end{bmatrix} \right) \tag{2.37b}$$

where:

$$\frac{1}{T_{v,x}} = \frac{c_{v,x,stat}|r\dot{\rho}_v|}{c_{v,s,stat}}, \frac{1}{T_{v,y}} = \frac{c_{v,y,stat}|r\dot{\rho}_v|}{c_{v,\alpha,stat}} \tag{2.38}$$

To determine the tire loads required to evaluate previous equation the normal forces of the tires at the front and the rear are [2]:

$$^V F_{v,z} = \frac{l_v}{l}mg \tag{2.39a}$$

$$^V F_{h,z} = \frac{l_h}{l}mg \tag{2.39b}$$

The principle of momentum conservation at the front and the rear wheel with respect to the wheel center is then [2]:

$$\theta_v\ddot{\rho}_v = M_{A,v} - sign\left(\dot{\rho}_v\right)M_{B,v} - r^v F_{v,x} \tag{2.40a}$$

$$\theta_h\ddot{\rho}_h = M_{A,h} - sign\left(\dot{\rho}_h\right)M_{B,h} - r^h F_{h,x} \tag{2.40b}$$

Where $\theta$ is the moment of inertia. $\ddot{\rho}$ and $\dot{\rho}$ is the angular acceleration and velocity of the wheel. $M_A$ and $M_B$ is driving and brake torques for front and rear axle.

### 2.7.2   Driving Torques

A simple model of the driving torques distribution between the front and the rear axle $M_{A,v}$ and $M_{A,h}$ respectively, using a dimensionless factor $0 \le \xi_a \le 1$ can be described as [2]:

$$M_{A,v} = (1 - \xi_a)M_A = M_A - M_{A,h} \tag{2.41a}$$

$$M_{A,h} = \xi_a M_A \tag{2.41b}$$

Where $\xi_a = 0$ and $\xi_a = 1$ represent front and rear wheel drive respectively. Calculating the driving torque $M_A$ requires an approximation of the engine speed [2]:

$$\omega_M = i_D i_G(G)((1 - \xi_a)\dot{\rho}_v + \xi_a\dot{\rho}_h) \tag{2.42}$$

Where the drivetrain parameters $i_D$ and $i_G$ represent the transmission and the gearbox respectively and the selected gear is $G$. The total driving torque is interpolated from engine torque characteristic curve $M_M$ based on engine speed $\omega_M$ and acceleration pedal position $0 \leq P_F \leq 1$ [2]:

$$M_A = i_D i_G(G) M_M(\omega_M, p_F) \tag{2.43}$$

Similarly the brake torques are calculated as [2]:

$$M_{B,v} = (1 - \xi_b) M_B(p_B) = M_B(p_B) - M_{B,h} \tag{2.44a}$$
$$M_{B,h} = \xi_b M_B(p_B) \tag{2.44b}$$

Where $0 \leq \xi_b \leq 1$ is a dimensionless distribution parameter and $0 \leq P_B \leq 1$ is the brake pedal position.

### 2.7.3 Final Equations of Motion

From the past sections the complete set of equations of motion for the nonlinear single track model can be listed. First the Principle of conservation of linear momentum [2]:

$$\begin{bmatrix} m\ddot{x}_V \\ m\ddot{y}_V \end{bmatrix} = \begin{bmatrix} F_{v,x} + F_{h,x} - F_{W,x} \\ F_{v,y} + F_{h,y} - F_{W,y} \end{bmatrix} \tag{2.45}$$

Where:

$$F_{W,x} = \frac{1}{2} c_w \rho_L A \dot{x}_V \sqrt{\dot{x}_V^2 + \dot{y}_V^2} \tag{2.46a}$$
$$F_{W,y} = \frac{1}{2} c_w \rho_L A \dot{y}_V \sqrt{\dot{x}_V^2 + \dot{y}_V^2} \tag{2.46b}$$

$$F_{v,x} = \cos(\psi_V + \delta)\,{}^v F_{v,x} - \sin(\psi_V + \delta)\,{}^v F_{v,y} \tag{2.47a}$$
$$F_{v,y} = \sin(\psi_V + \delta)\,{}^v F_{v,x} + \cos(\psi_V + \delta)\,{}^v F_{v,y} \tag{2.47b}$$

$$F_{h,x} = \cos(\psi_V)\,{}^h F_{h,x} - \sin(\psi_V)\,{}^h F_{h,y} \tag{2.48a}$$
$$F_{h,y} = \sin(\psi_V)\,{}^h F_{h,x} + \cos(\psi_V)\,{}^h F_{h,y} \tag{2.48b}$$

Second the Principle of conservation of the angular momentum for the chassis in the vehicle fixed coordinate system [2]:

$$\theta_{zz} \ddot{\psi}_V = l_v{}^V F_{v,y} - l_h{}^V F_{h,y} \tag{2.49}$$

Where:

$$^V F_{v,y} = \sin(\delta)\,^v F_{v,x} + \cos(\delta)\,^v F_{v,y} \tag{2.50a}$$

$$^V F_{h,y} = {}^h F_{h,y} \tag{2.50b}$$

Last the Principle of conservation of the angular momentum for the front and rear axle [2]:

$$\theta_v \ddot{\rho}_v = M_{A,v} - M_{B,v}\,sign\,(\dot{\rho}_v) - r\,^v F_{v,x} \tag{2.51a}$$

$$\theta_h \ddot{\rho}_h = M_{A,h} - M_{B,h}\,sign\,(\dot{\rho}_h) - r\,^h F_{h,x} \tag{2.51b}$$

With the Dynamic tire forces [2]:

$$\begin{bmatrix} ^v\dot{F}_{v,x} \\ ^v\dot{F}_{v,x} \end{bmatrix} = \begin{bmatrix} \frac{c_{v,x,stat}|r\dot{\rho}_v|}{c_{v,s,stat}} & 0 \\ 0 & \frac{c_{v,y,stat}|r\dot{\rho}_v|}{c_{v,\alpha,stat}} \end{bmatrix} \left( \begin{bmatrix} ^v F_{v,x,stat} \\ ^v F_{v,y,stat} \end{bmatrix} - \begin{bmatrix} ^v F_{v,x} \\ ^v F_{v,y} \end{bmatrix} \right) \tag{2.52}$$

$$\begin{bmatrix} ^h\dot{F}_{h,x} \\ ^h\dot{F}_{h,y} \end{bmatrix} = \begin{bmatrix} \frac{c_{h,x,stat}|r\dot{\rho}_h|}{c_{h,s,stat}} & 0 \\ 0 & \frac{c_{h,y,stat}|r\dot{\rho}_h|}{c_{h,\alpha,stat}} \end{bmatrix} \left( \begin{bmatrix} ^h F_{h,x,stat} \\ ^h F_{h,y,stat} \end{bmatrix} - \begin{bmatrix} ^h F_{h,x} \\ ^h F_{h,y} \end{bmatrix} \right) \tag{2.53}$$

The equations of motion can then be transferred into the state space form:

$$\dot{\boldsymbol{x}} = \boldsymbol{f}(\boldsymbol{x}, t, \boldsymbol{u}) \tag{2.54}$$

Where the state vector and input vector is [2]:

$$\boldsymbol{x} = \left[ x_V, y_V, \psi_V, \dot{x}_V, \dot{y}_V, \dot{\psi}_V, \dot{\rho}_v, \dot{\rho}_h, {}^v F_{v,x}, {}^v F_{v,y}, {}^h F_{h,x}, {}^h F_{h,y} \right]^T \tag{2.55a}$$

$$\boldsymbol{u} = [\delta_H, p_F, p_B, G]^T \tag{2.55b}$$

$$\begin{bmatrix} \dot{x}_V \\ \dot{y}_V \\ \dot{\psi}_V \\ \ddot{x}_V \\ \ddot{y}_V \\ \ddot{\psi}_V \\ \ddot{\rho}_v \\ \ddot{\rho}_h \\ ^V\dot{F}_{v,x} \\ ^V\dot{F}_{v,y} \\ ^V\dot{F}_{h,x} \\ ^V\dot{F}_{h,y} \end{bmatrix} = \begin{bmatrix} \dot{x}_V \\ \dot{y}_V \\ \dot{\psi}_V \\ \frac{1}{m}(F_{v,x} + F_{h,x} - F_{W,x}) \\ \frac{1}{m}(F_{v,y} + F_{h,y} - F_{W,y}) \\ \frac{1}{\theta_{zz}}(l_v\,^V F_{v,y} - l_h\,^V F_{h,y}) \\ \frac{1}{\theta_v}(M_{A,v} - M_{B,v}\,sign\,(\dot{\rho}_v) - r\,^v F_{v,x}) \\ \frac{1}{\theta_h}(M_{A,h} - M_{B,h}\,sign\,(\dot{\rho}_h) - r\,^h F_{h,x}) \\ \frac{c_{v,x,stat}|r\dot{\rho}_v|}{c_{v,s,stat}}\,(^v F_{v,x,stat} - {}^v F_{v,x}) \\ \frac{c_{v,y,stat}|r\dot{\rho}_v|}{c_{v,\alpha,stat}}\,(^v F_{v,y,stat} - {}^v F_{v,y}) \\ \frac{c_{h,x,stat}|r\dot{\rho}_h|}{c_{h,s,stat}}\,(^h F_{h,x,stat} - {}^h F_{h,x}) \\ \frac{c_{h,y,stat}|r\dot{\rho}_h|}{c_{h,\alpha,stat}}\,(^h F_{h,y,stat} - {}^h F_{h,y}) \end{bmatrix} \tag{2.56}$$

## 2.8   Model Verification

Having established the equation of motion, it is possible to implement the model in Simulink. The implementation is described in further detail in Appendix A.1, including figures of the implemented subsystems. For verification of the model, the acceleration, velocity and position achieved after a step applied to the model is first considered. As the G8 car can reach 100 $[km/h]$ or 27.78 $[m/s]$ within 5 $[s]$, it is possible to calculate the acceleration and distance the model should reach.

The acceleration $a$, is given by the initial/final velocity and time, which can be formulated as:

$$a = \frac{\Delta v}{\Delta t} \tag{2.57}$$

where $v$ here is velocity and $t$ is time. The distance $d$ can then be found as:

$$d = \frac{1}{2}at^2 \tag{2.58}$$

From equation (2.57) and (2.58) the acceleration and distance is 5.56 $[m/s^2]$ and 69.44 $[m]$ respectively. In Fig. 2.10 and Fig. 2.11, a plot before and after tuning simulated over 60 and 10 $[s]$ respectively can be seen. This represent the output from a step applied to the model. Note that only first gear is considered for now and a step is 100 $[\%]$ of the accelerator.
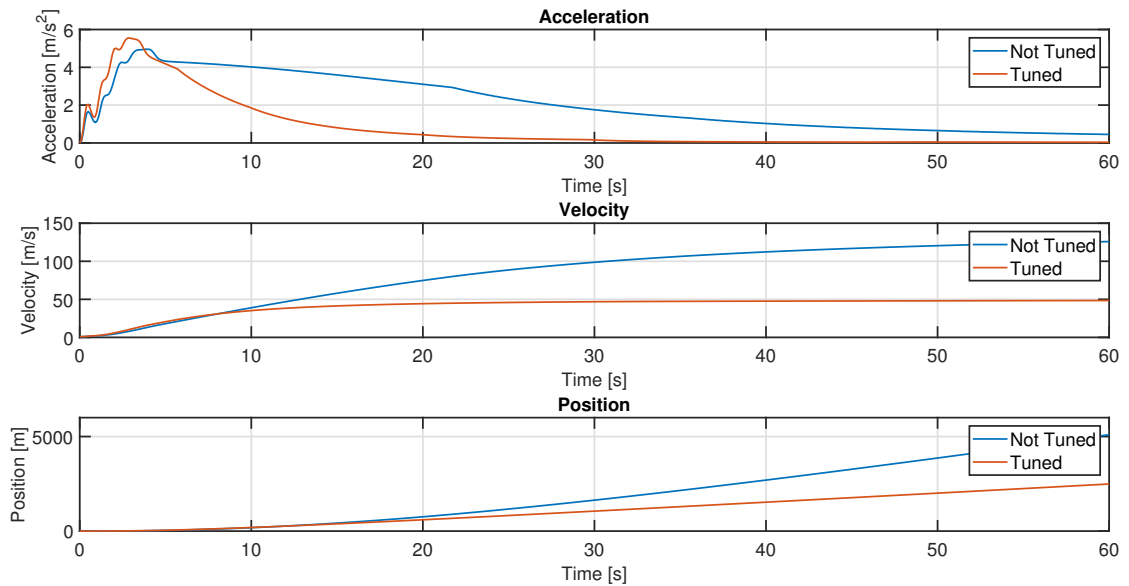


Figure 2.10: Plot of acceleration, velocity and position from a step applied to the Simulink model, before and after tuning.

Before any tuning to the model, the acceleration was found to peek at approximately 5 $[m/s^2]$ (after 4 $[s]$ of simulation) from the plot and thereby the 27.78 $[m/s]$ is first reached at approximately 7.3 $[s]$. Furthermore it can be observed that the acceleration is not a soft

curve between zero and four seconds, which will be discussed later in this section. The maximum velocity achieved is above the known top speed of 170 $[km/h]$ or 47.22 $[m/s]$ for the car. Since it is the aerodynamic drag that have the most influence at high speed, it is possible to tune the air resistance coefficient $c_W$ and the cross-sectional area $A$, to adjust the model. The $c_W$ is 0.2 for a car, 0.6 for a motorcycle and 1 for a truck according to [2]. Selecting a $c_W$ of 1 and adding 0.75 $[m^2]$ to the cross-sectional area results in a 49 $[m/s]$ top speed for the model. Note that the addition to the cross-sectional area changes it from 1.054 $[m^2]$ to 1.804 $[m^2]$ which is significantly larger. This could partially be due to use of simple shapes for approximation of the cross-sectional area and un-modeled dynamics. It should also be mentioned that change in gear would affect the amount of torque available for the vehicle and therefore a lower top speed.
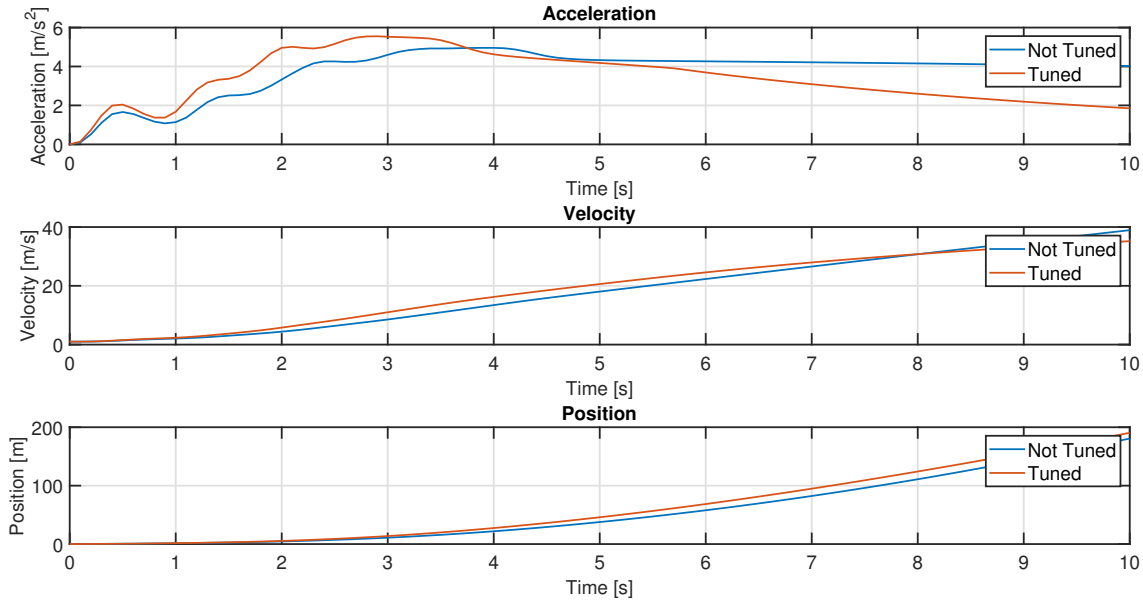


Figure 2.11: Plot of acceleration, velocity and position from a step applied to the Simulink model, before and after tuning.

The acceleration can be tuned by adjusting the inertia for the wheels from 33.36 $[kg \cdot m^2]$, obtained from SolidWorks, to 26 $[kg \cdot m^2]$. Thereby the the acceleration become 5.55 $[m/s^2]$. The velocity of 27.78 $[m/s]$ after tuning is reached at approximately 7 $[s]$ with a distance of 94.82 $[m]$, which is relatively close to the dynamic of the vehicle based on the acceleration. The non soft curve of acceleration, indicates that the velocity of the chassis is relatively faster than the wheels. This leads to a smaller slip and therefore less force will be applied to the chassis. This originates from the method of approximating the torque of the engine with the velocity of the wheels.

It is important that sufficient torque from the engine is applied to the wheels relative early, otherwise the subtracted torque of the slip, can in worst case cause the velocity of the wheel to become negative, failing the simulation. It should be noted that the maximum torque from engine is approximately 1000 $[Nm]$, but at max RPM it is approximately 900 $[Nm]$. Also it should be mentioned that as the vehicle approach the top speed, the velocity of the wheels continuous to rise, thereby the slip value will approach one over time. This is because the wheels and the frame is considered two parts in this model, where aerodynamic force is not applied to the wheels.

Plotting the torque, the difference of velocity between chassis and wheel and the slip can be seen in Fig. 2.12. Note at relative low velocity difference, between chassis and wheel

(between zero and one second) induces oscillatory behavior for the slip, which leads to a slow change of torque over time. Finally a plot of the torque, the acceleration and the slip, were a gear change from first to fifth gear is applied three seconds into the simulation, can be seen in Fig. 2.13. Note the drop in torque and the slowly increasing slip after the gear change. Over time the slip will settle around 0.25 instead of 1 as the difference of velocity between frame and wheel remain relative small, because of less torque applied to the wheel.
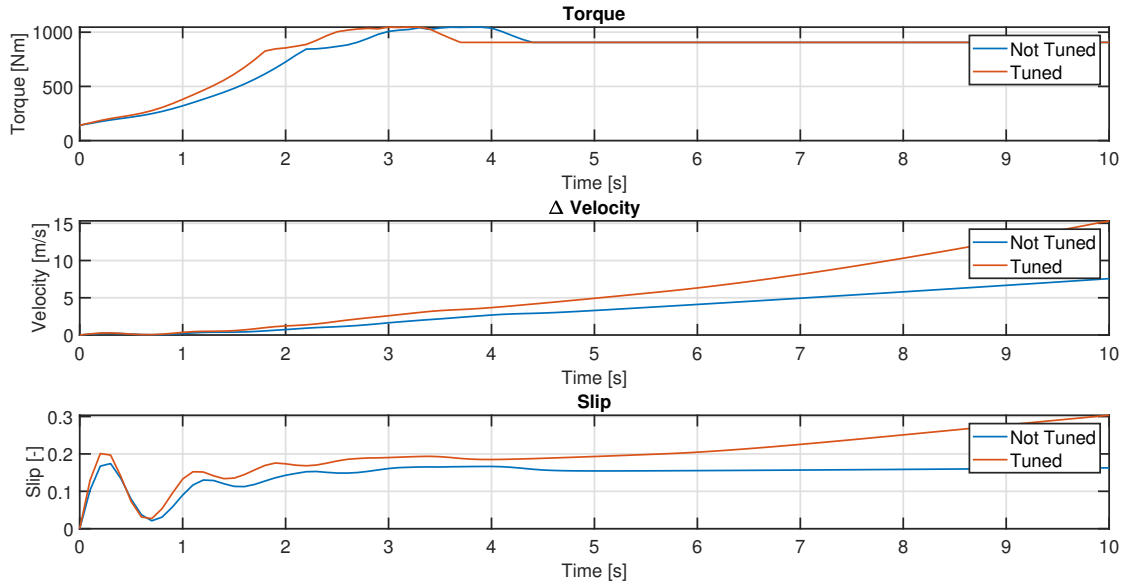


Figure 2.12: Plot of torque, velocity difference between chassis and wheel and slip from a step applied to the Simulink model, before and after tuning.
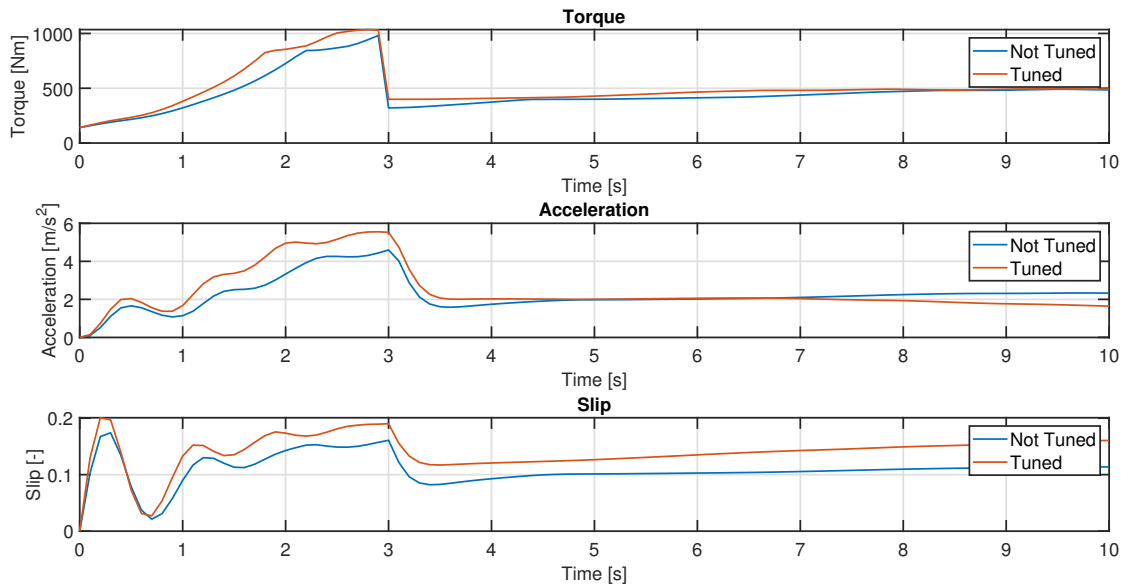


Figure 2.13: Plot of engine velocity, acceleration and slip from step applied to the Simulink model, before and after tuning. A gear change from first to fifth gear is applied three seconds into the simulation.

For lateral consideration the vehicle is driving at 10 $[m/s]$ plus/minus 0.1 $[m/s]$ and a step to the steering is applied at the start of the simulation (at time zero), where a positive

value causes the vehicle to turn left and a negative value causes a turn right. A maximum steering of 0.786 [*rad*] or 45 [*deg*] angle is used, although it assumed to be smaller for a race car. Plots of left and right turn from 10 to 100 [%], can be seen on Fig. 2.14 and Fig. 2.15. Note that negative signs are implied for a right turn.
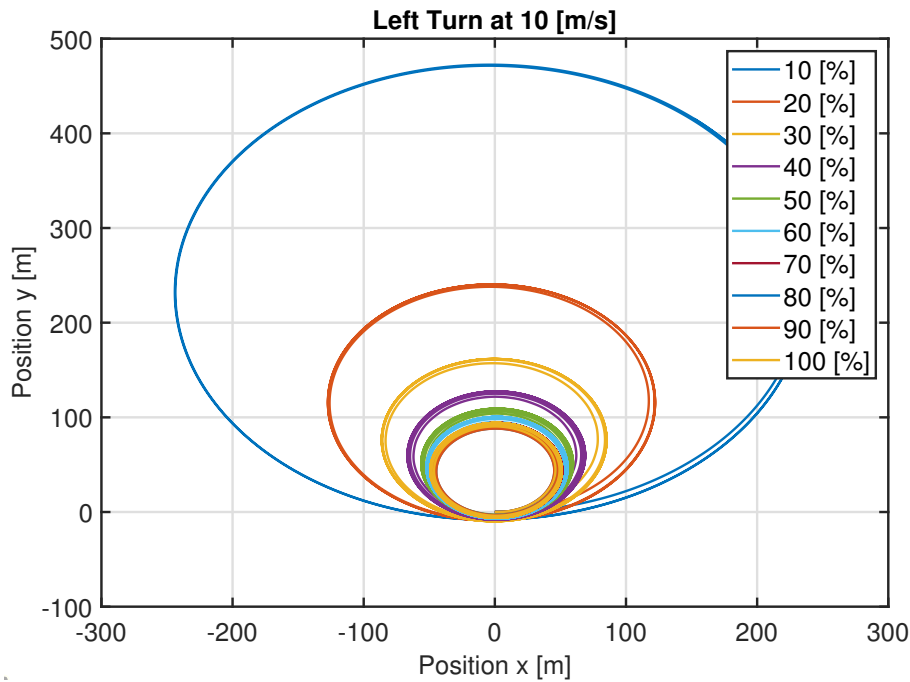


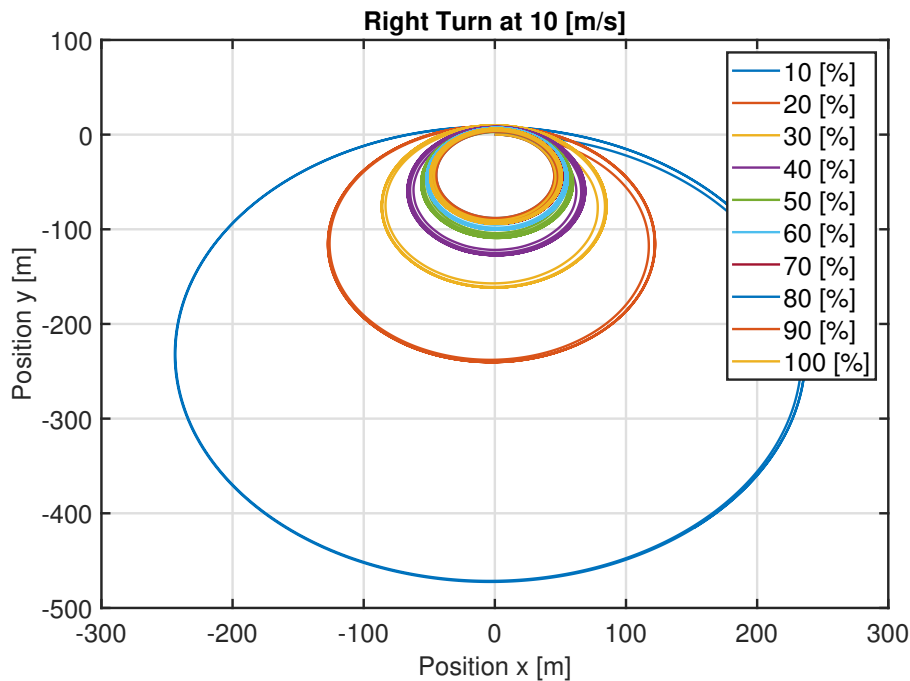Figure 2.14: Plot of left turn at approximately 10 [*m/s*], where a steering of 10 to 100 [%] have been applied.



Figure 2.15: Plot of right turn at approximately 10 [*m/s*], where a steering of 10 to 100 [%] have been applied.

Note that circles for left and right turns are identical. However, it is not possible to

determine whether the radius are accurate compared to a real vehicle, as data has not been obtained. Assuming the model is accurate, the largest and smallest radius is approximately 250 $[m]$ and 50 $[m]$ respectively when the velocity of the vehicle is 10 $[m/s]$. A plot of the lateral acceleration and lateral slip for the vehicle can be seen in Fig. 2.16 and Fig. 2.17 respectively. As expected the lateral acceleration is largest with a 100 percent turn and given it is above 0.4 $[m/s^2]$, which is the maximum for a linear model, it emphasize the need for the nonlinear model.
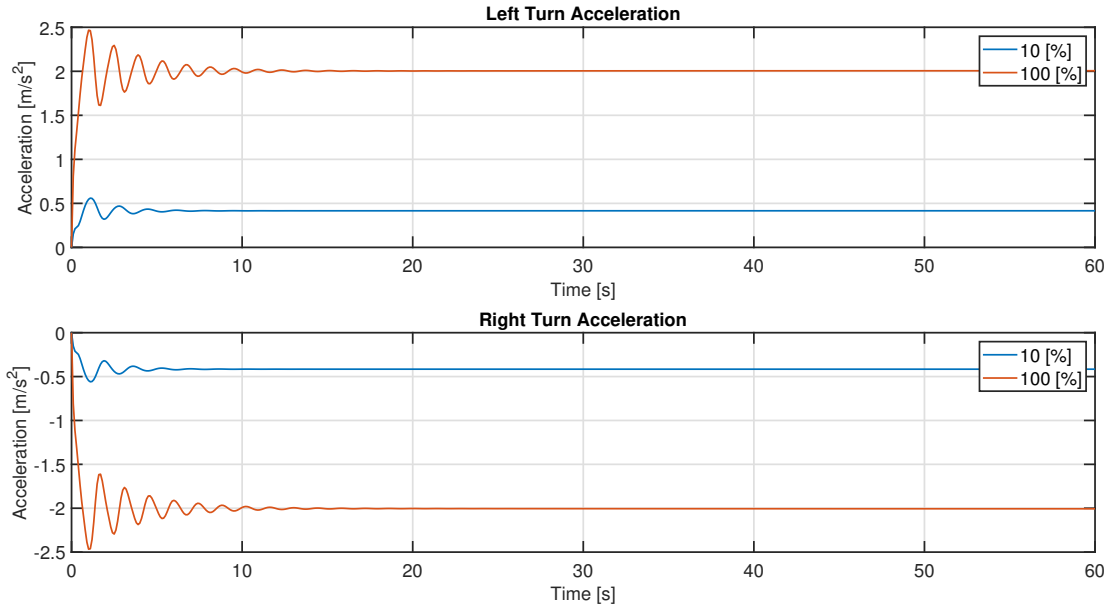


Figure 2.16: Plot of the lateral accelerations of the vehicle, where a steering of 10 and 100 [%] have been applied for a left and right turn.
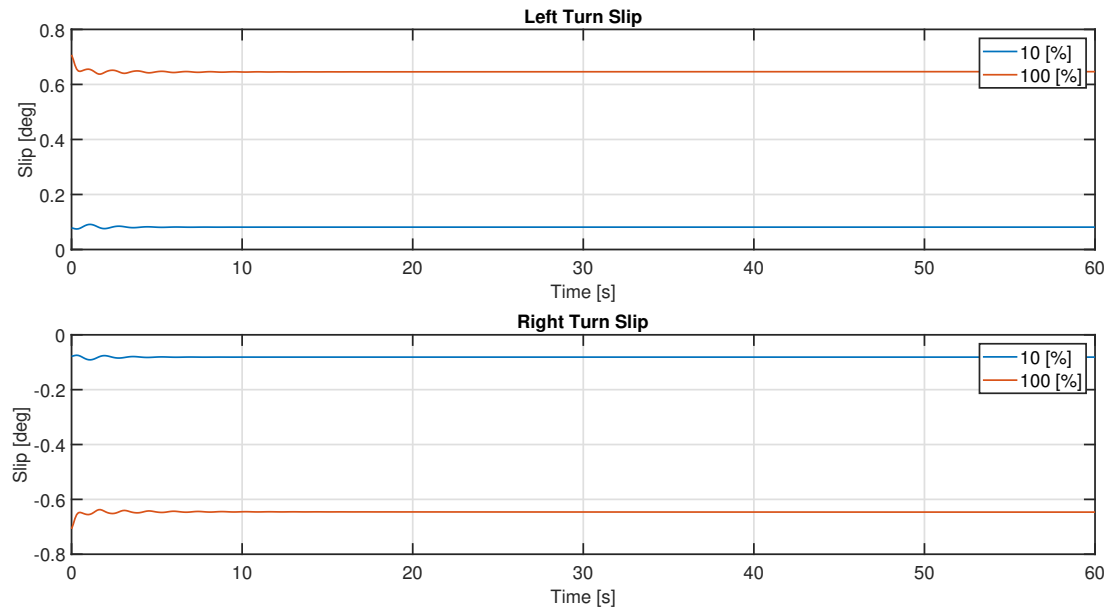


Figure 2.17: Plot of the lateral slip of the vehicle, where a steering of 10 and 100 [%] have been applied.

However the maximum value for the lateral slip is only around 0.7 degree angle, which is

relative low. It should be noted that the transition between traction and slip is around 4-5 degree angle and become increasing nonlinear after 2.5 degree angle and therefore could the lateral slip still be reasonable.

It should be mentioned that one of the important reasons for the nonlinear model was the handling of larger steering angles and higher lateral accelerations which has been shown in this section. However there are problems when considering lower velocities (generally below 10 $[m/s]$) as the model struggles with the oscillatory behavior from the longitudinal slip. The addition of the first order system for the wheel dynamics do improve the behavior from the longitudinal slip but does not solve it. Further improvement to the model could possible be achieved using other method of approximating the torque applied to the wheel, as the torque from the longitudinal slip overpower the torque from the engine, generally at low velocities. If the torque could be considered relative high from the start (45 $Nm$ at 0 RPM) it might be possible to improve the dynamics response at lower velocities.

# Control Strategy

<span style="font-size:3em">3</span>

In this chapter, an introduction to a possible track design, covering multiple aspect of a driving environment for the ARC is proposed. The requirements for a possible control scenarios are described. It furthermore includes a short evaluation of possible control strategies leading to a linearization of the nonlinear model for use in a linear quadratic regulator design.

## 3.1   Track Design

In this section a possible track design will be described based on Sec. 1.1.1, where the dynamic event skid pad, which have an inside and outside diameter of 15.25 $[m]$ and 21.25 $[m]$ respectively. Thereby is the width of the track 3 $[m]$, which is considered the minimum for all possible dynamic events [5].

The maximum and minimum outside diameter for an event is stated to be 50 $[m]$ and 9 $[m]$ respectively [5]. Based on the skid pad event, a reference track with a 180 degree turn could be used, as seen in Fig. 3.1. The radius for the reference track would then be 9.125 $[m]$, but given the knowledge from Sec. 2.8 this would not be possible. Increasing the radius to 60 $[m]$ would be within the operational region of the model, with the condition of a 10 $[m/s]$ vehicle velocity.
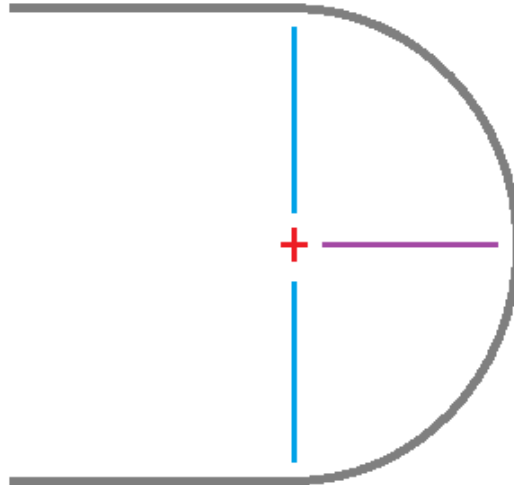


Figure 3.1: Sketch of the reference track (gray), where center (red), diameter (cyan) and radius (magenta) of the circle is represented.

The following concepts can be considered with the track design. First, the acceleration until the appropriate velocity for the turn, should be as high as possible without causing the tires to start spinning and thereby loss of traction. Second, following the turn at the highest possible velocity without causing the tires to slip laterally. Third, come to a hold from high velocity efficiently, meaning highest possible deceleration of the tires without blocking them causing the tires to slip longitudinally.

For now, only a speed regulator is considered. The initial condition of the vehicle must be 10 $[m/s]$ or above to avoid problem with the limitations of the model. This is based on Sec. 2.8, where torque supplied from the engine to the wheel, could be less than the torque subtracted, because of the longitudinal slip. A problem will arise when a controller is added, as no torque will be supplied from the engine, if the accelerator pedal is zero. This would be the case when brake is applied. Considering a brake action would increase the velocity difference between the wheel and the chassis, the slip would also increase. If one applied 100 $[\%]$ brake, the torque subtracted from the wheel would become close to that of the maximum torque deliver from the engine. Hence, the vehicle will not be able to recover as the torque from the engine depends on the velocity of the wheel.

The amount of brake must therefore be used cautiously such that the velocity difference is relative small. The problem is to quantified this in a meaningful way based on a limitation of the model. The best indication would be the tire force of the wheel, however it still depends on the amount of brake applied. One could also consider the de-acceleration of the wheel or the chassis, but it would depend on the amount of change between the reference speed, the vehicle have to perform. Also a value can not be determined before an actual control has been implemented, such that a value could be observed. The question is then, does it need to have a requirement. Based on Sec. 1.1 the brake is most important to stop the vehicle after an event have already been timed, with the exception of the autocross event. Otherwise the use of brake can be considered inefficient and could be neglected, given the limitation of the model.

When considering achieving a reference speed one should also consider the events. The importance on reaching a velocity fast, only applies to the acceleration and autocross event. For the skid pad event the precision of the reference speed is more important than the time it takes to reach it. Maintaining a precis reference speed leads to high knowledge of the turning radius, as found in Sec. 2.8. No problem was observed regarding the lateral slip, which is likely due to the lack of dynamics, such as pitch and roll in the model. A requirement should therefore be placed on the precision of the reference speed. No requirement will be placed on the time to reach the speed, given the limitation of the model and since efficiency is not considered no requirement is put on the accelerator. This means acceleration to a reference speed would be fast, which is acceptable for most events. The uses of brake must be limited such that the model will continue to function, but do otherwise not have an requirement.

## 3.2  Control requirements

In this section, the requirements for the controller will be defined including a short explanation for each requirement. As mentioned in Sec. 3.1, it is desired to implement a control strategy that can regulate and maintain the speed with a relative high precision. Any overshoot is not considered a problem given all events have a straight segments at the start, before any maneuvering. The main requirement for the speed control are:

1. The controller must regulate the speed to be greater than or equal to -0.1 $[m/s]$ and less than or equal to 0.1 $[m/s]$ of the reference speed.

Note that the value is based on [10], which consider speed indication between true speed of the vehicle and the speed displayed on a speedometer. To ensure a reliable simulation. The uses of brake will be limited such that a change of reference speed between the maximum and the minimum speed, of a selected region, will not cause a failure of the simulation. This leads to the following sub requirement.

1(a). The simulation must be able run the full simulation time without a failure, due to uses of the brake from a change between the maximum and the minimum speed, of a selected region.

This requirement does not specify how to limit the uses of the brake, which can be achieved in multiple ways. A failure to simulate is when a brake action increase the velocity difference between the wheel and the chassis to the point where the subtracted force from the wheel overcome the force form the engine.

## 3.3   Controller Consideration

As discussed in the previous section, the controller is required to regulate the speed of the vehicle. Here classical control such as Proportional (P), Proportional-Integral (PI) and Proportional-Integral-Derivative (PID) could be used. However a better option would be to use a Linear Quadratic Regulator (LQR), which minimizing a cost function related directly to the goals of the control task instead of choosing locations for the poles. However both methods have limitation, as they can not handle constraints with varying disturbances without using *ad hoc* fixes [9, p. 5].

This leads to the Model Predictive Control (MPC) that can operate closer to constraints and takes actuator limitations into account which could be beneficial for the race car events. The main limiting factor of MPC is the computation time, and is therefore mostly used for relative slow system [9, p. 2].

Linear quadratic regulator can be linked to the MPC, if the prediction horizon is sufficiently long. The main difference is how the optimization problem is solved. LQR is solves within a fixed window or infinite horizon in contrast to MPC that use a moving horizon window. The advantages form a moving horizon window includes real-time optimization with hard constraints on variables [12, p. xii].

As a first approach the controller could be a LQR design, which is convenient for comparison of performance with other methods of controller such as MPC or possibly Sliding Mode Control (SMC). The nonlinear model would need to be linearized in order to implement a LQR design.

## 3.4   Model Linearization

In this section, the system described in Sec. 2.7 will be linearize based on (2.56) and is an approximation of the nonlinear function which allows it to be analyzed with tools for linear systems close to a desired point.

Given the model is nonlinear, several linear approximations must be performed for the linearization to succeed, including torque, brake and slip. However this means the linear system only is accurate within a small a region. If multiple linearizations is performed a control system could switch between them. The necessary number of linearizations will depend on the region of operation.

A general nonlinear system $\dot{\boldsymbol{x}} = \boldsymbol{f}(\boldsymbol{x}, t, \boldsymbol{u})$, can be approximated around a point $\boldsymbol{x}^*$, by a linear system with input $\boldsymbol{u}^*$. Thereby it is possible to approximate $\boldsymbol{f}(\boldsymbol{x}, t, \boldsymbol{u})$ near $(\boldsymbol{x}^*, \boldsymbol{u}^*)$, by the first order term of the Taylor expansion [8]:

$$\frac{d\boldsymbol{x}}{dt} \approx \boldsymbol{f}(\boldsymbol{x}^*, \boldsymbol{u}^*) + \frac{\partial f}{\partial \boldsymbol{x}}\bigg|_{\boldsymbol{x}=\boldsymbol{x}^*, \boldsymbol{u}=\boldsymbol{u}^*} (\boldsymbol{x} - \boldsymbol{x}^*) + \frac{\partial f}{\partial \boldsymbol{u}}\bigg|_{\boldsymbol{x}=\boldsymbol{x}^*, \boldsymbol{u}=\boldsymbol{u}^*} (\boldsymbol{u} - \boldsymbol{u}^*) \tag{3.1}$$

Where the expressions:

$$\frac{\partial f}{\partial \boldsymbol{x}}\bigg|_{\boldsymbol{x}=\boldsymbol{x}^*, \boldsymbol{u}=\boldsymbol{u}^*} \quad \text{and} \quad \frac{\partial f}{\partial \boldsymbol{u}}\bigg|_{\boldsymbol{x}=\boldsymbol{x}^*, \boldsymbol{u}=\boldsymbol{u}^*} \tag{3.2}$$

Are the jacobians of the evaluated point $(\boldsymbol{x} = \boldsymbol{x}^*, \boldsymbol{u} = \boldsymbol{u}^*)$. For convenience, $t$ is implied as only continuous time is used for this project. The jacobians is denoted by matrix $\boldsymbol{A} \in \mathbb{R}^{n \times n}$ and $\boldsymbol{B} \in \mathbb{R}^{n \times p}$ respectively. The number of states are represented by $n$ and the number of inputs by $p$. Any new values can then be defined as $\tilde{\boldsymbol{x}} = \boldsymbol{x} - \boldsymbol{x}^*$ and $\tilde{\boldsymbol{u}} = \boldsymbol{u} - \boldsymbol{u}^*$, representing the deviation from the point $(\boldsymbol{x}^*, \boldsymbol{u}^*)$. Given $\boldsymbol{x}^*$ is a constant value of $\boldsymbol{x}$, it is possible to write $\frac{d\tilde{\boldsymbol{x}}}{dt} = \frac{d\boldsymbol{x}}{dt}$. The linear model is then:

$$\frac{d\tilde{\boldsymbol{x}}}{dt} = \boldsymbol{A}\tilde{\boldsymbol{x}} + \boldsymbol{B}\tilde{\boldsymbol{u}} + \boldsymbol{f}(\boldsymbol{x}^*, \boldsymbol{u}^*) \tag{3.3}$$

Choosing an equilibrium point for $(\boldsymbol{x} = \boldsymbol{x}^*, \boldsymbol{u} = \boldsymbol{u}^*)$, ensure that $\boldsymbol{f}(\boldsymbol{x}^*, \boldsymbol{u}^*) = 0$ and the term can be dropped:

$$\frac{d\tilde{\boldsymbol{x}}}{dt} = \boldsymbol{A}\tilde{\boldsymbol{x}} + \boldsymbol{B}\tilde{\boldsymbol{u}} \tag{3.4}$$

Before a linear approximation can be performed, the torque from the engine, the brake and the longitudinal/lateral slips must be linearized. Considering the torque plot in Sec. 2.3 (see Fig. 3.2 below), a constant value can be chosen between 53 and 55 $[Nm]$ if the angular velocity are between 6500 and 11000 $[RPM]$.
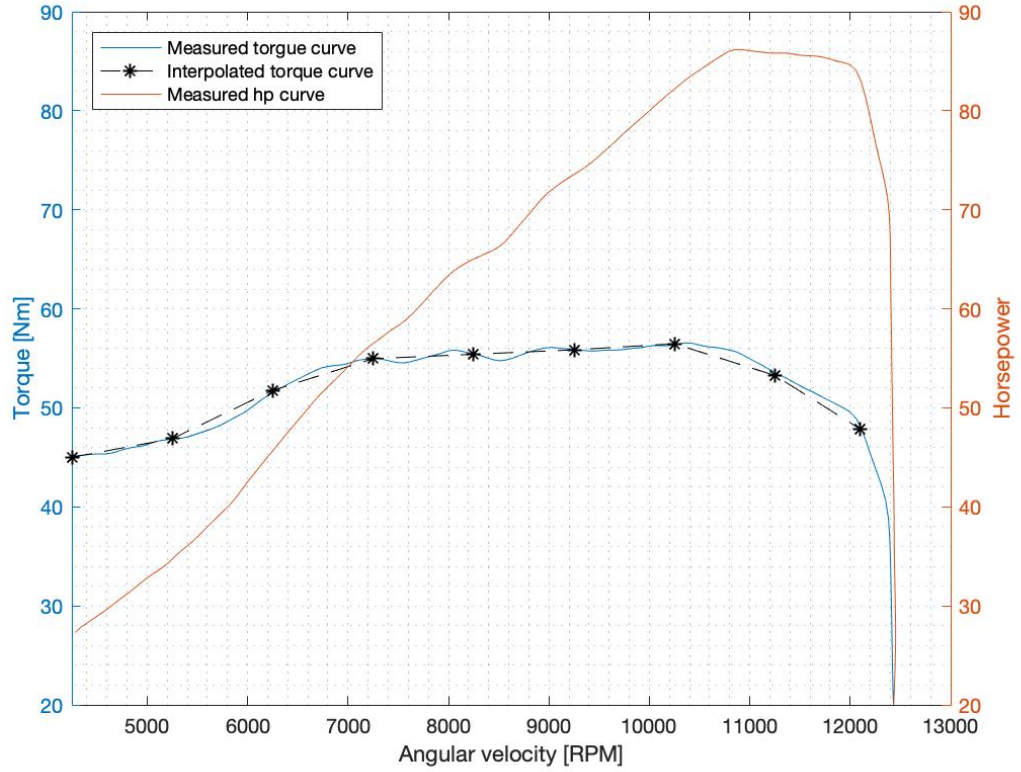
Figure 3.2: Plot of torque and horsepower given the angular velocity of the engine.

No data was found for the brakes, but it can be considered as follows, based on [2]:

$$f_{brake} = 3500P_B + 0 \tag{3.5}$$

There are to parts to consider for the longitudinal slip, first the tire data found in Appendix A.3, given the following functions:

$$f_{Fvx} = 3473.8s_v + 144.2 \tag{3.6a}$$
$$f_{Fhx} = 5322.1s_h - 86.2 \tag{3.6b}$$

The second part is given by the (3.7) (see below) from Sec. 2.7.1, since acceleration slip and brake slip are found, based on different velocities (chassis and wheel). However if the difference is relative small it can be considered the same.

$$s_h = \frac{r\dot{\rho}_h - {}^h\dot{x}_h}{max\left(|r\dot{\rho}_h|, |{}^h\dot{x}_h|\right)} \tag{3.7}$$

Finally the lateral slip, can be linearized from the tire data found in Appendix A.3, given the following functions:

$$f_{Fvx} = -585\alpha_v + 0 \tag{3.8a}$$
$$f_{Fhx} = -923.2\alpha_h + 0 \tag{3.8b}$$

Now it is possible find a linear approximation of the nonlinear model near an equilibrium point $(\boldsymbol{x}^*, \boldsymbol{u}^*)$ based on (3.4). The jacobians, $\boldsymbol{A}$ and $\boldsymbol{B}$, where found using MatLab's jacobian function. They can however not be found in this report as the forces from the tires leads to large equations, but can be found on the Database.

Now, to obtain a linear model an equilibrium point must be define. $\dot{x}_V^* = 10\ [m/s]$ is chosen as an equilibrium point for the vehicle where no turn is performed. This value is chosen based on the lower region of the model which is know to be working. The remaining states values for the equilibrium point is found so the system of equations $\boldsymbol{f}(\boldsymbol{x}^*, u^*) = 0$, using the Simulink model.

Hence, the state space model of the system is described by the following equation.

$$\dot{\tilde{\boldsymbol{x}}} = \boldsymbol{A}\tilde{\boldsymbol{x}} + \boldsymbol{B}\tilde{\boldsymbol{u}} \tag{3.9a}$$
$$\tilde{\boldsymbol{y}} = \boldsymbol{C}\tilde{\boldsymbol{x}} \tag{3.9b}$$

Where $\boldsymbol{x}$ and $\boldsymbol{u}$ are the state vector and the input vector respectively.

$$\boldsymbol{x} = \left[x_V, y_V, \psi_V, \dot{x}_V, \dot{y}_V, \dot{\psi}_V, \dot{\rho}_v, \dot{\rho}_h, {}^vF_{v,x}, {}^vF_{v,y}, {}^hF_{h,x}, {}^hF_{h,y}\right]^T \tag{3.10a}$$
$$\boldsymbol{u} = [\delta_H, p_F, p_B, G]^T \tag{3.10b}$$

For simplicity $\boldsymbol{x}$ and $\boldsymbol{u}$ will be note as;

$$\boldsymbol{x} = \left[x_1, x_2, x_3, x_4, x_5, x_6, x_7, x_8, x_9, x_{10}, x_{11}, x_{12}\right]^T \tag{3.11a}$$
$$\boldsymbol{u} = [u_1, u_2, u_3, u_4]^T \tag{3.11b}$$

and $\boldsymbol{A}$ and $\boldsymbol{B}$ are the evaluated jacobians in the equilibrium point:

$$\boldsymbol{A}_{1-6} = \begin{bmatrix} 0 & 0 & 0 & 1 & 0 & 0 \\ 0 & 0 & 0 & 0 & 1 & 0 \\ 0 & 0 & 0 & 0 & 0 & 1 \\ 0 & 0 & 0 & -0.098 & -4.898\text{e-}9 & 0 \\ 0 & 0 & 0.49 & -4.898\text{e-}9 & -0.049 & 0 \\ 0 & 0 & 0 & 0 & 0 & 0 \\ 0 & 0 & 0 & 0 & 0 & 0 \\ 0 & 0 & 0 & 0 & 0 & 0 \\ 0 & 0 & -1.174 & 0 & 0.117 & 0.073 \\ 0 & 0 & 1.629\text{e-}4 & 0 & -1.629\text{e-}5 & -1.012\text{e-}5 \\ 0 & 0 & 0.151 & -5329 & -0.016 & 0.015 \\ 0 & 0 & 2.96\text{e}4 & 0.006 & -2963 & 2901 \end{bmatrix} \tag{3.12}$$

$$
\boldsymbol{A}_{7-12} =
\begin{bmatrix}
0 & 0 & 0 & 0 & 0 & 0 \\
0 & 0 & 0 & 0 & 0 & 0 \\
0 & 0 & 0 & 0 & 0 & 0 \\
0 & 0 & 0.005 & 0 & 0.005 & 0 \\
0 & 0 & 0 & 0.005 & 0 & 0.005 \\
0 & 0 & 0 & 0.004 & 0 & -0.006 \\
0 & 0 & -0.010 & 0 & 0 & 0 \\
0 & 0 & 0 & 0 & -0.010 & 0 \\
-1.505\text{e-}9 & 0 & -10.81 & 0 & 0 & 0 \\
2.784\text{e-}13 & 0 & 0 & -10.38 & 0 & 0 \\
0 & 1366 & 0 & 0 & -10.39 & 0 \\
0 & -0.002 & 0 & 0 & 0 & -10.38
\end{bmatrix}
\tag{3.13}
$$

$$
\boldsymbol{B} =
\begin{bmatrix}
0 & 0 & 0 & 0 \\
0 & 0 & 0 & 0 \\
0 & 0 & 0 & 0 \\
0 & 0 & 0 & 0 \\
0 & 0 & 0 & 0 \\
0 & 0 & 0 & 0 \\
0 & 0 & 0 & 0 \\
0 & 39.05 & 134.6 & 1.108 \\
-1.174 & 0 & 0 & 0 \\
1.629\text{e-}4 & 0 & 0 & 0 \\
0 & 0 & 0 & 0 \\
0 & 0 & 0 & 0
\end{bmatrix}
\tag{3.14}
$$

Note that $\boldsymbol{A}_{1-6}$ indicate column 1 to 6 and $\boldsymbol{A}_{7-12}$ indicate column 7 to 12, as $\boldsymbol{A} = [\boldsymbol{A}_{1-6} \ \boldsymbol{A}_{7-12}]$.

Also note that the model is initialized at the velocity of 10 $[m/s]$ for the chassis, 39.02 $[rad/s]$ for the wheels and the force for the rear tire is 108.3 $[N]$. The acceleration is adjusted, such that 10 $[m/s]$ is the equilibrium giving the following values for the equilibrium point in Tab. 3.1.

| Variable | Values | Unit |
|:---:|:---:|:---:|
| $\dot{x}_1^*$ | 10 | $[m/s]$ |
| $\dot{x}_2^*$ | 1.0e-6 | $[m/s]$ |
| $\dot{x}_3^*$ | 0 | $[rad/s]$ |
| $\dot{x}_4^*$ | 2.1e-4 | $[m/s^2]$ |
| $\dot{x}_5^*$ | $-4.9$e-8 | $[m/s^2]$ |
| $\dot{x}_6^*$ | 0 | $[rad/s^2]$ |
| $\dot{x}_7^*$ | 0 | $[rad/s^2]$ |
| $\dot{x}_8^*$ | $-3.9$e-4 | $[rad/s^2]$ |
| $\dot{x}_9^*$ | 5.9e-8 | $[N/s]$ |
| $\dot{x}_{10}^*$ | $-5.4$e-12 | $[N/s]$ |
| $\dot{x}_{11}^*$ | 1.9e-4 | $[N/s]$ |
| $\dot{x}_{12}^*$ | -0.003 | $[N/s]$ |
| $u_1^*$ | 0 | $[rad]$ |
| $u_2^*$ | 2.84 | $[\%]$ |
| $u_3^*$ | 0 | $[\%]$ |
| $u_4^*$ | 1 | $[-]$ |

Table 3.1: Values for the equilibrium point

It should be noted that $\dot{x}_2^*$ can not be zero, given the jabcobians require elements to be divided by $\dot{x}_2^*$. Also note that not all values are zero, which is likely due to numerical error and the linearized torque, brake and slips.

Given the equilibrium point $(\boldsymbol{x^*}, \boldsymbol{u^*})$, it is possible to compare and verify the linear model (State Space) against the nonlinear model (Simulink) by plotting them together with different initial conditions or input deviations. Note that chassis and wheel will have the same initial conditions, meaning the longitudinal slip is zero at the start of the simulation.

Lets first consider the two models with no deviation ($\tilde{x}_4 = 0 \ [m/s], \tilde{u}_2 = 0 \ [\%]$) as seen in Fig. 3.3. There is nearly no inconsistency between the nonlinear and linear model, the linearization is a good approximation of the nonlinear. Note the relative small change over time is likely due to numerical error for the initialization of the dynamic tire force for the rear wheel. Also note the time, at which point the vehicle reach the equilibrium point, is relative large, although change of velocity is relative small.
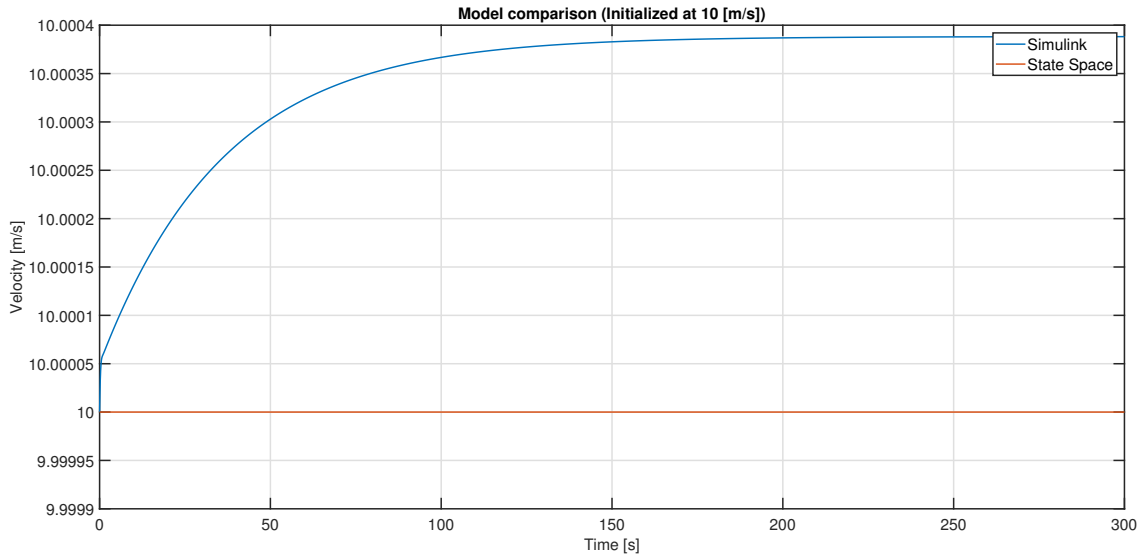
Figure 3.3: Plot of the Simulink and State Space model initialized at 10 $[m/s]$ with no deviation ($\tilde{x}_4 = 0$ $[m/s], \tilde{u}_2 = 0$ $[\%]$).

Now consider the two models with a deviation in the initial condition ($\tilde{x}_4 = 5$ $[m/s], \tilde{u}_2 = 0$ $[\%]$) as seen in Fig. 3.4. The vehicle starts at 15 $[m/s]$ and reach 10 $[m/s]$ after approximately 150 seconds. The two models conform to the same path relatively well.
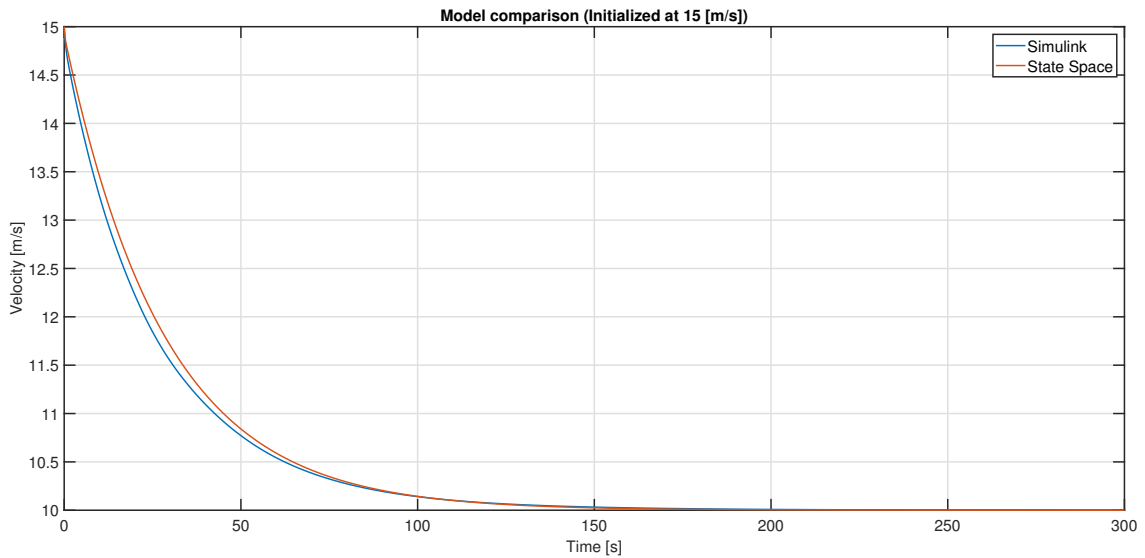


Figure 3.4: Plot of the Simulink and State Space model initialized at 15 $[m/s]$ with a deviation ($\tilde{x}_4 = 5$ $[m/s], \tilde{u}_2 = 0$ $[\%]$).

Next consider the two models with a deviation in the input ($\tilde{x}_4 = 0$ $[m/s], \tilde{u}_2 = 2$ $[\%]$) as seen in Fig. 3.5. The vehicle is initialized at 10 $[m/s]$ and reach 13.24 and 13.52 $[m/s]$ for the nonlinear and linear model respectively. The difference is likely due to the aerodynamic force given it contained a squared term before linearization.
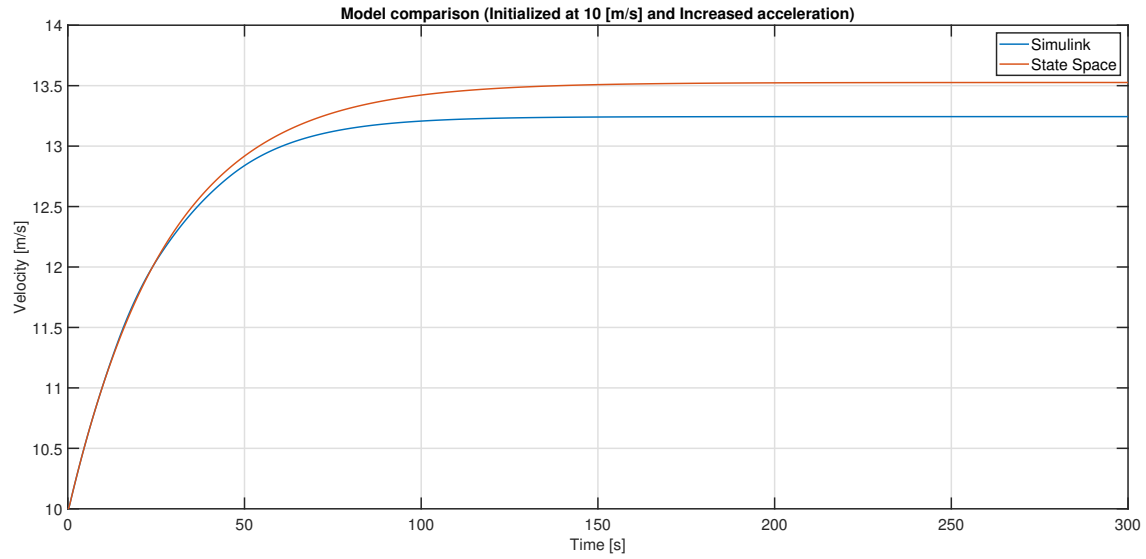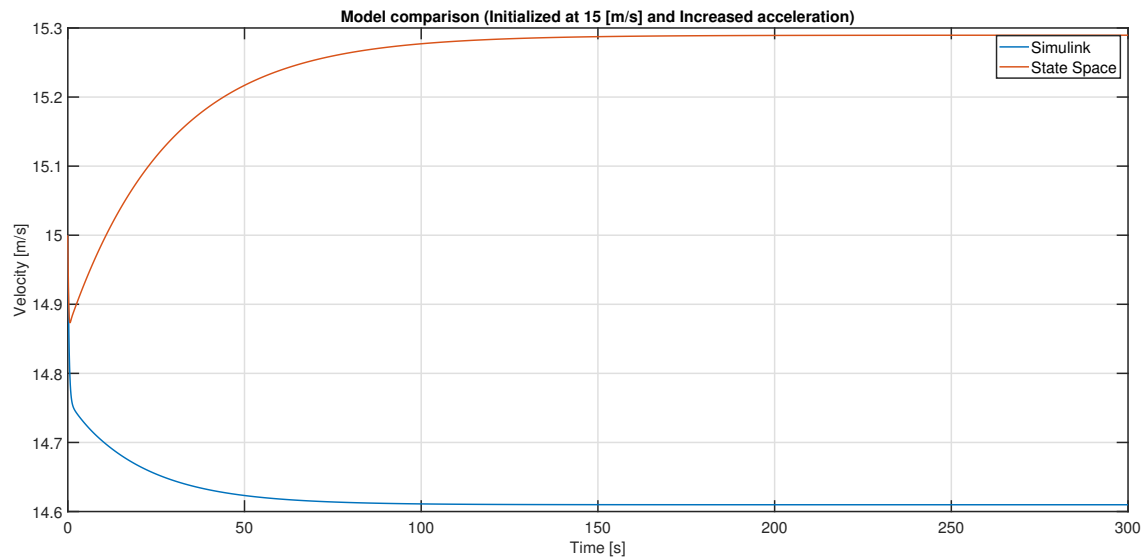
Figure 3.5: Plot of the Simulink and State Space model initialized at 10 $[m/s]$ with a deviation ($\tilde{x}_4 = 0$ $[m/s], \tilde{u}_2 = 2$ $[\%]$).

Then consider the two models with a deviation in the initial condition and the input ($\tilde{x}_4 = 5$ $[m/s], \tilde{u}_2 = 3$ $[\%]$) as seen in Fig. 3.6. The vehicle is initialized at 15 $[m/s]$ and reach approximately 14.61 and 15.29 $[m/s]$ for the nonlinear and linear model respectively. Clearly the nonlinear model starting to deviate from the linear model, compared to the previous plot.



Figure 3.6: Plot of the Simulink and State Space model initialized at 15 $[m/s]$ with a deviation ($\tilde{x}_4 = 5$ $[m/s], \tilde{u}_2 = 3$ $[\%]$).

Last consider the two model with a deviation in two of the inputs ($\tilde{x}_4 = 0$ $[m/s], \tilde{u}_2 = 3$ $[\%], \tilde{u}_3 = 1$ $[\%]$) as seen in Fig. 3.7. The vehicle is initialized at 10 $[m/s]$ where both acceleration and brake have been applied. A clear difference in velocity can be seen, which is because the nonlinear model reach a region of less torque from the engine, meaning around 45 $[Nm]$ compared to the 54 $[Nm]$ of the linear model.
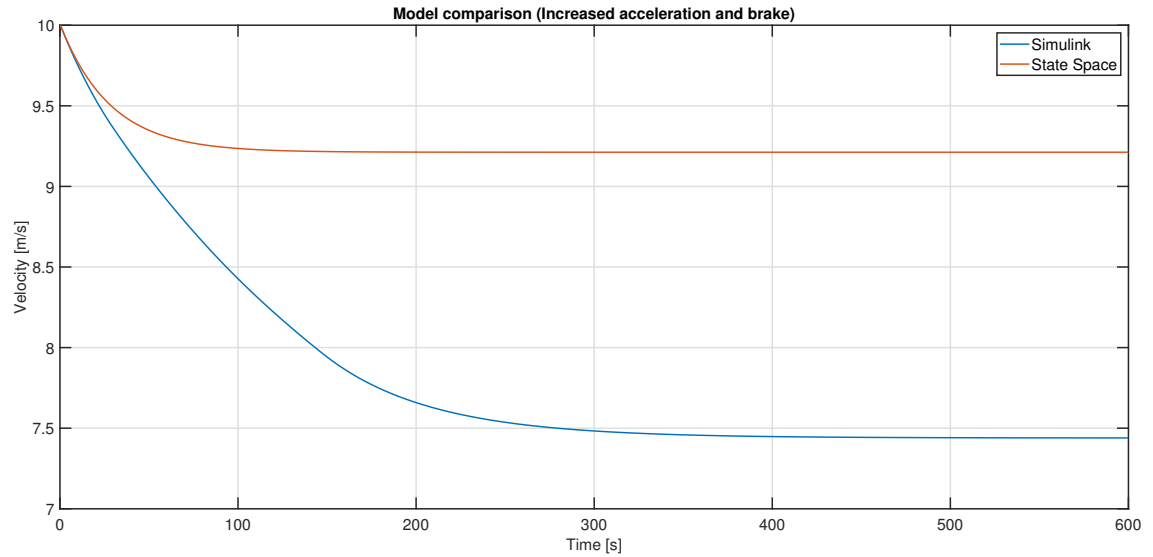
Figure 3.7: Plot of the Simulink and State Space model initialized at $10\ [m/s]$ with a deviation $(\tilde{x}_4 = 0\ [m/s], \tilde{u}_2 = 3\ [\%], \tilde{u}_3 = 1\ [\%])$.

The linearization of the nonlinear model, can be said to be a good approximation within a region between of approximately $8\ [m/s]$ and $15\ [m/s]$. A new linearization is needed if one consider other regions. Particular lower regions as torque varies more than higher regions.

## 3.5   LQR Controller

In the previous section a linearization of the equations of motion at the equilibrium point, was performed. A close loop control law, tracking the reference of the vehicle speed $(x_4)$ can then be implemented using a LQR design.

The LQR find the optimal state-feedback control law $\boldsymbol{u} = -\boldsymbol{Kx}$ that minimizes the quadratic cost function (3.15), and penalizes the states and the inputs of the system by weighting them with the symmetric matrices $\boldsymbol{Q}$ and $\boldsymbol{R}$ respectively [3]:

$$J(\boldsymbol{u}) = \int_0^\infty (\boldsymbol{x}^T \boldsymbol{Q} \boldsymbol{x} + \boldsymbol{u}^T \boldsymbol{R} \boldsymbol{u}) dt \tag{3.15}$$

Subject to the system dynamics:

$$\dot{\tilde{\boldsymbol{x}}} = \boldsymbol{A}\tilde{\boldsymbol{x}} + \boldsymbol{B}\tilde{\boldsymbol{u}} \tag{3.16}$$

Where $\boldsymbol{Q} \geq 0$ and $\boldsymbol{R} > 0$ can be tuned to find a balanced control law between error correction and control authority. A relative simple method of choosing the weights is to set $\boldsymbol{Q} = I$ and $\boldsymbol{R} = \epsilon I$, where $I$ is the identity matrix and $\epsilon$ is a scalar factor.

In addition, the gain matrix $\boldsymbol{K}$ is obtained by solving the Riccati equation [3]:

$$0 = \boldsymbol{P}\boldsymbol{A} + \boldsymbol{A}^T \boldsymbol{P} - \boldsymbol{P}\boldsymbol{B}\boldsymbol{R}^{-1}\boldsymbol{B}^T \boldsymbol{P} + \boldsymbol{Q} \tag{3.17}$$

Suppose that for the given system there is a feasible trajectory and a compensator can be design, such that the deviation of the states goes to zero as time goes to infinity. This is the trajectory tracking problem. Given (3.16), it can be written as [3]:

$$\boldsymbol{u} = \boldsymbol{K}_{(\tilde{\boldsymbol{r}} - \tilde{\boldsymbol{x}})} + \boldsymbol{u}^* \qquad (3.18)$$

The controlled variables, are the deviations between the current states and the reference trajectory, which can be written as:

$$\tilde{\boldsymbol{r}} = \boldsymbol{r} - \boldsymbol{x}^* \qquad (3.19a)$$
$$\tilde{\boldsymbol{x}} = \boldsymbol{x} - \boldsymbol{x}^* \qquad (3.19b)$$

By finding the eigenvalues of the system, it is established that the system has poles in the Right Half Plane (RHP), meaning it is unstable at the equilibrium point. The poles in the Left Half Plane (LHP) and RHP have the following values:

$$\lambda_1 = 0$$
$$\lambda_2 = 0$$
$$\lambda_3 = -0.648 + 4.300i$$
$$\lambda_4 = -0.648 - 4.300i$$
$$\lambda_5 = -9.133$$
$$\lambda_6 = -5.137 + 3.416i$$
$$\lambda_7 = -5.137 - 3.416i$$
$$\lambda_8 = -10.810$$
$$\lambda_9 = -10.379$$
$$\lambda_{10} = -0.035$$
$$\lambda_{11} = 2.112e\text{-}5$$
$$\lambda_{12} = 1.412e\text{-}12$$

To find a proper pole placement for the close-loop system with state-feedback $\boldsymbol{u} = -\boldsymbol{K}\boldsymbol{x}$, one must first ensure that the system is controllable and observable, by evaluating the rank of the following equation:

$$Co = \begin{bmatrix} \boldsymbol{B} & \boldsymbol{A}\boldsymbol{B} & \boldsymbol{A}^2\boldsymbol{B} & ... & \boldsymbol{A}^{n-1}\boldsymbol{B} \end{bmatrix} \qquad (3.21a)$$

$$Ob = \begin{bmatrix} \boldsymbol{C} \\ \boldsymbol{C}\boldsymbol{A} \\ \boldsymbol{C}\boldsymbol{A}^2 \\ ... \\ \boldsymbol{C}\boldsymbol{A}^{n-1} \end{bmatrix} \qquad (3.21b)$$

It is found that only 9 out of 12 states are controllable and only 7 out of 12 states are observable, hence the system is underactuated. Two possible methods to manage this can be considered. One is to eliminate uncontrollable or unobservable state from the state space model while still preserving the response characteristics of the original system. The other separates the controllable states from the uncontrollable, thereby it is possible to design a LQR on the controllable part. However the uncontrollable states must be stable as it otherwise may affect the system.

To separate the controllable states $\boldsymbol{A}_c$ from uncontrollable states $\boldsymbol{A}_{uc}$ the Matlab function *ctrbf* can be used. Which finds a unitary similarity transformation matrix $\boldsymbol{T}$ such that:

$$\bar{\boldsymbol{A}} = \boldsymbol{T}\boldsymbol{A}\boldsymbol{T}^T, \quad \bar{\boldsymbol{B}} = \boldsymbol{T}\boldsymbol{B}, \quad \bar{\boldsymbol{C}} = \boldsymbol{C}\boldsymbol{T}^T \tag{3.22}$$

Which transformed the system to the following form:

$$\bar{\boldsymbol{A}} = \begin{bmatrix} \boldsymbol{A}_{uc} & 0 \\ \boldsymbol{A}_{21} & \boldsymbol{A}_c \end{bmatrix}, \quad \bar{\boldsymbol{B}} = \begin{bmatrix} 0 \\ \boldsymbol{B}_c \end{bmatrix}, \quad \bar{\boldsymbol{C}} = \begin{bmatrix} \boldsymbol{C}_{uc} & \boldsymbol{C}_c \end{bmatrix} \tag{3.23}$$

If all nine controllable states are chosen, one of the uncontrollable state is unstable. Taking only eight controllable states, the remaining four uncontrollable states of the system have the following values:

$$\lambda_1 = -11.180$$
$$\lambda_2 = -0.379$$
$$\lambda_3 = -1.696\text{e-}11$$
$$\lambda_4 = -1.441\text{e-}5$$

Then a LQR controller can be implemented on the controllable portion of the system, with the gain matrix $\boldsymbol{K}$. To verify the poles are in the LHP, one could consider the close loop controllable system in the following form:

$$\dot{\boldsymbol{x}}_c = (\boldsymbol{A}_c - \boldsymbol{B}_c\boldsymbol{K})\boldsymbol{x}_c \tag{3.25}$$

Where the poles for the controllable part of the system have the following values:

$$\lambda_1 = -97.419 + 96.834i$$
$$\lambda_2 = -97.419 - 96.834i$$
$$\lambda_3 = -10.874$$
$$\lambda_4 = -10.379$$
$$\lambda_5 = -1.130$$
$$\lambda_6 = -0.084$$
$$\lambda_7 = -0.055$$
$$\lambda_8 = -0.001$$

Augmenting the $K$ matrix back to the full system will require it to be padded with zeros. The amount of zeroes depends on the number of control inputs and number of uncontrollable states. Applying the transformation matrix $T$ to the padded gain matrix restore it back to the full system. Where the poles have the following values:

$$\lambda_1 = -97.419 + 96.834i$$
$$\lambda_2 = -97.419 - 96.834i$$
$$\lambda_3 = -11.764$$
$$\lambda_4 = -9.374 + 1.437i$$
$$\lambda_5 = -9.374 - 1.437i$$
$$\lambda_6 = -0.539 + 4.479i$$
$$\lambda_7 = -0.539 - 4.479i$$
$$\lambda_8 = -1.244 + 0.390i$$
$$\lambda_9 = -1.244 - 0.390i$$
$$\lambda_{10} = -0.004$$
$$\lambda_{11} = 1.875e\text{-}5$$
$$\lambda_{12} = 4.526e\text{-}14$$

The last two eigenvalues are located in the RHP and therefore the full system can not be said to be stable in the neighbourhood of the equilibrium point. However an implementation on the linearized model was performed, since the last two eigenvalues is relative small and therefore could be numerical errors. In Fig. 3.8 and Fig. 3.9, the error of the states $x_4$, $x_8$ and $x_{11}$ and the control effort of $u_2$ and $u_3$, for the controlled linearized model can be seen.
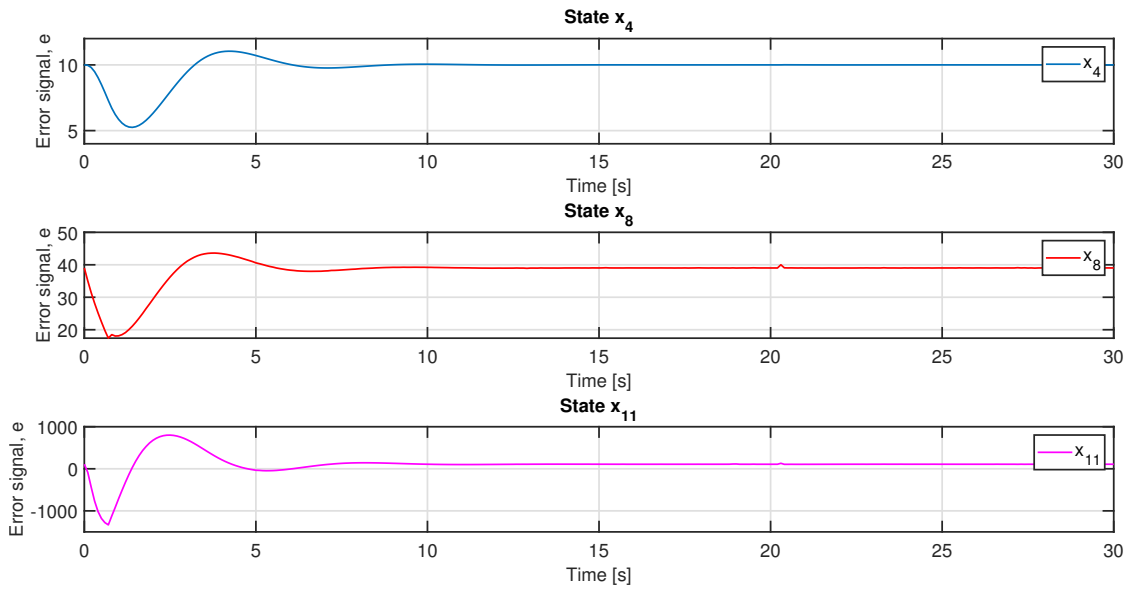


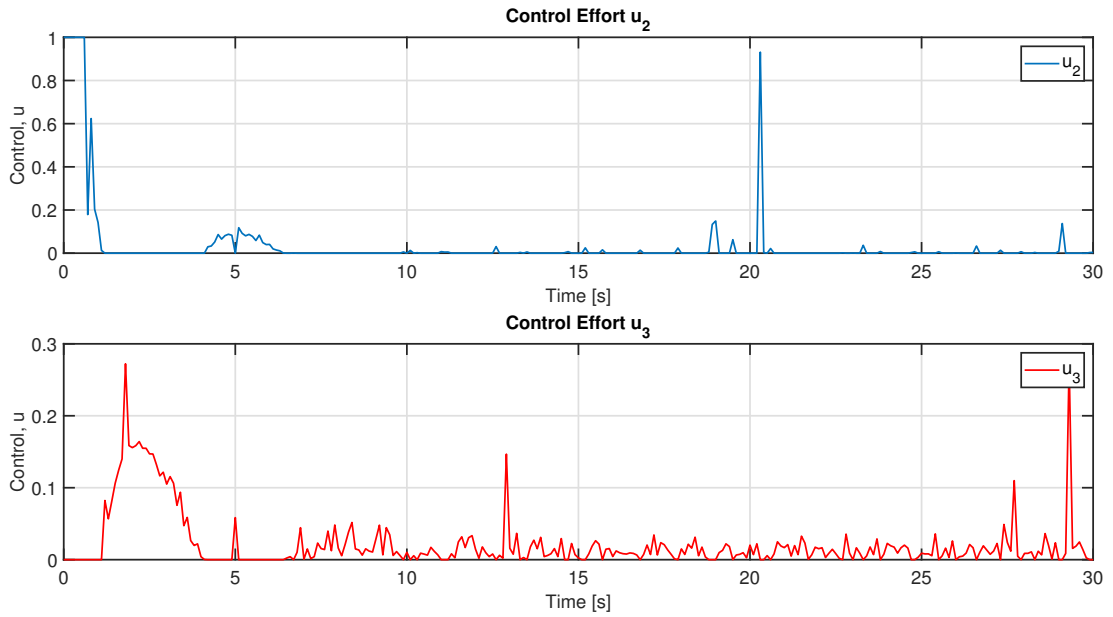Figure 3.8: Plot of the states $x_4$, $x_8$ and $x_{11}$ error signal for the controlled linearized model.

Figure 3.9: Plot of the control effort for $u_2$ and $u_3$, of the controlled linearized model.

The vehicle is initially driving at 10 $[m/s]$ with no steering applied and at time zero of the simulation, the controller should maintain the 10 $[m/s]$ velocity. The error of state $x_4$ in particular should go to zero, as it is the one relevant to control, but the dynamic response return to where it started. The control effort should remain minimal which is not the case and it rely more on the brake.

The problem could be due to the control of multiple states, of which for now, only one is desired. State $x_8$ should be controllable, given three of four control input applies to this state and it is therefore likely that $x_1$, $x_4$ and possibly $x_{11}$ is controllable. Since only the accelerator and brake pedal is considered for now, the last two could also be removed from the design.

A weight matrix with only the controllable state included can be defined, by using the similarity transformation matrix $\boldsymbol{T}$ such that:

$$\bar{\boldsymbol{Q}} = \boldsymbol{T}\boldsymbol{Q}\boldsymbol{T}^T \tag{3.28}$$

A new LQR was design, with only two inputs, where the weights can be adjusted from $\boldsymbol{Q}$. This design have poles in the LHP for both the uncontrollable part and the augmented full system. They are however still relative small, like the first design.

The region the model should be able to manage, based on the linearized model, is between 8 and 15 $[m/s]$. By integrating the speed reference one gets the position reference and by dividing speed reference with the radius of the wheel, one gets the reference for the wheel's angular velocity. There is no simple solution to determine the tire forces reference so it will be set to zero. Thereby is $\boldsymbol{Q} = [1\text{e-}6\ 0\ 0\ 1\ 0\ 0\ 0\ 1\text{e-}6\ 0\ 0\ 0\ 0]$, which is a diagonal matrix.

Fig. 3.10 and Fig. 3.11, represents the error of the state $x_4$ and the control effort of $u_2$ and $u_3$ for the new LQR design, implemented on the linear and nonlinear model. The controller is enabled after 10 seconds and should follow a reference of 15 $[m/s]$. After 40

seconds the reference is change to 8 $[m/s]$. The larger error of state $x_4$, after the controller is enable for the linear model, is an issue with Simulink. The behavior is now as desired, which also can be said for the nonlinear model. The control effort react as expected, but the time spent on braking is longer for the nonlinear. A large weight have been placed on the brake input ($\boldsymbol{R} = [1 \; 1e4]$), given the issue with de-acceleration of the wheel. The control effort between the two models is similar, however the linear model may subtract more force from the wheel, making it faster.
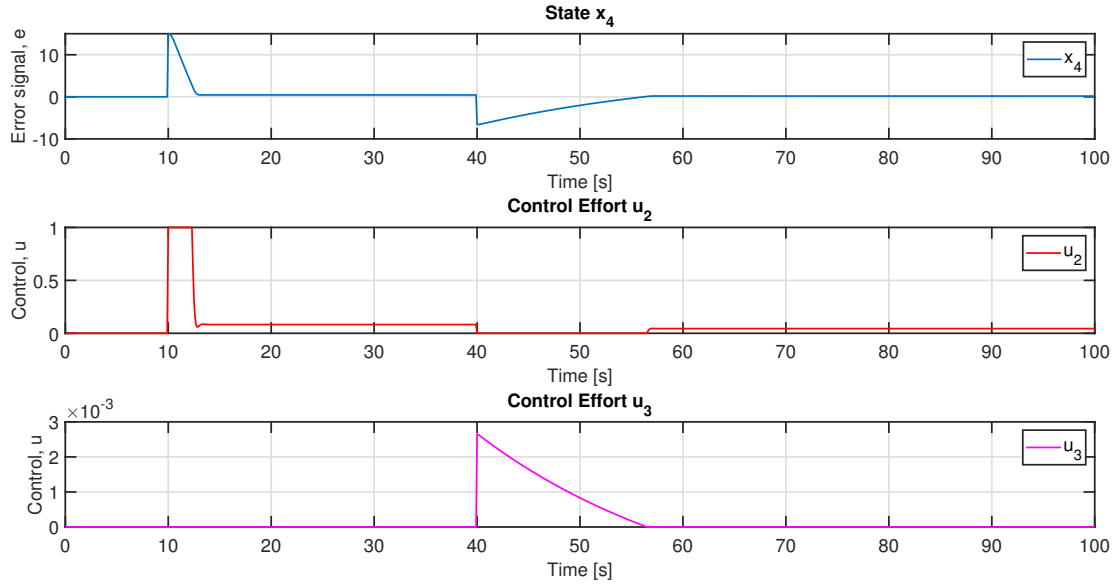


Figure 3.10: Plot of the state $x_4$ error signal and the control effort of $u_2$ and $u_3$, for the controlled linearized model.
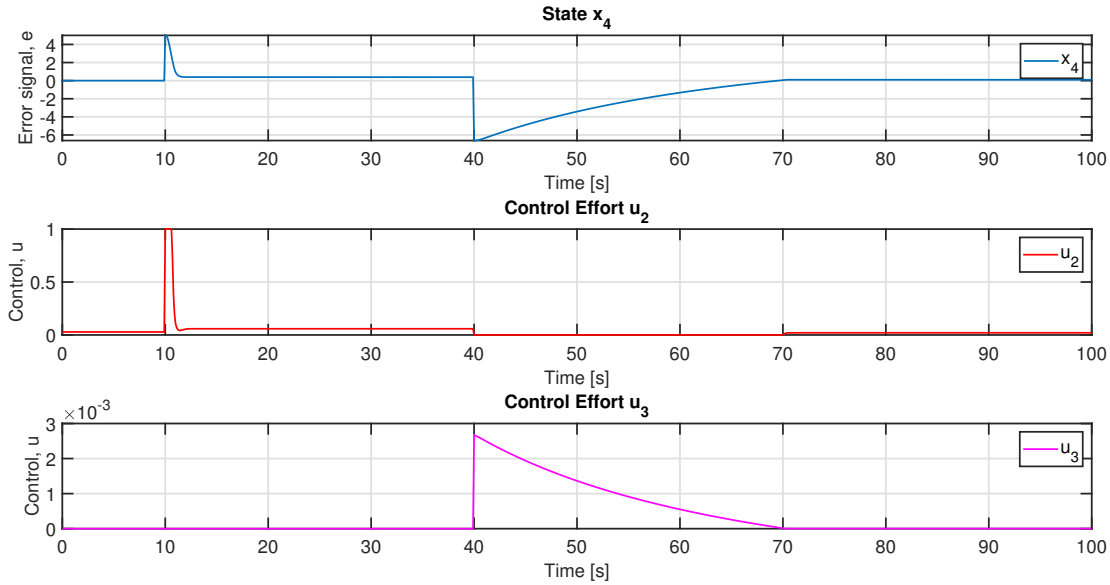


Figure 3.11: Plot of state $x_4$ error signal and the control effort of $u_2$ and $u_3$, for the controlled nonlinear model.

Fig. 3.12, represents the controlled velocity of the vehicle with the new LQR design,

implemented on the nonlinear model. The control is enabled after 10 seconds and should follow a reference of 15 $[m/s]$. After 40 seconds the reference is changed to 8 $[m/s]$. Note the steady state error at both reference velocity.
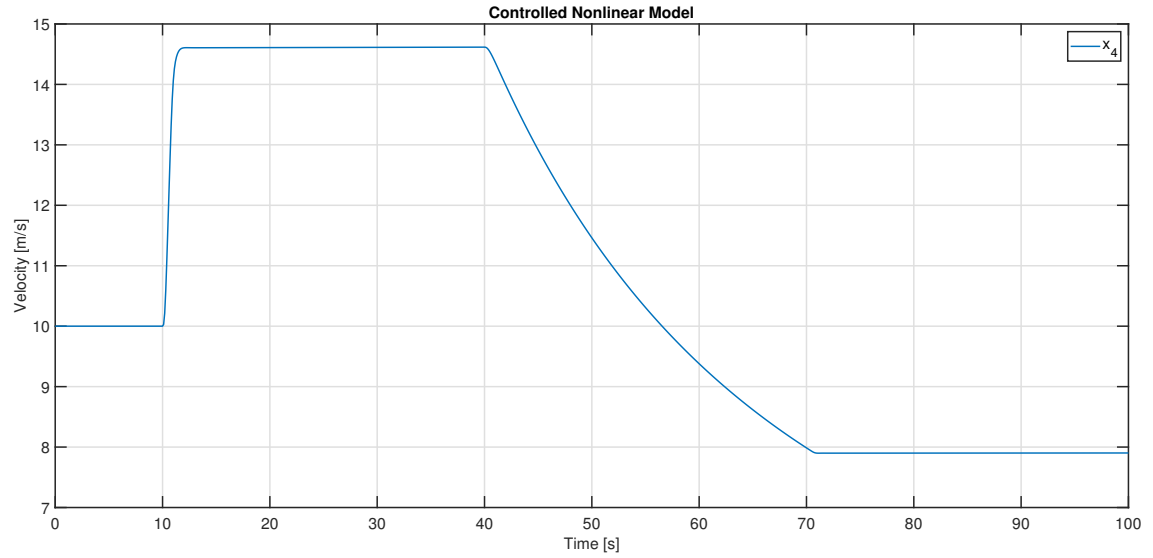


Figure 3.12: Plot of the velocity for the controlled nonlinear model.

To remove the steady state error one should implement integral feedback, which use an integrator to provide zero steady state error by augmenting the system with a new state $z$ [3]:

$$\begin{bmatrix} \dot{\tilde{x}} \\ \dot{\tilde{z}} \end{bmatrix} = \begin{bmatrix} A\tilde{x} + B\tilde{u} \\ \tilde{r} - C\tilde{x} \end{bmatrix} \qquad (3.29)$$

Given the augmented system, the control law would be [3]:

$$\boldsymbol{u} = \boldsymbol{K}_{(\tilde{\boldsymbol{r}} - \tilde{\boldsymbol{x}})} + \boldsymbol{K}_i z + \boldsymbol{u}^* \qquad (3.30)$$

Given that the controllable part still must be separate together with the inclusion of the integral part, an implementation is thereby not straightforward. However it is possible to implement and verify integration by increasing the penalty on the position. Changing the weight to be $\boldsymbol{Q} = [0.002\ 0\ 0\ 1\ 0\ 0\ 0\ 1\text{e-}6\ 0\ 0\ 0\ 0]$ and testing it on the linear model, leads to the result seen in Fig. 3.13.

However it is clear that the integral action is relative slow given this method should be considered more an *ad hoc* than true integral feedback. A trade off can be made by adjusting the weights to be $\boldsymbol{Q} = [0.004\ 0\ 0\ 150\ 0\ 0\ 0\ 1\text{e-}6\ 0\ 0\ 0\ 0]$, such that a relative small steady state error is achieved quickly and will over time become zero. The plot seen in Fig. 3.14 represent this, though the integral action can not be perceived, it does indeed goes to zero slowly.
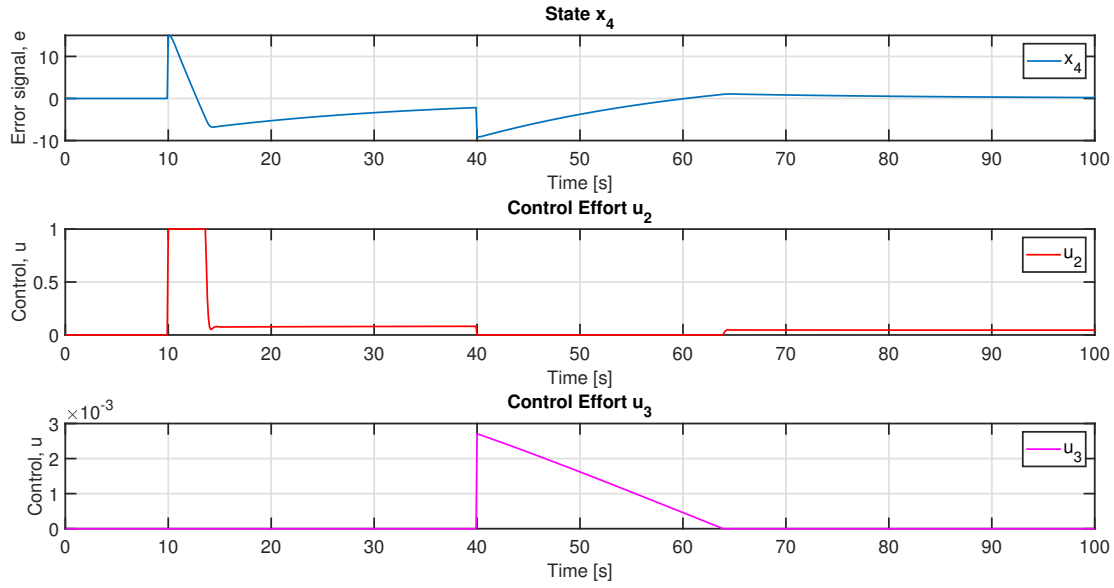
Figure 3.13: Plot of the state $x_4$ error signal and the control effort of $u_2$ and $u_3$, for the controlled linearized model to verify integral action.
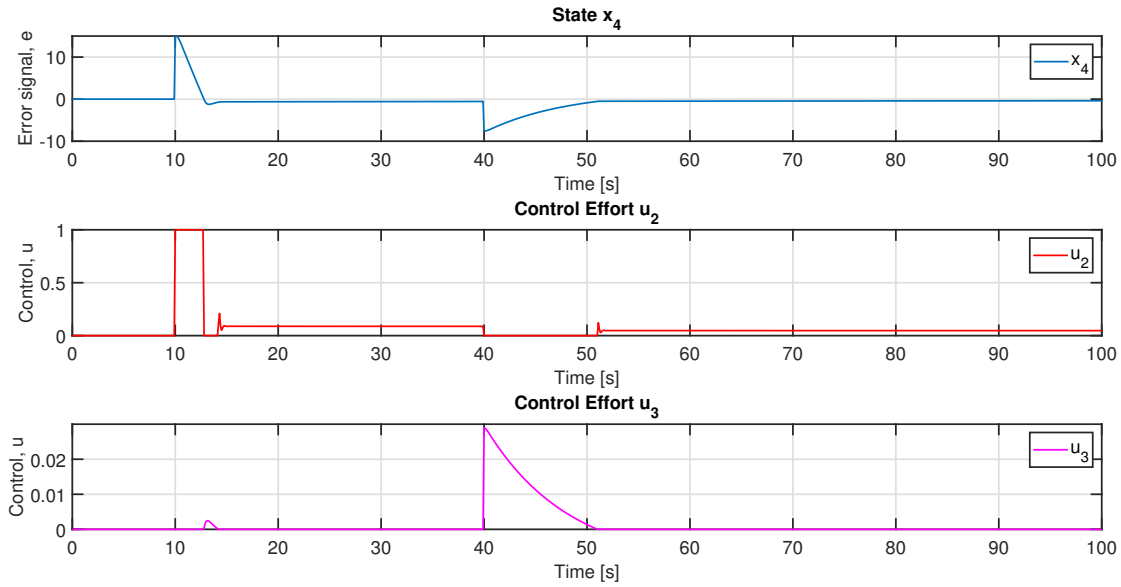


Figure 3.14: Plot of the state $x_4$ error signal and the control effort of $u_2$ and $u_3$, for the controlled linearized model with adjusted weights.

In Fig. 3.15, the error of the state $x_4$ and control effort of $u_2$ and $u_3$ with the adjusted weights, is implemented on the nonlinear model. In Fig. 3.16, the velocity of the controlled vehicle with adjusted weights is compared to the non-adjusted weights, that was seen in Fig. 3.12. The controller is enabled after 10 seconds and should follow a reference of 15 $[m/s]$, then at 40 seconds the reference is change to 8 $[m/s]$. There is a clear improvement in regards to reaching the reference speed, but also in regards to the braking time for the nonlinear model, compared to the linear. There is an overshoot but this is not considered a problem as it is relative small.
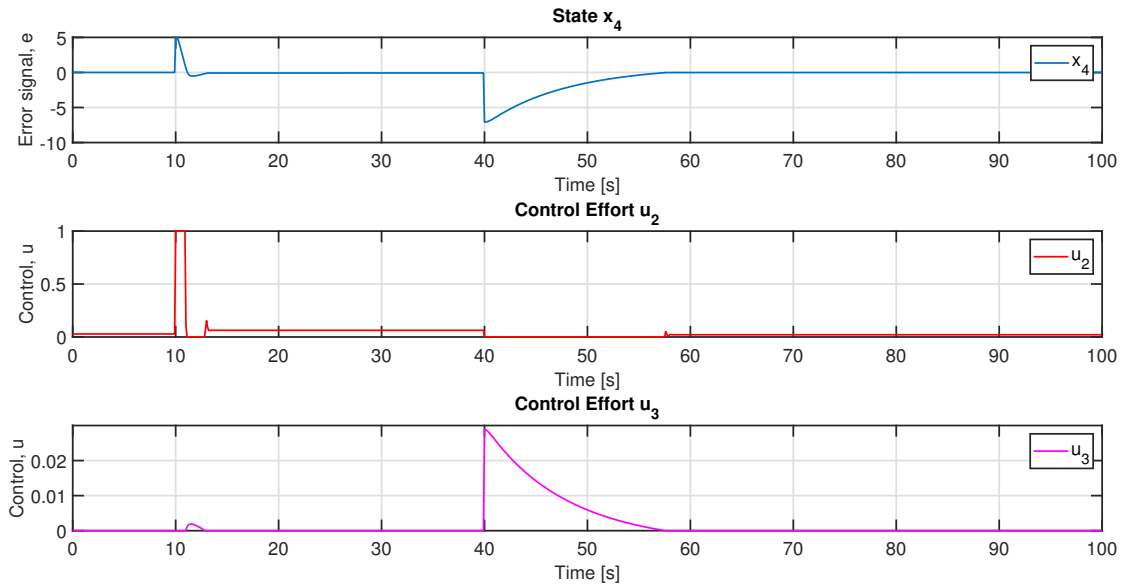
Figure 3.15: Plot of the state $x_4$ error signal and the control effort of $u_2$ and $u_3$, for the controlled nonlinear model with adjusted weights.
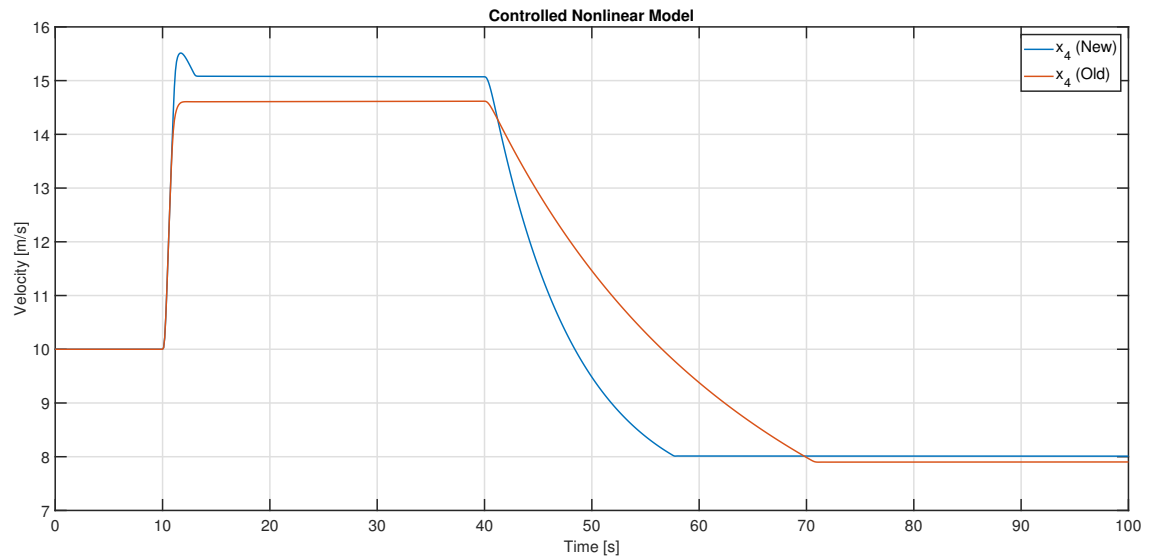


Figure 3.16: Plot of the velocity for the controlled nonlinear model with adjusted weights (New) and the non-adjusted weights (Old).

In Fig. 3.17, another plot of the controlled vehicle can be seen. The control is enabled after 10 seconds and should follow a reference of 11 $[m/s]$, at 40 seconds the reference is change to 9 $[m/s]$. The controller is performing well, given the steady state is small and over time it will reach the reference speed. To visualize the integral action the reference is set to 10 $[m/s]$, where the controller enabled after 10 seconds. Two weight matrices can then be considered, the old $\boldsymbol{Q}_{old} = [$1e-6 0 0 150 0 0 0 1e-6 0 0 0 0$]$ with state $x_4$ set to 150 and the new $\boldsymbol{Q}_{new} = [$0.004 0 0 150 0 0 0 1e-6 0 0 0 0$]$. From Fig. 3.18 it is clear that over time the integral action will bring the steady state error to zero.
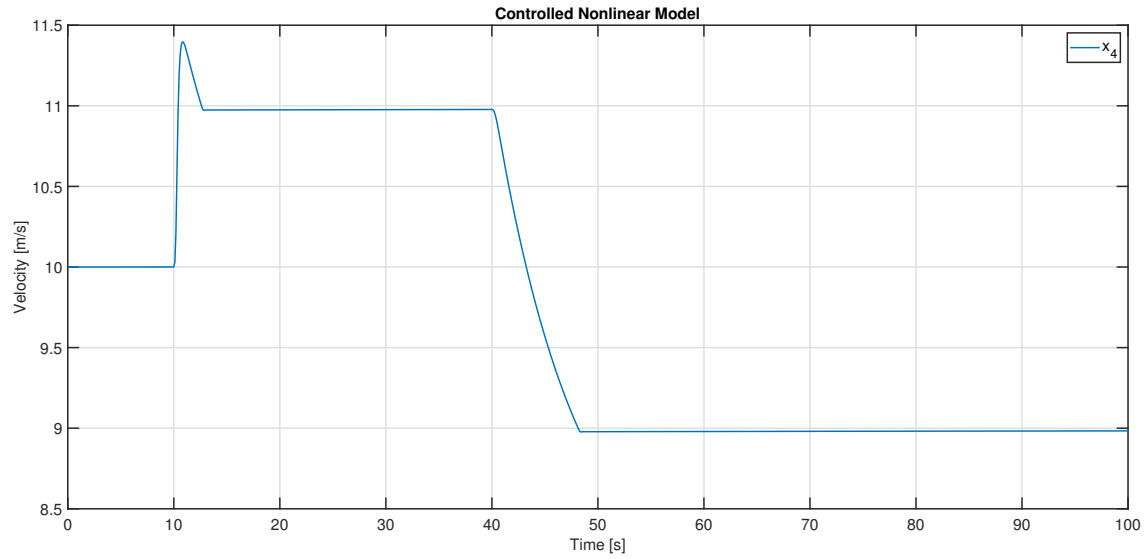
Figure 3.17: Plot of the velocity for the controlled nonlinear model at a lower reference speeds.
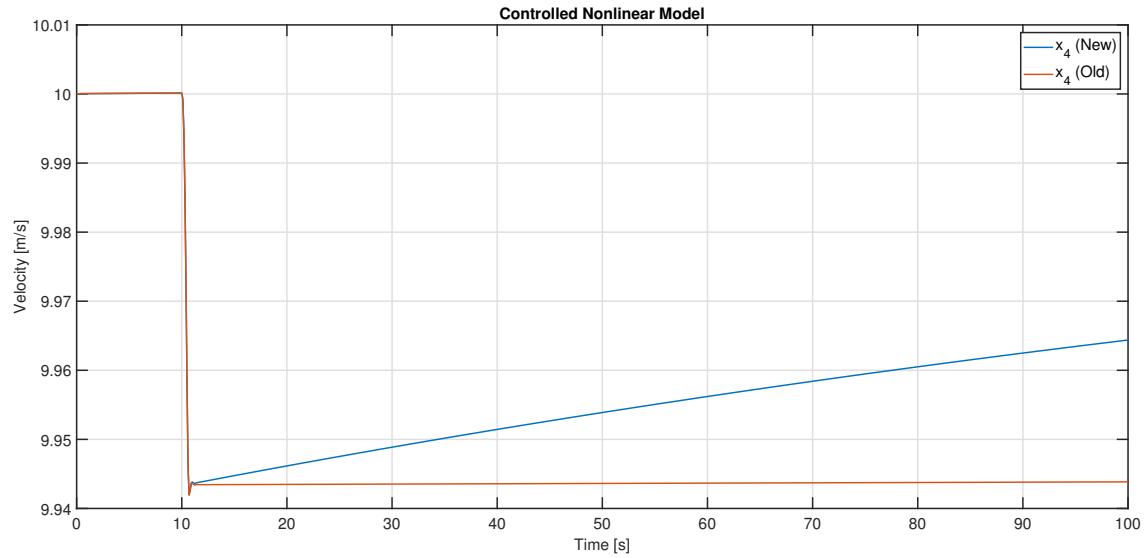


Figure 3.18: Plot of the velocity for the controlled nonlinear model to visualize the integral action.

Note that a more optimal weight matrix may exist and implementing a true integral feedback would improve the performance of the controller. However the found controller, within the selected region, does fulfilled the requirement 1. and requirement 1(a). The velocity obtained from Fig. 3.16 is 15.08 $[m/s]$ after 13 $[s]$ and 8.013 $[m/s]$ after 58 $[s]$, which is within 0.1 $[m/s]$ of the requirement. The velocity obtained from Fig. 3.17 is 10.97 $[m/s]$ after 13 $[s]$ and 8.98 $[m/s]$ after 49 $[s]$, also within the requirement. Therefore the controller can be said to work within the region of 15 to 8 $[m/s]$.

# Discussion, Conclusions and
# Future work

<span style="float:right; font-size:3em; color:gray;">4</span>

This thesis considered multiple aspects related to modeling and control of an existing race car. This chapter discusses the results and concludes the overall project. Furthermore is suggestions and recommendations for future work given.

## 4.1   Discussion

The implemented nonlinear showed good response for both longitudinal and lateral dynamics, above the 10 $[m/s]$ threshold and even for lower velocities with the control applied for the longitudinal direction. The model can however be configured from a rear to front or all wheel drive of which only rear and front have been attempted. A problem was observed when applying both longitudinal and lateral forces for the front wheel drive, where the simulation trying to solve stiff differential equations, would become very slow or fail entirely. Possibly this problem could also affect all wheel drive. The cause of the problem was not ascertained throughout the work on this thesis and therefore the performance only applies to rear wheel drive. The importance of this is worth mentioning since improvements to the vehicle includes electrical motors for all wheels in the future. Furthermore for front wheel drive, a velocity to the rear wheel must be applied as no lateral force will be passed on otherwise to evaluate the angular momentum of the vehicle.

The velocity limitation of the model has primarily been associate with the model for the engine in this thesis. No other model was considered as knowledge of the problem was first realised late into the project, given that the used model from [2], should be sufficient. Nevertheless, an improvement could be to set a minimum torque even at zero angular velocity for the wheels, or a more complex model could be implemented. The inclusion of longitudinal slip, complicated the problem further due to the oscillation nature of it. Sources that include the longitudinal slip were difficult to find and often it was neglected. Given the mentioned problem with front wheel drive, one could possibly consider modeling the slip as a disturbance on the tire forces, based on the difference in speed between the chassis and the wheels. However it can not be substantiated, whether or not, it would work and would require a relative large data set to be obtained.

For this thesis, only aerodynamic disturbances on the vehicle has been considered. Other disturbances is assumed to be have includes in the data from the Formula SAE Tire Test. It also assumed that the data resemble the mathematical description of the Magic Formula Model. Therefore it can not be excluded, that the tire model may not represent the data accurately in the Simulink model. An mathematical approximation from the tire data, using the Magic Formula as baseline, would be an improvement to the model. The constructed Simulink model includes a large variety of blocks to perform various functions, such as the switch, the saturation and the integrator block. It can not be guaranteed that the implemented model is constructed optimally, which could lead to unexpected errors

when running the simulating. Some part of the model could possibly be optimized using blocks designed for a certain function, leading to a faster computation and easier fault detection.

The linearization of the model perform well near the equilibrium point as expected, but degraded fast with negative deviations because of the lower available torque supplied from the engine. For positive deviations the linear model degraded slower, which is likely due to increasing aerodynamic disturbances. However the torque will also decrease at higher RPMs, hence an equilibrium point placed at higher RPMs would experience the reverse effect.

Although the performance of the LQR was found to track the speed reference well in this thesis, it could be clear that for better performance an implementation of integral feedback is necessary. The system could not be fully stabilized, as it was not fully controllable, which could limited the overall system. It can be said that the implemented control system performed well given the limitation of the system. Ideally the system should be fully stabilized, but as in real life, is not guaranteed.

With the implementation of the controller, limitation of the model was accounted for by limiting the use of the brake. However, there might be a potential problem with the model, which could be related to the use of brake. Until the implementation of the controller, the model have not been tested with only the brake applied. Therefore, it can not be excluded that the nonlinear model might react unexpectedly when only the brake is applied.

## 4.2  Conclusion

The goal of the project was to model, design and development of a control strategy for an autonomous racing car, for uses in a educational engineering competition, that have two types of events. Both was investigated and lead to a study for possible subsystems for the vehicle. It was suggested to use LIDAR, GPS and IMU to accomplish the goal of an autonomous car.

It was found that a nonlinear model would be necessary to get an accurate description of the dynamics for the vehicle. For simplification only a single track model was considered and implemented. The model included aerodynamic disturbances, a simple engine model, a tire model which include both longitudinal and lateral slips and tire forces build up through a first order system.

The model was implemented in Simulink, using data obtained from a SolidWorks model and the G8 race car. It has been verified to work both longitudinally and laterally in rear wheel drive mode. However the the model performed poorly at lower speeds likely due to the engine model.

Linearization of the nonlinear model has been proven to accurately capture the dynamics of the vehicle in small region. Only one linearization was performed for test and verification of the control system. The implemented LQR control was verified to work on both the linear and nonlinear model in simulink, with both requirements fulfilled.

## 4.3   Future work

Through this thesis some possible future improvements have already been mentioned. Based on the experiences gained, the following recommendations and suggestions are provided for future work.

- The nonlinear model implemented in Simulink is a good representation of the dynamic systems. It should however be expanded upon to include all four wheel and at least a simple suspension system. Thereby, pitch and roll of vehicle would be taken into account.

- The simplified engine model proved to be a problem in this project and it is therefore recommended to further investigate this subject. A short-term solution could be to set a minimum torque output regardless of the velocity of the wheel.

- Currently the model uses rear wheel drive mode, but allows for front and four wheel drive. The last two modes should be evaluated and verified for possible uses in the future.

- The tire model is based on data from Calspan's research facility. The AAU race team have however requested a mathematical model, possibly based on the Magic Formula. A mathematical model based on the tire data should therefore be explored further.

- The controller in this project do not have true integral feedback and only cover a small region of operation. Multiple linearizations would be required to cover all regions, with improved performance of the controller by implementing integral feedback.

- The LQR design can not by nature handle constraints with varying disturbances or takes actuator limitations into account. It is therefore recommended to implement a MPC controller in the future.

# Bibliography

[1] M. E. Bernd Heißing. *Chassis Handbook*. Vieweg+Teubner Verlag, 2011.

[2] R. B. Dieter Schramm, Manfred Hiller. *Vehicle Dynamics Modeling and Simulation*. Springer, 2018.

[3] V. L. S. Frank L. Lewis, Draguna L. Vrabie. *Optimal Control*. John Wiley & Sons, Inc., third edition edition, 2012.

[4] F. S. Germany. An outlook on fsg 2021 and the following seasons, 2018. Last visited on 2019-03-14, [https://www.formulastudent.de/pr/news/details/article/an-outlook-on-fsg-2021-and-the-following-seasons/](https://www.formulastudent.de/pr/news/details/article/an-outlook-on-fsg-2021-and-the-following-seasons/).

[5] F. S. Germany. Formula student rules 2019, 2019. Last visited on 2019-03-14, [https://www.formulastudent.de/fileadmin/user_upload/all/2019/rules/FS-Rules_2019_V1.1.pdf](https://www.formulastudent.de/fileadmin/user_upload/all/2019/rules/FS-Rules_2019_V1.1.pdf).

[6] F. S. Germany. Fsg competition handbook 2019, 2019. Last visited on 2019-03-14, [https://www.formulastudent.de/about/concept/](https://www.formulastudent.de/about/concept/).

[7] F. S. Germany. What is the formula student germany competition, 2019. Last visited on 2019-03-14, [https://www.formulastudent.de/about/concept/](https://www.formulastudent.de/about/concept/).

[8] H. K. Khalil. *Non Linear Systems*. Prentice Hall, third edition edition, 2001.

[9] J. M. Maciejowski. *Predictive control with constraints*. Prentice Hall, 2002.

[10] U. NATIONS. Un regulation no. 39 - rev.2, 2018. Last visited on 2019-08-29, [http://www.unece.org/fileadmin/DAM/trans/main/wp29/wp29regs/2018/R039r2e.pdf](http://www.unece.org/fileadmin/DAM/trans/main/wp29/wp29regs/2018/R039r2e.pdf).

[11] T. E. Toolbox. Air - density, specific weight and thermal expansion coefficient at varying temperature and constant pressures, 2019. Last visited on 2019-07-04, [https://www.engineeringtoolbox.com/air-density-specific-weight-d_600.html](https://www.engineeringtoolbox.com/air-density-specific-weight-d_600.html).

[12] L. Wang. *Model Predictive Control System Design and Implementation Using MATLAB*. Springer, 2009.

## A.1   ARC Simulink Model

In this appendix, each subsystem for the implemented Simulink model representing the nonlinear model is described. Figure for the subsystems is used to illustrate important points. Furthermore will modification to the model be explained. The parameters used in the model can be found in Appendix A.2.

The constructed model in Simulink of the ARC is based on the equation of motion found in Sec. 2.7. The linear momentum of the chassis is evaluated from the approximated momentum of the wheels and therefore the subsystem for the wheels is considered first. The subsystem is located in the vehicle dynamics (see Fig. A.1).
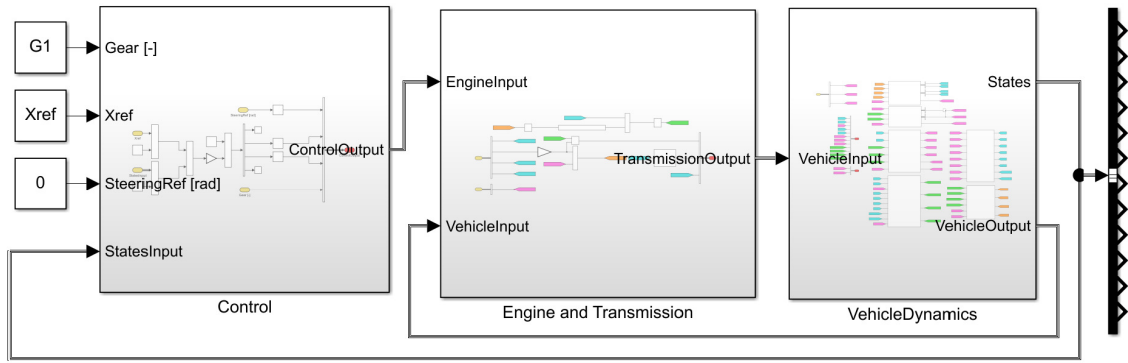


Figure A.1: Diagram of ARC model in Simulink.

A diagram of the implemented equation (2.40) can be seen in Fig. A.2. The subsystem approximate the velocity of the front/rear wheel, used for the slip calculation and approximating the engine torque. It is therefore a critical subsystem since it depends on three of the control input, the accelerator, the brake and the gear. At relative low velocity, the torque from the engine can become less than the torque subtracted from the wheels, caused by the longitudinal slip. This can lead to a negative velocity of the wheels which the model is not designed to handle.

The selection of $\xi_a$ and $\xi_b$ also important, as the torque from the engine and the brake is distributed over the front/back wheel. If the torque is fully distributed to one wheel the other will have no velocity, which lead to no steering capability, if the torque is not applied to the front wheel. Distributing torque to both wheel cause less torque for each wheel making the problem mentioned before even worse. It should be note that rear wheel drive is used, but to allow for steering the velocity from the rear wheel is also used for the front wheel.
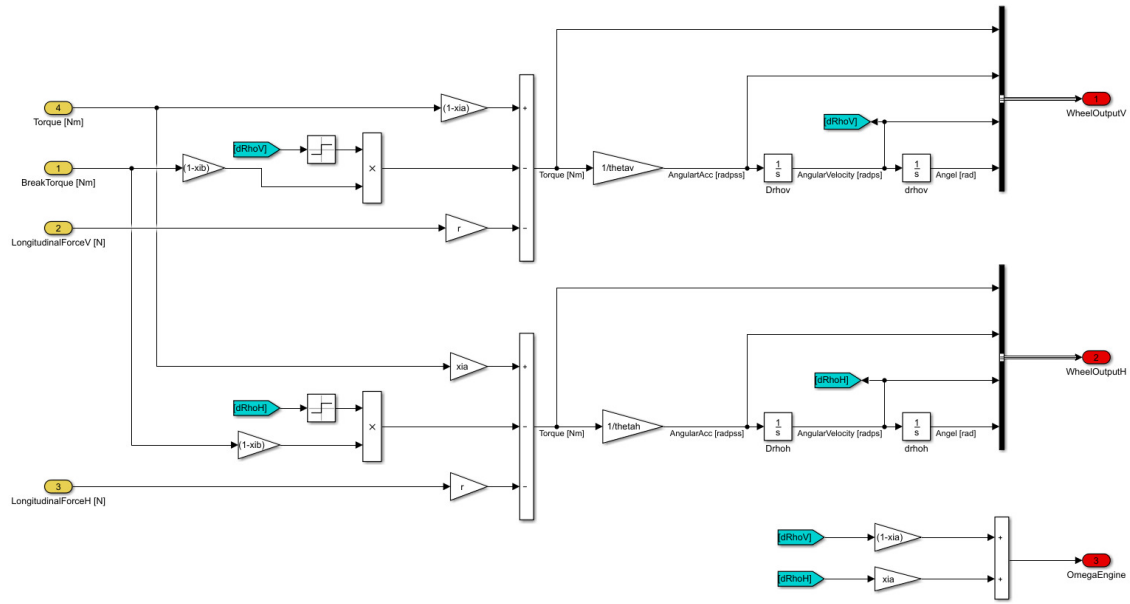
Figure A.2: Diagram of the implemented equation (2.40) in Simulink, that evaluate the velocity of wheels.

To initialize the simulation the velocity of the wheel and chassis must be relative large, to avoid the problem of negative velocity, or one could apply a sufficiently large input from the accelerator pedal. If the wheel and chassis are initialize at large different velocity, a slip will arise quickly. Whereas initialize at equal or slightly different velocity, the slip will be slightly delayed or low.

The velocity of the wheels is also used to approximate the RPM of the engine which determines the torque applied to the wheels. The model for the engine is placed in the engine and transmission subsystem as seen in Fig. A.1 and Fig. A.3 and is based on Sec. 2.7.2.
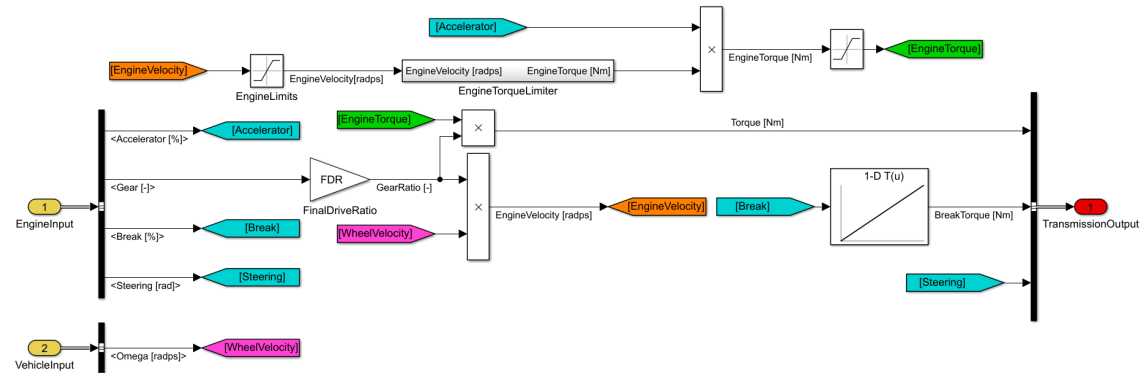


Figure A.3: Diagram of the implemented engine and transmission in Simulink, that approximate the torque from the engine and the brake.

The velocity of the wheels is multiplied with the selected gear ratio and the FDR to approximate the velocity of the engine. Which is converted to RPM and applied in a look-up table, specifying the torque from an engine map, located in the subsystem engine torque limiter. The torque is multiplied with the accelerator value, gear ratio and FDR to determined the torque applied to the wheels. Depending on the engine map, a relative high torque will first be available at a relative high RPM. Therefore is the selection of gear and

use of the accelerator important at relative low velocity. The brake torque is approximated from a look-up table based on the percentages of brake applied and subtracted from the wheels.

Having implemented the engine and the wheels, it is possible to consider the longitudinal and lateral slip. In Fig. A.4, a diagram of the implemented slip calculation can be seen, which is based on equation (2.31) and (2.32) in Sec. 2.7.1. A switch determines whether it is drive or brake slip, where drive is considered a positive slip and brake a negative slip. Note that a switch is implemented to avoid singularities in Simulink and a gain just before the output $SaV$ and $SaH$, enable or disable the slip. This is to remove longitudinal slip (no traction) from the front wheel but allow lateral slip to be evaluated.
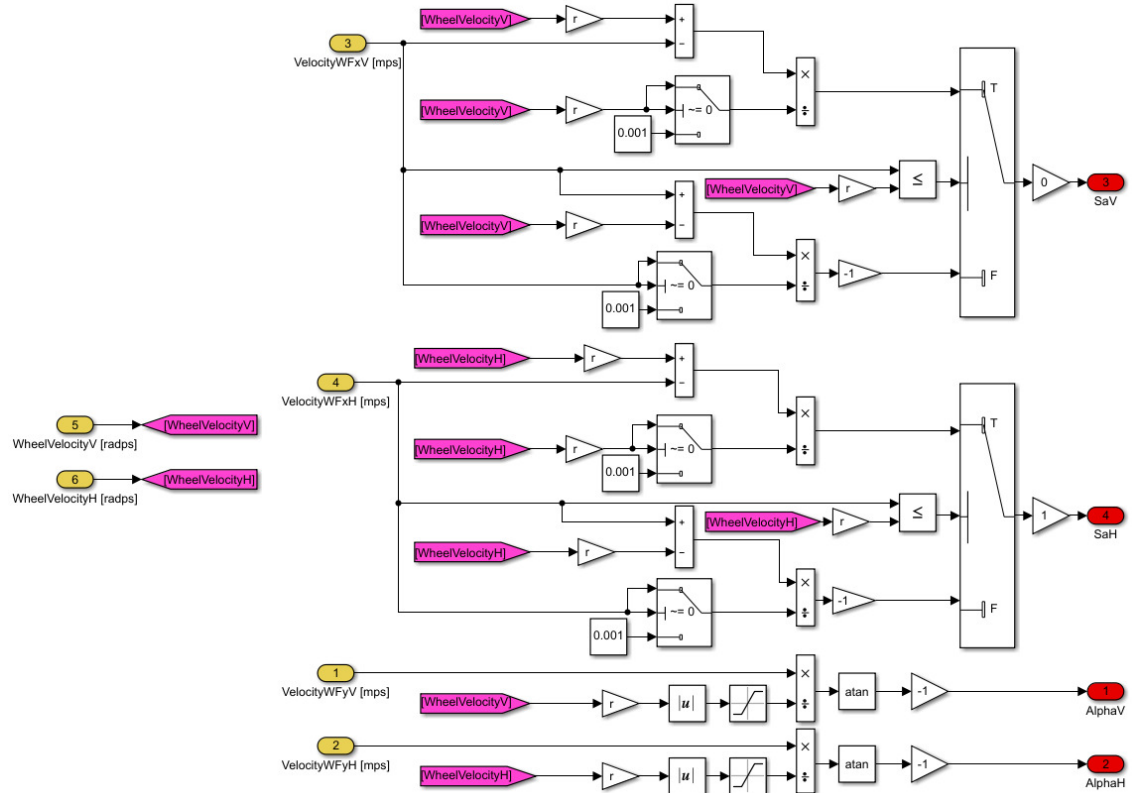


Figure A.4: Diagram of the implemented subsystem to determine longitudinal and lateral slip of the wheels.

Furthermore, the slip depends on velocity of the wheel center point which is calculated from the vehicle (chassis), but as mentioned before is not possible to steer unless front drive is chosen with the modification, as the forces will be zero and thereby no change in direction, regardless of the steering input. This can be seen in Fig. A.5, which is the implemented angular motion of the vehicle based on equation (2.25). Hence to allow steering, velocity from the rear wheel is applied to the front wheel. Having a front driven vehicle with no modification, means no forces on the rear wheel and therefore the angular motion would only depend the front wheel.

The velocity of both wheels center point is nevertheless calculated in the model as seen in Fig. A.6, where the implementation is based equation (2.27) and (2.28). However for the slip values, the velocities must be in the wheel fixed coordinate system requiring another transformation to be implemented based on equation (2.29) and (2.30). This can be seen in Fig. A.7.
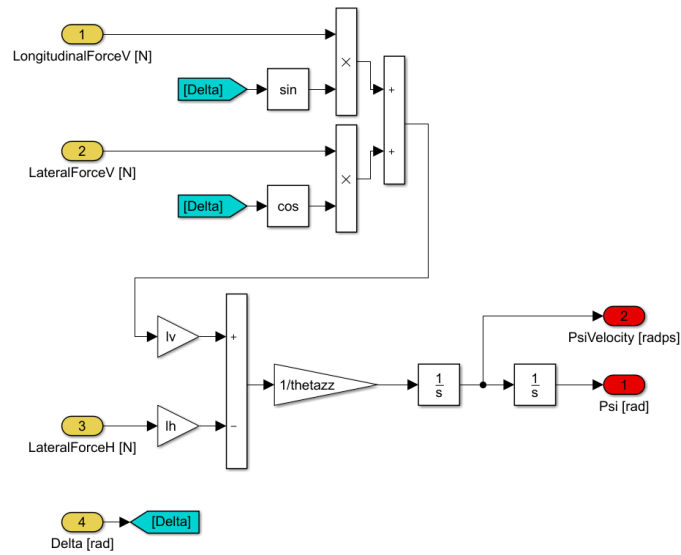
Figure A.5: Diagram of the implemented subsystem to determine the angular motion of the vehicle around the z-axis.
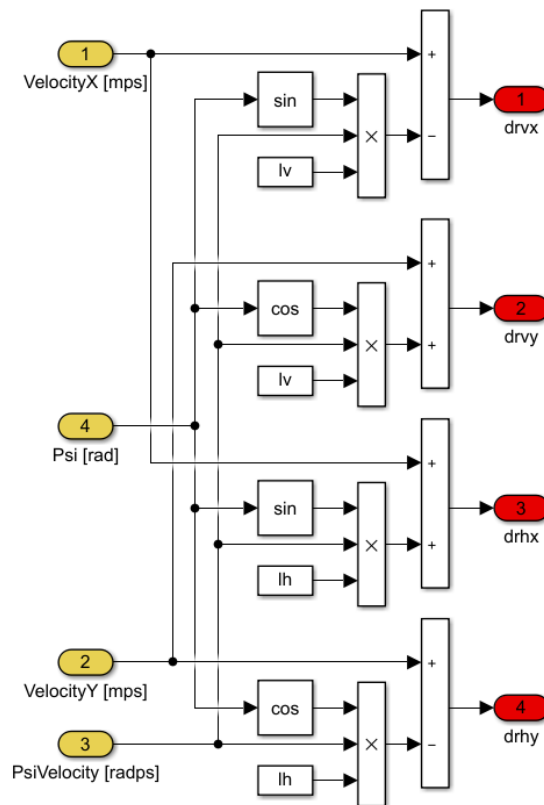


Figure A.6: Diagram of the implemented subsystem to determine the velocity of the wheels center points.
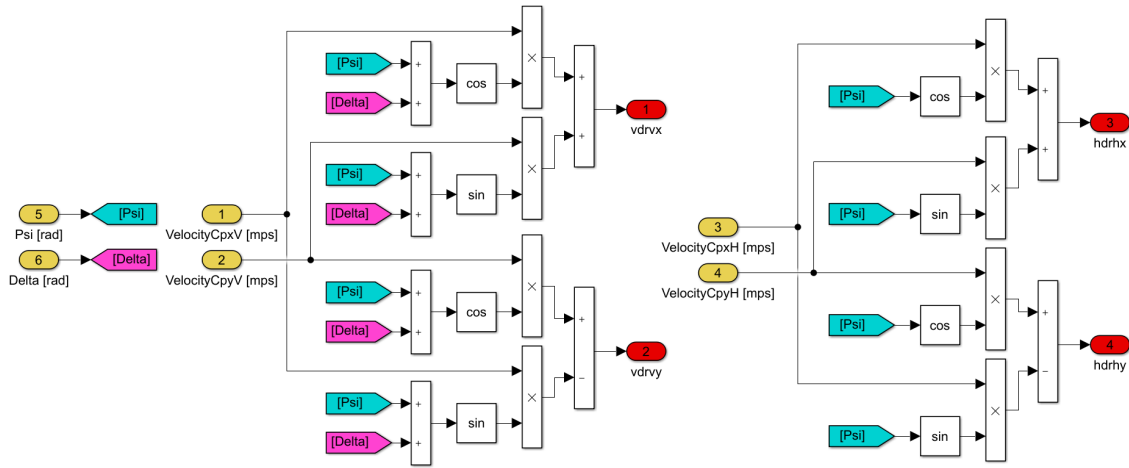
Figure A.7: Diagram of the implemented subsystem to determine the velocity in the wheel fixed coordinate system.

Having found the slip values, a normalized slip is needed in order to consider the effects of both longitudinal and lateral slip and the direction of the slip during a driving situation. For which implementation can be seen in Fig. A.8 and is based on equation (2.7) and (2.8). Note that the protection against singularity mean a small total slip is always present.
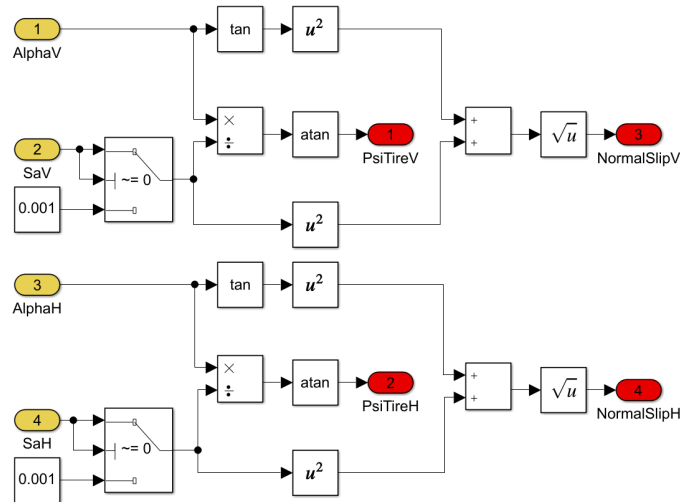


Figure A.8: Diagram of the implemented subsystem to determine the normalized total slip.

The magnitude of the resulting tire forces is then calculated and the tire forces in the wheel fixed coordinate system can be determined. The implementation of this can be seen in Fig. A.9 and is based on equation (2.9) and (2.10). However the resulting slip forces requires the static forces, determined from a look-up table, as shown in Fig. A.10 and Fig. A.11, which also consider the settling time of the tires, from the resulting tire forces. Note that no tire forces is passed on if the wheel velocity is zero. The time constant is calculated using (2.38).
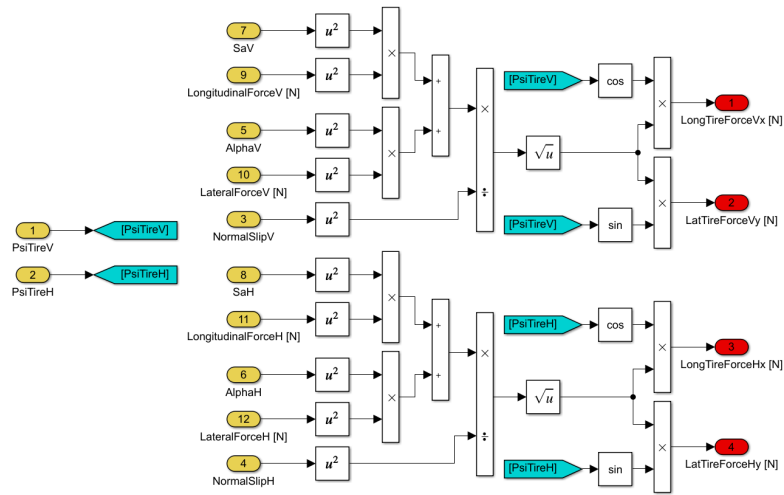
Figure A.9: Diagram of the implemented subsystem to determine the resulting tire forces in the wheel fixed coordinate system.
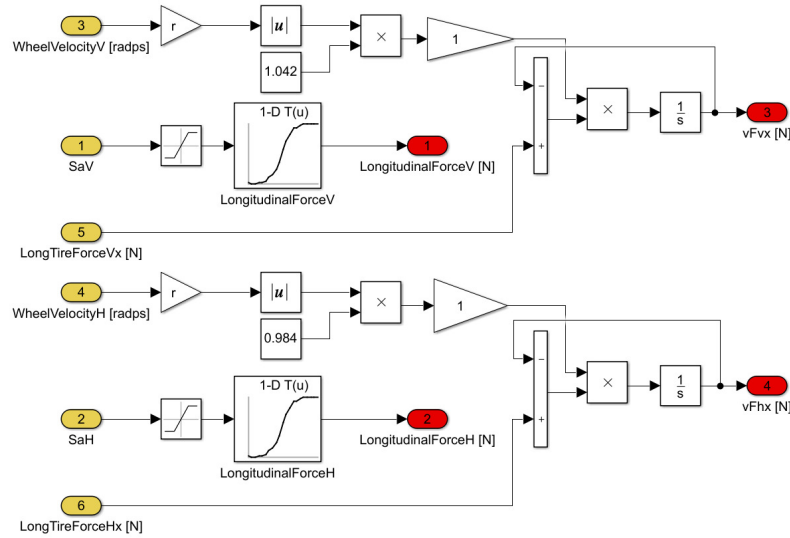


Figure A.10: Diagram of the implemented subsystem to determine the longitudinal slip force, the settling time of the tires and the final tire forces.
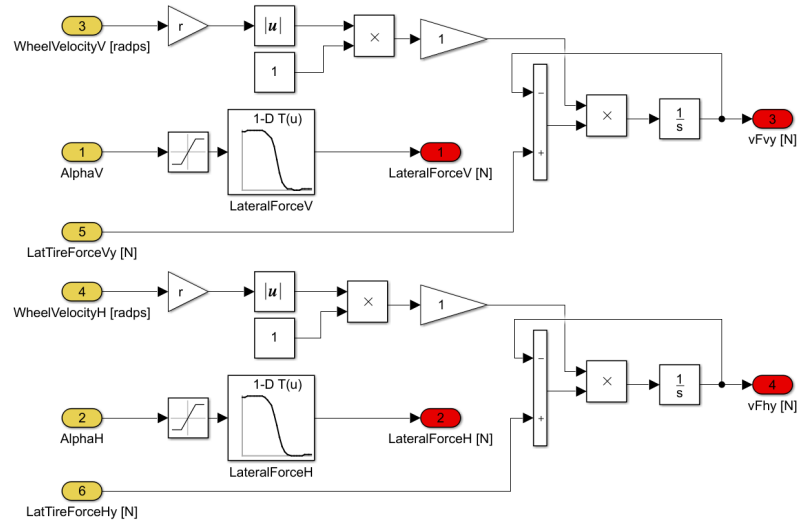
Figure A.11: Diagram of the implemented subsystem to determine the longitudinal slip force, the settling time of the tires and the final tire forces.

Finally the forces applied to the chassis can be determined from the implemented subsystem in Fig. A.12 and the linear momentum on the chassis can determined as seen in Fig. A.13.
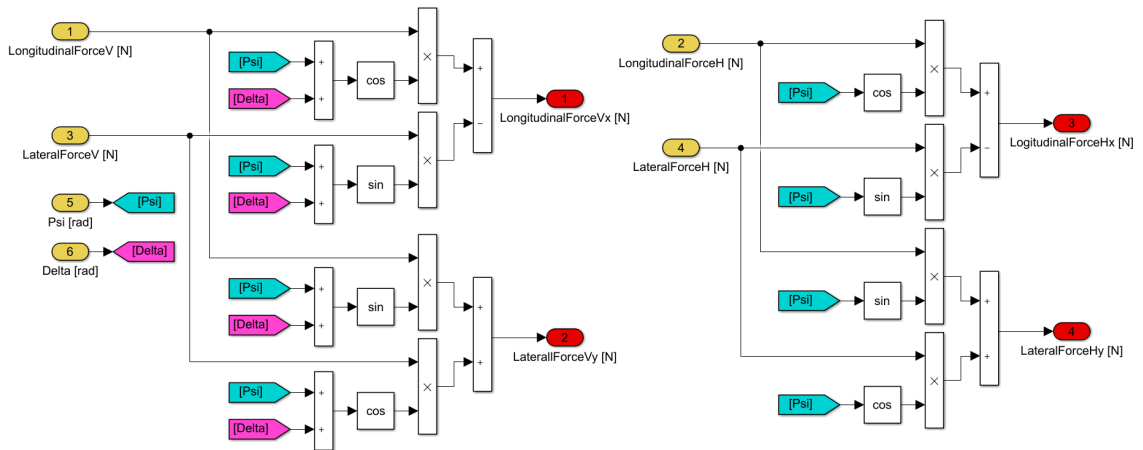


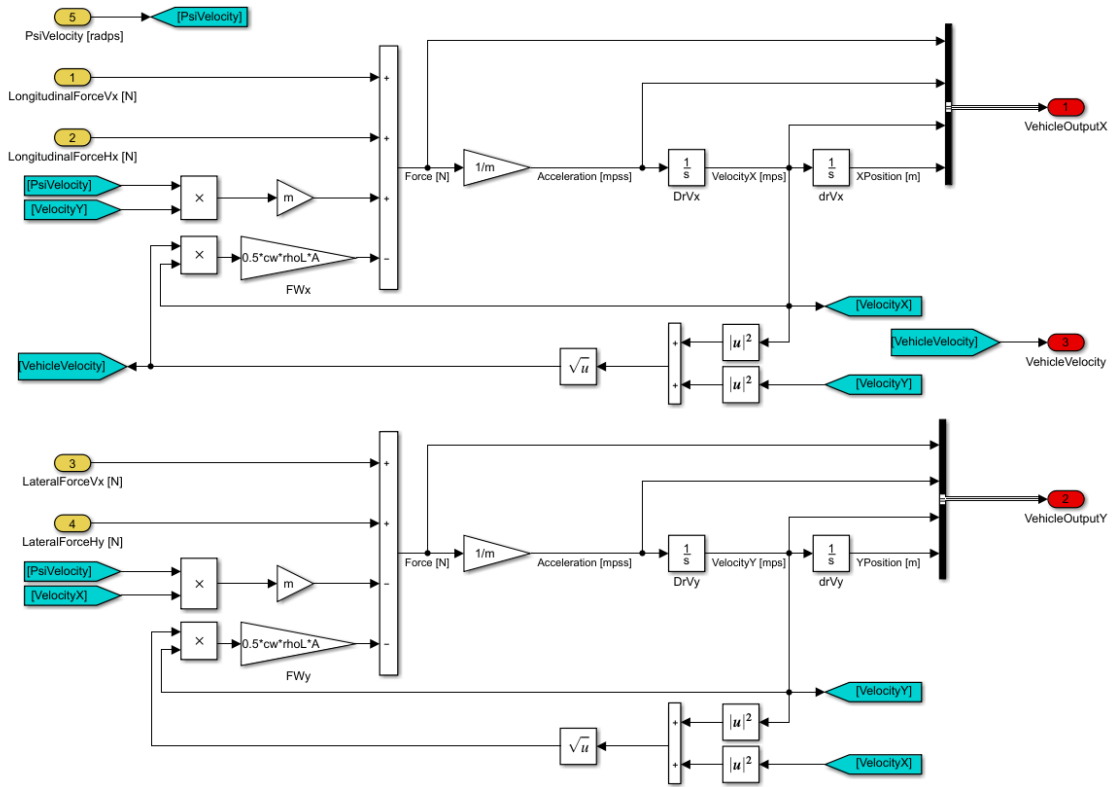Figure A.12: Diagram of the implemented subsystem to determine the forces applied to the chassis.

Figure A.13: Diagram of the implemented subsystem to determine the linear momentum on the chassis.

Last the control of the vehicle velocity is placed in the control subsystem as seen in Fig. A.1 and Fig. A.14 and is based on equation (3.18) in Sec. 3.5. The controller tracks the deviation between the reference velocity and the selected equilibrium point $X_{eq}$. The inputs required to maintain the equilibrium $U_{eq}$ is then added to the control gain and is passed on to the vehicle.
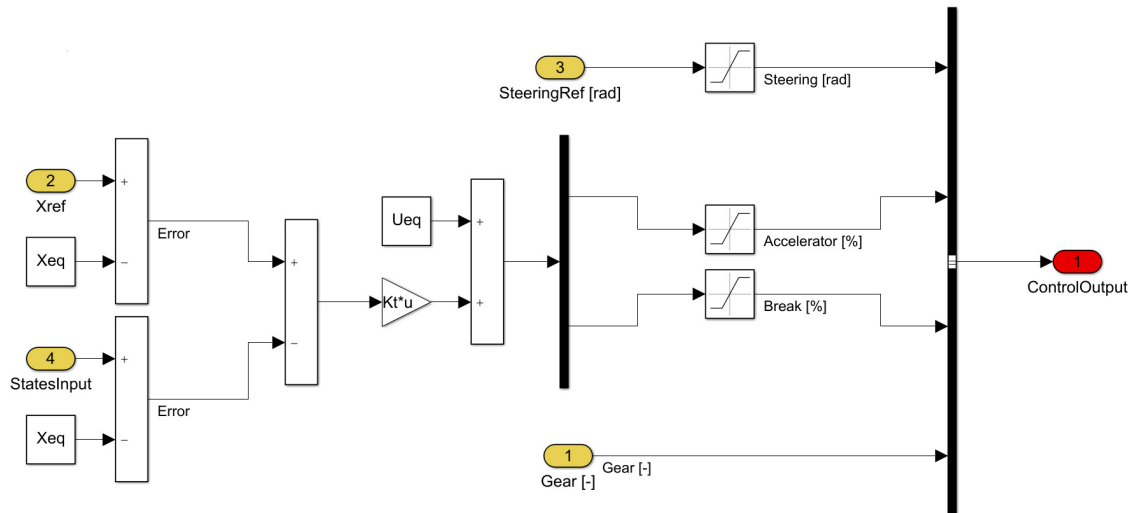


Figure A.14: Diagram of the implemented subsystem to control the vehicle.

## A.2   Data Parameter

This appendix contains the parameter used in the ARC model. The data can be seen in Tab. A.1. The parameters were found from a SolidWorks model and using the equations found in Sec. 2.7

| Data | Value | Unit |
|------|-------|------|
| $m$: Vehicle mass | 221 | $[kg]$ |
| $\theta_{zz}$: Moment of inertia about the vertical axis | 168.8 | $[kg \cdot m^2]$ |
| $\theta_v$: Moment of inertia (front wheel) | 26 | $[kg \cdot m^2]$ |
| $\theta_h$: Moment of inertia (rear wheel) | 26 | $[kg \cdot m^2]$ |
| $l$: Wheel base | 1.6 | $[m]$ |
| $l_v$: Distance between CoG and front axle | 0.621 | $[m]$ |
| $l_h$: distance between CoG and rear axle | 0.979 | $[m]$ |
| $r$: Radius of wheels | 0.266 | $[m]$ |
| $A$: Cross-sectional area | 1.804 | $[m^2]$ |
| $c_W$: Air resistance coefficient | 1.0 | $[m/s^2]$ |
| $\rho_L$: Air density at (20 Celsius) | 1.2 | $[kg/m^3]$ |
| $\xi_a$: Factor represent a front/rear wheel drive | 1 | $[-]$ |
| $\xi_b$: Factor represent brake distribution | 1 | $[-]$ |
| $T_{v,x}$: Time delay constant | 1.042 | $[-]$ |
| $T_{h,x}$: Time delay constant | 0.984 | $[-]$ |
| $T_{v,y}$: Time delay constant | 1 | $[-]$ |
| $T_{h,y}$: Time delay constant | 1 | $[-]$ |

Table A.1: Table of data set for the model.

## A.3    Formula SAE Tire Data

The Formula SAE Tire Test Consortium provide high quality tire data to participating teams for use in their race cars. Data on different constructions of tires was measured at Calspan's Tire Research Facility.

The relevant tire data can be plotted using a MatLab script provided by AAU Racing Team. The front tire type is Hoosier 20.5 x 6.0-13 while the rear tire is Hoosier 20.5 x 7.0-13, with the camber angle set to zero as it is not considered and the tire pressure set to the default 12 [$psi$]. Plots of front and rear tire data can be seen in Fig. A.15 and Fig. A.16 respectively. The loads was calculated using equation (2.39) from Sec. 2.7.1, giving a vertical load of 841 [$N$] and 1326 [$N$] for the front and rear wheel respectively. Hence the yellow curve was used for the front wheel and the read curve for the rear wheel.
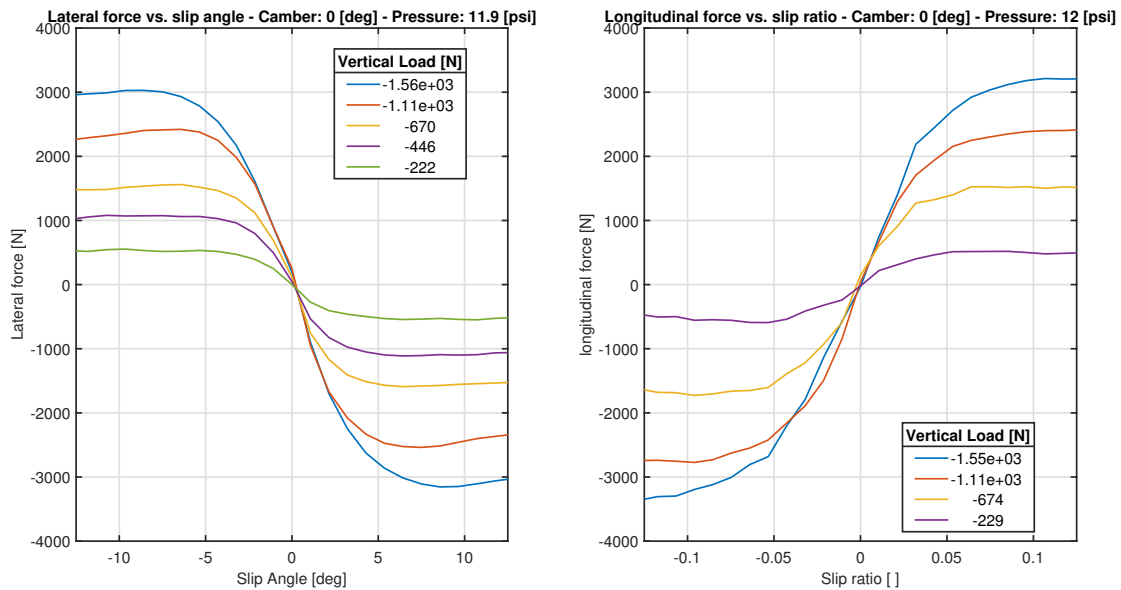


Figure A.15: Plot of lateral and longitudinal forces for front tire given the slip angel and slip ratio, for multiple vertical loads.
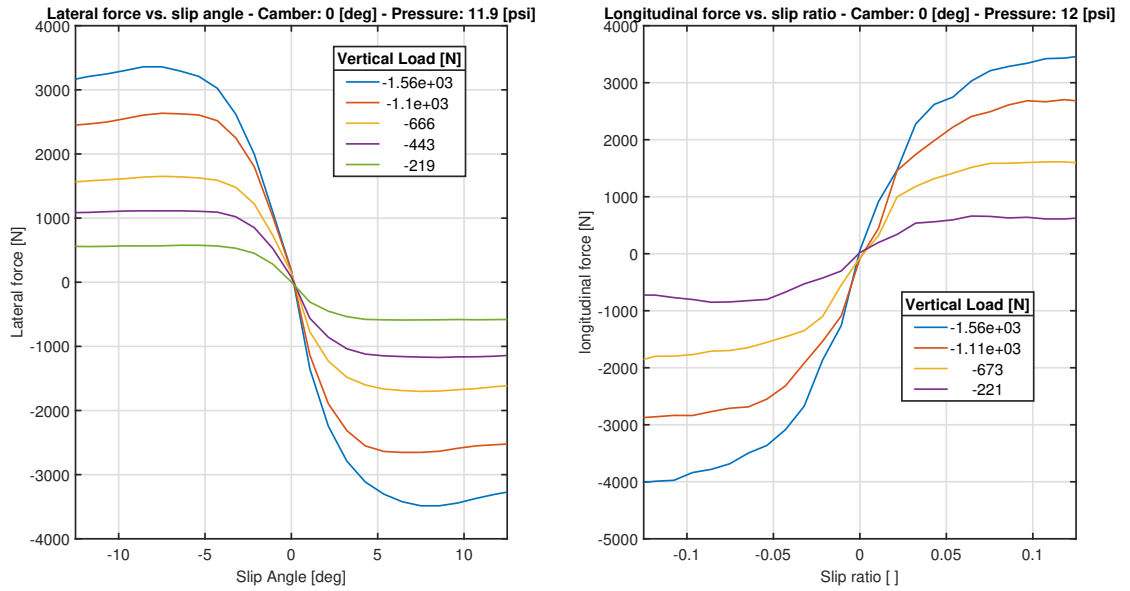
Figure A.16: Plot of lateral and longitudinal forces for rear tire given the slip angel and slip ratio, for multiple vertical loads.

Note that the slip ratio does not follow the typically slip given in percentage considered in [2]. Assuming the curvature data is similar to that of the most widely used tire models (the Magic Formula Model), a model based on the data could be approximated

The Magic Formula Model is a mathematical description of the relationship between the input/output and tire-road contact under stationary conditions, to connect the force variables with the rigid body slip using mathematical functions. It is capable of describing the longitudinal force and lateral force as functions of the longitudinal and lateral slip with high accuracy [2]:

$$f(\kappa) = F_z \cdot D \cdot sin(C \cdot arctan(B\kappa - E(B\kappa - arctan(B\kappa)))) \tag{A.1}$$

where B, C, D, and E are dimensionless coefficients corresponding to stiffness, shape, peak, and curvature respectively. $\kappa$ is the wheel slip and $F_z$ is the Vertical load. Note that notation used only applies in this appendix.